Quantum and Classical Effects in Brane-World Large Distance Modified Gravity

The DGP Model With Two Branes

Max Warkentin

München 2022

Quantum and Classical Effects in Brane-World Large Distance Modified Gravity

The DGP Model With Two Branes

Max Warkentin

Dissertation
an der Fakultät für Physik
der Ludwig-Maximilians-Universität
München

vorgelegt von
Max Warkentin
aus Syktywkar

München, den 11. Mai 2022

Erstgutachter: Prof. Dr. Georgi Dvali
Zweitgutachter: Prof. Dr. Goran Senjanović
Tag der mündlichen Prüfung: 21. Juni 2022

Zusammenfassung

Diese Dissertation befasst sich mit grundlegenden Fragestellungen in Bezug auf gravitative Phänomene auf großen Längenskalen, adressiert durch die Untersuchung sowohl einer modifizierten Gravitationstheorie als auch eines Modells der Dunklen Materie (DM).

Im ersten Teil setzen wir uns mit einer Verallgemeinerung des Dvali-Gabadadze-Porrati-Modells (DGP-Modell) auseinander, bei der eine zweite 3+1-dimensionale (4D) Bran, welche ebenfalls mit einem lokalisierten Krümmungsterm ausgestattet ist, im 4+1-dimensionalen (5D) Bulk eingebettet ist. In diesem modifizierten System decken wir neue, phänomenologisch interessante Erscheinungen auf. Wir beginnen mit der Analyse der klassischen Theorie, wobei wir sowohl die volle 5D-Darstellung als auch die Kaluza-Klein-Beschreibung gebrauchen. Dabei untersuchen wir die Gravitationsgesetze, indem wir die Gravitationsenergie zwischen zwei statischen Punktquellen berechnen, welche auf unterschiedlichen Branen lokalisiert sind. Wir entdecken eine neue Längenskala, die gleich dem geometrischen Mittelwert aus der kritischen DGP-Längenskala (welche die Übergangsregion zwischen 4D- und 5D-Gravitation im Einzel-Bran-Modell markiert) und dem Abstand der beiden Branen entlang der zusätzlichen Dimension ist. Während wir für Abstände, die größer sind als diese neue Längenskala, das ursprüngliche Resultat des DGP-Modells reproduzieren, erhalten wir für kleinere Abstände ein schwächeres Gravitationspotential. Außerdem existiert eine Region, in der ein 4D-Beobachter eine abstandsunabhängige Kraft misst. Wir diskutieren eine mögliche Anwendung des hier zugrunde liegenden Szenarios für die Herleitung von Rotationskurven in Low Surface Brightness-Galaxien. Da dieses physikalische System die Existenz eines Sektors erlaubt, in dem die Teilchensorten beliebig schwach mit „unserem“ Sektor wechselwirken, beleuchten wir weiterhin die Auswirkungen dieses Umstandes auf Schwarze Löcher und die Beschränkung der Anzahl von Teilchensorten. Als nächstes widmen wir uns der Untersuchung quantenmechanischer Erscheinungen in diesem System. Dabei erkunden wir insbesondere den Casimir-Effekt, dem zwei Branen in Anwesenheit der „infrared transparency“ unterliegen. Als letztere bezeichnet man den Tatbestand, dass die ultravioletten Moden des 5D-Gravitons auf den Branen unterdrückt sind, während die infraroten (IR) Moden diese ungestört durchdringen können. Zunächst bestätigen wir, dass die DGP-Branen als „effektive“ (impulsabhängige) Randbedingungen für das Gravitationsfeld fungieren, sodass tatsächlich eine (gravitative) Casimir-Kraft zwischen den Branen auftritt. Des Weiteren entdecken wir, dass die Anwesenheit einer IR transparency-Region für die diskreten Moden die gewöhnliche Casimir-Kraft – wie man sie für ideale Dirichlet-Randbedingungen herleitet – auf zwei konkurrierende Weisen modifiziert: i) Der Ausschluss der weichen Moden vom diskreten Spektrum führt zu einer Ver-

stärkung der Casimir-Kraft. ii) Die Abweichung der Randbedingungen von ihrem idealen Pendant führt zu einem „leakage“ der harten Moden. Als Resultat der Effekte i) und ii) wird die Casimir-Kraft schwächer. Da der Herleitung dieses Ergebnisses nur die lokalisierten kinetischen Terme eines Quantenfeldes auf parallelen Flächen (der Kodimension eins) zugrunde liegen, ist davon auszugehen, dass die hergeleitete Casimir-Kraft in einer Vielfalt an Systemen in beliebigen Dimensionen auftritt.

Im zweiten Teil dieser Arbeit untersuchen wir ein DM-Modell, welches durch ein komplexes Skalarfeld mit abstoßender, biquadratischer Selbstwechselwirkung gegeben ist, sowie dessen Auswirkungen auf die Struktur von galaktischen Halos. Da wir DM-Teilchen mit ultraleichten Massen betrachten, kann ein solches Bosegas in den inneren Halo-Regionen mit hoher Dichte einem Phasenübergang zur suprafluiden Phase unterliegen, wobei ein homogener galaktischer Kern gebildet wird. Unter Berücksichtigung der Tatsache, dass das Jeans-Kriterium eine obere Schranke an die Größe einer solchen Struktur setzt, diskutieren wir den erlaubten Parameter-Raum für ein Szenario mit Kernen, die einige Kiloparsec umfassen. Wir zeigen, dass die Parameter durch die Restriktion des Selbstwechselwirkungsquerschnitts, welche man durch Beobachtungen von Zusammenstößen von Galaxienhaufen ableitet, stark eingeschränkt werden. Obwohl eine solche Restriktion wohlbekannt ist, demonstrieren wir, dass im Falle von ultraleichter DM, welche einen massiv entarteten Phasenraum besetzt, diese Beschränkung durch eine vergrößerte Wechselwirkungsrate signifikant verschärft wird. Daraus resultierend erfordert das betrachtete Szenario eine noch leichtere DM-Teilchensorte und einen thermalisierten Kern, der in eine Ansammlung aus kleineren, suprafluiden Tröpfchen zerfällt.

Abstract

This thesis addresses fundamental questions concerning gravitational phenomena at large distances by investigating in turn a model of modified gravity and a dark matter (DM) model.

In the first part we study a generalization of the DGP model by embedding a second 3+1-dimensional (4D) brane, also endowed with a localized curvature term, in the 4+1-dimensional (5D) bulk. In this modified system we uncover phenomenologically interesting, new phenomena. We start with a classical analysis, working in both the full 5D description and the Kaluza-Klein language, and investigate the laws of gravity by calculating the gravitational potential energy between two static point sources localized on different branes. We discover a new length scale, which is equal to the geometric mean of the DGP cross-over scale (that marks the interpolation region between 4D and 5D gravity in the single-brane model) and the separation of the two branes in the extra dimension. For distances that are larger than this new length scale we recover the original DGP result, but for smaller distances the gravitational potential is weaker. Furthermore, a region emerges where a 4D observer measures a distance-independent force. We discuss a possible application of the present scenario for deriving rotation curves of low surface brightness galaxies. Moreover, since this setup allows for the existence of a sector of particle species that are interacting arbitrarily weakly with "our" sector, we explore the implications of this circumstance for black holes and the bound on the number of species. Next, we turn to the investigation of quantum phenomena in this system. In particular, we explore the Casimir effect perceived by the two branes in the presence of infrared (IR) transparency, meaning that the ultraviolet modes of the 5D graviton are suppressed on the branes, while the IR modes can penetrate them freely. First, we find that the DGP branes act as "effective" (momentum-dependent) boundary conditions for the gravitational field, so that a (gravitational) Casimir force between them indeed emerges. Second, we discover that the presence of an IR transparency region for the discrete modes modifies the standard Casimir force—as derived for ideal Dirichlet boundary conditions—in two competing ways: i) The exclusion of soft modes from the discrete spectrum leads to an increase of the Casimir force. ii) The non-ideal nature of the boundary conditions gives rise to a "leakage" of hard modes. As an effect of i) and ii), the Casimir force becomes weaker. Since the derivation of this result involves only the localized kinetic terms of a quantum field on parallel surfaces (with codimension one), the derived Casimir force is expected to be present in a variety of setups in arbitrary dimensions.

In the second part of this thesis we investigate a DM model given by a complex scalar field with repulsive, quartic self-interactions and its effect on the structure of galactic halos. Since we consider DM particles with an ultra-light mass, they

can undergo a phase transition to the superfluid phase in the inner high-density regions of a halo, thereby forming a homogeneous core. Taking into account that the gravitational Jeans instability sets an upper limit on the size of such a structure, we discuss the allowed parameter space for a scenario with kpc-size cores. We demonstrate that the parameters get severely constrained by a bound on the self-interaction cross section, obtained from observations of galaxy cluster collisions. Although this constraint is well-known, we show that in the case of ultra-light DM, which occupies a highly degenerate phase space, the bound tightens significantly due to the enhanced interaction rate. As a result, the considered scenario requires an even lighter DM species, and a thermalized core that has fragmented into a collection of smaller superfluid droplets.

Publications

This thesis is based on research that I conducted at the Ludwig-Maximilians-Universität München and that has been published in Refs. [1–3]. In particular, part I of this thesis is based on my work published in

[1] M. Warkentin, "Modification of the laws of gravity in the DGP model by the presence of a second DGP brane", *JHEP* **03** (2020) 015 [1908.01227],

[2] M. Warkentin, "The Casimir effect in the presence of infrared transparency", *JHEP* **05** (2021) 071 [2011.02985].

Part II is rested on research performed in collaboration with Lasha Berezhiani and Giordano Cintia, which was published in

[3] L. Berezhiani, G. Cintia and M. Warkentin, "Core fragmentation in simplest superfluid dark matter scenario", *Phys. Lett. B* **819** (2021) 136422 [2101.08117].

The authors of that paper share the principal authorship and are listed alphabetically as is conventional in high energy physics.

Some parts of the abstract and the introductory chapter 1 contain verbatim passages of the abstracts and introductions of Refs. [1, 2]. Chapters 3 and 4 follow very closely the Refs. [1] and [2], respectively. They are, to a large extent, verbatim reproductions (in text, equations and figures) of the latter, although some material has been modified or expanded. Chapter 6 is based on the collaborative work of Ref. [3] and contains figures as well as equations that are taken from that paper. Appendices B, C and D are also largely extracted verbatim from the appendices of Refs. [1, 2].

Contents

Conventions, Notation, and Units

We use the "mostly minus" metric signature, i.e. the Minkowski metric is given by $\eta_{\mu\nu} = \mathrm{diag}(1, -1, -1, -1)$, and employ the Einstein summation convention.

We further make use of the *reduced Planck mass*, $M_{\mathrm{P}} \equiv (8\pi G)^{-1/2}$, where G is the gravitational constant.

When labeling spacetime coordinates, capital roman and greek letters take values $A \in \{0, 1, 2, 3, 5\}$ and $\mu \in \{0, 1, 2, 3\}$, respectively. Lower-case roman letters are used for spatial coordinates (unless stated otherwise in the text), $i \in \{1, 2, 3\}$.

The abbreviation "c.c." denotes *complex conjugation*.

Finally, we use a subset of the Planck units throughout this thesis where the speed of light, the reduced Planck constant, and the Boltzmann constant are set to unity ($\hbar = c = k_{\mathrm{B}} = 1$).

1

Introduction

1.1 Large Distance Modified Gravity

With the proud age of over a century, Einstein's theory of general relativity (GR) is still the standard theory to describe gravitational phenomena, having passed all experimental tests so far [4–6]. However, most physicists consider it necessary to modify this theory. Indeed, a modification on short distance scales seems reasonable on the grounds that GR, being a classical theory, is incompatible with the presumably more fundamental quantum theory and has to date rejected attempts to be quantized (unless it is treated as an effective quantum field theory valid up to some cutoff energy [7][1]). A modification on large distance scales,[2] on the other hand, is sometimes deemed less well-motivated. Hence, in the following we shall present arguments in favor of such a modification.

One substantial incentive for a large distance modification of gravity has its origin in the supernova survey conducted at the end of the last century [10, 11]. In order to properly put the existing arguments into context, it is worthwhile to examine the situation carefully. Those supernova observations (which were later supported by measurements of the Cosmic Microwave Background anisotropies [12] and baryon acoustic oscillations [13]) indicate that currently the expansion of the universe is accelerating.[3] According to our standard cosmological model [14] (see also e.g. Refs. [15, 16]), also called *ΛCDM model*, the accelerated expansion of the universe can be explained without the need for a modification of gravity if

[1] See also e.g. the reviews [8, 9].

[2] In this thesis we will use the term *large distance* in the context of modified gravity for distance scales greater than the solar system size.

[3] It is accelerating in the sense that $\ddot{a} > 0$, where a is the scale factor and $\dot{()}$ denotes time derivatives. Note that the Hubble parameter H actually decreases, $\dot{H} < 0$, so the actual *rate* of expansion (as measured by H) decreases as well.

one postulates a dominating energy component of the universe that behaves as (positive) vacuum energy ρ_{vac} (and hence has negative pressure) or at least varies slowly enough with time and space to approximate a vacuum energy. In this latter, more general, case it is also called *dark energy* [17, 18] (see also Ref. [19]). The simplest realization of dark energy that is consistent with observations is a vacuum energy, or *cosmological constant* $\Lambda \equiv \rho_{\text{vac}}/M_{\text{P}}^2$. Thus, it is adopted in the standard cosmological model (and features in the name "ΛCDM") that is used to deduce the observational value $\rho_{\text{vac}} \sim 10^{-47}\,\text{GeV}^4$ [20].

Such an explanation for the accelerating expansion of the universe, however, which involves invoking that particular energy content for the universe, has led to a widely recognized puzzle, called *cosmological constant problem* [21]: why is the net (observed) cosmological constant so small compared to the assumed contributions to it, such as the zero-point energy from the Standard Model (SM) quantum fields.[4] Even though this latter contribution is not calculable without an underlying high energy theory, it is considered reasonable that it should be proportional to the fourth power of the cutoff scale, and hence $\rho_{\text{vac}} \sim 10^{72}\,\text{GeV}^4$ if one uses the Planck scale as a cutoff (assuming no new physics between the weak scale and the Planck scale).

Although the cosmological constant problem might be one reason why some physicists seek to explain the accelerated expansion of the universe by modifying gravity at large distances rather than the universe's energy-momentum content, note that the cosmological constant problem is not solved if one merely modifies gravity in such a way that late-time cosmology without a cosmological constant is reproduced. In the absence of a net cosmological constant one would still expect the large quantum corrections and hence an extremely delicate cancellation of all the terms contributing to the vacuum energy (including the bare value). However, there exist modified gravity proposals that show in principle that it might be possible to solve the cosmological constant problem by employing a (zero-mode) graviton that couples very weakly to sources with a large wavelength (such as the spatially constant vacuum energy), so that even a large cosmological constant does not curve space significantly, allowing it to be consistent with observations.[5]

It should also be mentioned that Dvali, demanding the applicability of the S-matrix formulation for quantum gravity and applying consistency requirements, recently argued that the (net) cosmological constant should be identically zero [31, 32] (see also earlier but related work [33–35]).[6] If this were true, it would propel an even greater need to modify gravity at large distance scales.[7]

[4] There are also related puzzles like the "coincidence problem" or the question of why the observed cosmological constant is not exactly zero, but we will not comment on them further.

[5] This class of ideas is called *degravitation* [22–25] and was inspired by the DGP model, which is the central actor of this thesis. Realizing that the original DGP proposal is just on the border of not being able to degravitate the cosmological constant motivated further developments, such as higher-dimensional DGP [26, 27] (see also the earlier work in Ref. [28]) and *cascading gravity* [29, 30].

[6] It is argued that in the limit of a rigid de Sitter spacetime (no back-reactions from particle scattering), the S-matrix for graviton scattering would be trivial for a cosmological constant $\Lambda > 0$.

[7] It should be noted that a number of recent surveys indicates that the isotropy of the universe,

But even setting aside the cosmological constant, the current cosmological model seems to be in tension with observations (see e.g. Ref. [39] for a recent overview). Modifying GR is a widely used approach to alleviate at least some of those tensions. Even if eventually the ΛCDM model should turn out to be capable of explaining all observations, it is crucial to have alternative models to be able to "stress-test" the ΛCDM model or certain aspects of it, like its reliance on GR [40]. Therefore, consistent theories of a modification of GR at large distances are called for.

The previous discussion was intended to point out that it might ultimately be necessary to modify gravity at large distance scales in order to explain the cosmological (especially late-time) evolution. Another, commonly applied motivation for a large distance modification of gravity is the *missing mass problem*. Among the earliest accounts for the existence of such a discrepancy were the observations of orbital motions of galaxies in clusters [41] and gas and stars in galaxies [42, 43] that were not explicable with the baryonic matter inside those structures. Similar to the above-mentioned late-time evolution of the universe, these observations can be attributed to an additional (matter) component in the universe, called *dark matter* (DM), that interacts mostly gravitationally with ordinary matter, which is then also incorporated in the ΛCDM model (where CDM stands for *cold dark matter*). Later, many other observations, e.g. gravitational lensing or various features in the cosmic microwave background radiation, called for a dark component (see e.g. the reviews [44, 45]). Hence, nowadays DM is not just associated with the problem of explaining observations on galactic scales, but is also needed to explain large-scale structures in the cosmological context.

Although a majority of scientists in this field attempts to solve the missing mass problem by invoking such DM, and in particular very often yet undiscovered particles, one can still make a case that a failure to explain large-scale gravitational observations with known physics cries for the need to modify gravity at large distances. Also, recently a growing number of problems (or at least curiosities) with the standard CDM paradigm has been reported, particularly on galactic and subgalactic scales [46] (see section 1.2 for more details).

One of the most famous examples of an alternative to DM that is particularly successful in providing a different explanation for the behavior on galactic scales, avoiding many of the small-scale challenges of CDM, is the *Modified Newtonian Dynamics* (MOND) [47–50] (see also e.g. the review [51]). In this proposal the gravitational acceleration a of objects in galaxies interpolates between two expressions,

$$a = \begin{cases} a_\mathrm{b}\,, & a_\mathrm{b} \gg a_0\,, \\ \sqrt{a_\mathrm{b} a_0}\,, & a_\mathrm{b} \ll a_0\,, \end{cases} \tag{1.1}$$

which is the underpinning of the standard cosmological model, is not yet established securely (see e.g. Refs. [36, 37]). Some authors even doubt the validity of the observation of an accelerated cosmological expansion [38], thereby apparently disposing of the necessity to modify either gravity or the energy-momentum content (of the universe). However, even if future observations would confirm their assertions, the resulting departure from the standard cosmological model does not necessarily reinforce the validity of GR at large distances. In fact, it might even increase the need for its modification.

where $a_{\rm b}$ is the Newtonian acceleration due to baryons (ordinary matter) and $a_0 \simeq 1.2 \times 10^{-8}\,{\rm cm/s^2}$ (see e.g. Ref. [51]).[8] This so-called *Milgrom's law* (or MOND law) works astoundingly well in explaining many of the small-scale puzzles that are challenging for the conventional DM paradigm. Thus, one should not prematurely disregard the possibility that modified gravity is needed to explain the missing mass.

Since the need for DM arises in many different situations and on different scales (not all on which the MOND theory matches the observations satisfactory), it is conceivable that both approaches do not exclude each other. We will provide a particular example in this thesis of how a modification of GR at large distances can help to solve part of the missing mass problem (see section 3.2). Moreover, nowadays it is most common to view Milgrom's law (1.1) as an empirical law and look for DM models that can reproduce the encoded dynamics on galactic scales. The model that we will discuss in the second part of this thesis draws part of its motivation from this very viewpoint (see again section 1.2).

Finally, there are compelling theoretical reasons to study the modification of GR at large distances. At the very least, one can learn a great deal about this theory by attempting to deform it. Since GR is the unique theory of a spin-2 graviton consistent with Poincaré invariance, locality and quantum mechanics, modifying GR at large distances (while leaving these principles intact) introduces new degrees of freedom, and hence turns out to necessarily alter gravity at short distances as well [53–55]. We will illustrate a different example of this interconnection between large and short distance scales in section 3.4 of this thesis. Hence, much of the structure of GR has been understood by trying to modify it.

A particularly fruitful avenue in this regard was the study of massive gravity, since a very natural way to modify gravity at large distances is to give the graviton a mass. This turns the massless messenger that mediates a long-range force, $1/r^2$, to a massive messenger (with mass m) that mediates a Yukawa-type force that falls off exponentially for $r \gtrsim m^{-1}$. As stated before, this modification necessarily introduces additional degrees of freedom. Therefore, letting the graviton mass go to zero does not recover GR but a theory of a massless spin-2, a massless spin-1 and a massless spin-0 particle. This fact is most dramatically apparent in the so-called *vDVZ discontinuity* [56, 57], where a deviation from GR predictions by 25% is obtained in the limit of $m \to 0$, using the linearized gravity theory. However, it can be shown [55, 58] that in the $m \to 0$ limit non-linearities become important and a graviton mass will lead to strong self-interactions of the scalar degree of freedom at short distances, screening the modification of gravity below the so-called *Vainshtein radius*. Besides this classical scale, there is also another distance scale—the ultraviolet (UV) cutoff (or strong coupling scale) of the theory that signals the breakdown of the classical theory and indicates that a more complete quantum theory is required (see e.g. Ref. [59] for a review of this topic). In some massive gravity theories this cutoff is so low (with the associated distance even

[8] One possible way to achieve this behavior is to utilize an additional scalar field that mediates a force on top of the one mediated by the graviton [50] (see also the relativistic extension in Ref. [52], where additionally a vector field is used as a mediator).

larger than the Vainshtein radius) that there is no region where one can trust the classical non-linearities and hence a regime where GR is recovered [60]. But there are also examples where the UV cutoff is high enough so that the screening can be applied in a certain range of distances (see e.g. Refs. [61, 62]).[9]

Despite this immense progress in understanding the modification of gravity, our knowledge is not yet complete, and further surprises about the nature of gravity might lurk around the corner. Much of the development summarized here (and even more of it not mentioned here) was initiated or facilitated by studying a model to which we will turn in the next section. We will also show in the present thesis that the model in question has even more hitherto undiscovered features that could potentially have interesting phenomenological consequences.

1.1.1 The DGP Model

In this thesis we will study a particular model of large distance modified gravity. This model was suggested by Dvali, Gabadadze, and Porrati [64], originally in order to address questions of supersymmetry breaking and the cosmological constant problem,[10] and has been known since as the *DGP model*. Although there have been many proposals to modify gravity (see e.g. the review [68]), the DGP model stands out because it was the first generally covariant, non-linear and ghost-free model of large distance modified gravity. Also, it remains one of the few examples of a calculable, consistent effective theory that modifies spin-2 gravity at large distances while reproducing the predictions of GR at intermediate scales. Moreover, as already alluded to above, it has been an extraordinarily fruitful theoretical laboratory for understanding general features of large distance modified gravity, as e.g. providing the first explicit example where the Vainshtein mechanism was realized [55], or spawning the wide research field devoted to the study of *Galileons* [69].

The DGP model belongs to a class of models, often described as the *brane-world scenario*, that involve extra dimensions (more than four spacetime dimensions) and the idea that certain fields (typically all except the graviton field) are localized on a 3-brane (which is our 3+1-dimensional, observable universe), while the graviton can propagate into the extra dimensions. Extra-dimensional models can be naturally thought of as massive gravity theories, since the dimensional reduction introduces a (typically discrete) tower of massive Kaluza-Klein (KK) modes. In the DGP model, the massive graviton turns out to be a resonance instead of a normalizable zero-mode [66, 70, 71]. However, whereas most of those models modify gravity at short distances, the DGP model modifies it at long distances.

Another attractive feature of that model is the possible quantum origin of its action, more precisely that the 4+1-dimensional (5D) graviton propagator gets quantum corrections from the SM fields, which are localized on the 3-brane and running in the loop, as illustrated in Figure 1.1. That renormalized graviton prop-

[9] In certain theories, like the DGP model, the cutoff scale for fluctuations around non-trivial background configurations can even be raised further, which renders these theories calculable—and consistent with observations—for gravitational processes down to microscopic scales [63] (see also Ref. [53]).

[10] See e.g. Refs. [65–67] for discussions of these matters.

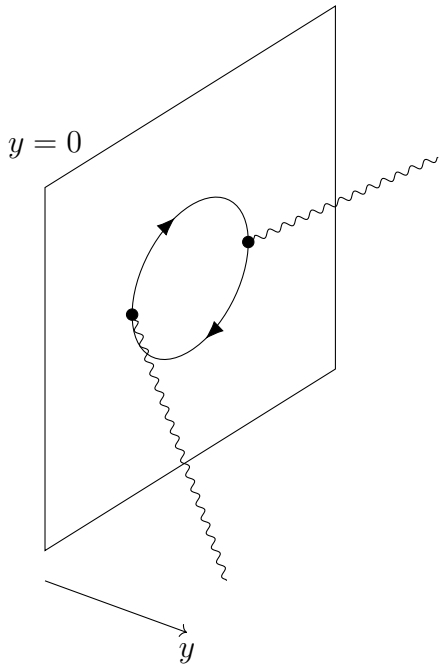

Figure 1.1: The 5D bulk graviton propagator (wavy line) gets renormalized on the brane through loop corrections (solid line), due to the SM fields. The coordinate of the extra dimension is denoted by y.

agator on the brane is then responsible for the seemingly 3+1-dimensional (4D) gravity below a certain length scale.

The action of the DGP model is given by

$$S = M_*^3 \int \mathrm{d}^5X \, \sqrt{G}\mathcal{R}_{(5)} + M_\mathrm{P}^2 \int \mathrm{d}^4x \, \sqrt{|g|}\mathcal{R}_{(4)} \,, \tag{1.2}$$

where M_* is the fundamental (5D) Planck mass, while M_P is the 4D Planck mass, observed in our world.[11] The bulk action contains the bulk metric with its determinant G and the bulk Ricci scalar $\mathcal{R}_{(5)}$, whereas g and $\mathcal{R}_{(4)}$ are the corresponding (localized) quantities on the brane (with the induced metric $g_{\mu\nu}(x^\mu)$ on the brane).

One of the characteristic features of the theory in (1.2) is that the graviton propagates as four-dimensional over length scales smaller than r_c, but changes its behavior to 5D propagation for scales larger than r_c, where the *cross-over scale* (sometimes also called *DGP scale*) is set by

$$r_\mathrm{c} \equiv \frac{M_\mathrm{P}^2}{M_*^3} \,. \tag{1.3}$$

This property is often described as that the graviton is a resonance which decays into a tower of KK modes for large distances. One way to think about this behavior is to note that the brane suppresses hard modes (frequencies larger than r_c^{-1}) of the graviton, while it is transparent to soft modes (frequencies smaller than r_c^{-1}). This

[11] We suppress here the localized matter action and are not careful with correct numerical factors and signs. This will be remedied in section 2.1.

phenomenon, which in fact originated from the DGP model, is called *infrared (IR) transparency*.[12] It has been demonstrated explicitly, using a 4D mode expansion (into KK modes), for the case of a single brane in Refs. [70, 71] (for a compact extra dimension and an infinite extra dimension, respectively).

Let us briefly review the mechanism. The mode functions $\psi_m(y)$ of the KK modes, i.e. the basis functions of the space along the extra dimension with coordinate y, have the form

$$|\psi_m(y=0)| \propto \frac{1}{\sqrt{4+m^2 r_c^2}}$$

on the brane ($y=0$), with m the masses of the KK modes.[13] Hence, the amplitude of the 5D field, which scales as $\propto \psi_m(y)$, is suppressed on the brane and vanishes for KK modes with $m \gg r_c^{-1}$. This affects the potential energy between two static sources (separated by the distance r), which is given by

$$V(r, y=0) \propto -\frac{1}{M_*^3} \int_0^\infty \mathrm{d}m \, |\psi(y=0)|^2 \frac{\mathrm{e}^{-mr}}{r} \,,$$

leading to a 4D gravitational potential ($1/r$) for distances $r \ll r_c$ and a 5D gravitational potential ($1/r^2$) for $r \gg r_c$ (see section 2.3.1 for more details).

Another interesting implication of the localized term in (1.2), that can be traced back to the IR transparency phenomenon, is the following. Since the brane "screens" the 5D gravitational force between two point sources on opposite sides of the brane (separated along the extra dimension), the situation is somewhat analogous to the so-called image problem in classical electrostatics. There, a point charge in the vicinity of a perfectly conducting plate effectively induces a mirror image charge on the opposite side of the plate. In the DGP scenario, the brane effectively introduces a mirror image with a negative mass for a point mass in the brane's vicinity. Therefore, a source interacts non-trivially even with an empty brane: it gets repelled (see also section 2.3.2).

One of the main goals of the present thesis is to demonstrate that this model possesses even more distinctive features, which were not originally intended by the authors. Of course, as we will see, the derived effects are closely tied to the presence of the localized curvature terms, that also play the key role for modifying gravity at large distances, and are related to the properties stated above. We will show that the novel applications, which so far have not been explored, follow from both classical and quantum mechanical considerations and can have implications for various research fields, as we will briefly discuss.

In order to extract those effects, we have to consider a setup with two parallel branes. The intriguing property concerning the analogy to mirror charges, pointed out above, already suggests that the model might show interesting behavior if two

[12] This phenomenon's physical meaning was explained in Ref. [28], where also the term infrared transparency was coined. Later, Ref. [54] showed that any ghost-free, large distance modified gravity theory should exhibit such a phenomenon. Furthermore, this phenomenon has been generalized for massless gauge fields [72].

[13] We will derive the mode functions explicitly for the case of two branes (from where the limit of one brane follows straightforwardly) in section 2.2.2 and appendix B.

such branes were placed next to each other. From the phenomenological side it is crucial to investigate setups with a multitude of branes (more than one brane), since they feature in a number of physical proposals in the literature. One example is brane inflation [73]. In that scenario, inflation in our universe could have been caused by a relative motion of branes. Another example was given in Ref. [74], where it was suggested that (anti-)baryons could be transported to such a parallel brane, leading to a new mechanism of baryogenesis on our brane. In this thesis we will show how the physical implications of the DGP model are modified and what novel signatures appear if there exists a second brane with a localized curvature term. Despite the theoretical interest, this can also provide important new "handles" to experimentally test the DGP model as well as brane-world scenarios with several branes, such as those mentioned above. We discuss these matters in chapter 5.

A first study in that direction was already carried out in Ref. [70]. Since a setup with a single brane and a compact extra dimension is equivalent to a setup with infinitely many branes, Ref. [70] also showed that the phenomenon of IR transparency is independent of the number of branes. We want to note, however, that the system in that paper is nonetheless not equivalent to the system that we will consider in the present work: two parallel branes separated along an *infinite* extra dimension.[14] This fact will be illustrated in chapter 3, where a modification of the gravitational laws as compared to the standard DGP model (containing just a single brane) is demonstrated. For example, we will show that (in the limit of $R \ll r_c$, where R is the separation of the branes) the gravitational potential between two sources on the same brane interpolates between the standard 4D potential $V_{4D}(r)$, for $r \ll \rho$, and $V_{4D}(r)/2$, for $\rho \ll r \ll r_c$. The emergent length scale

$$\rho \equiv \sqrt{R r_c}\,, \tag{1.4}$$

which does not arise in Ref. [70],[15] is essential for understanding the decrease of the gravitational force in this case. Furthermore, we will show in this thesis that the scale ρ also plays an important role for another physical implication—an emerging Casimir force.

In the previously existing literature there have also appeared other works studying the properties of the DGP model by modifying it through the addition of a second brane (see e.g. Refs. [75–77]), but the properties studied in the present thesis have not been discussed yet.

In order to provide a clear presentation and not complicate the necessary calculations, we will study the present setup in the context of a slightly simplified (prototype) model, involving a massless scalar field with a localized kinetic term rather than the massless tensor field. In reality, the richer structure of the gauge theory associated with the full spin-2 model involves additional degrees of freedom,

[14] In fact, in the present thesis we will consider two branes in both an infinite and a compact extra dimension. The latter case, however, will be just a computational tool, and we will send the size of the extra dimension to infinity at the end.

[15] We suspect that the reason for this is that in the setup with the compact dimension, there are infinitely many branes and infinitely many sources that contribute to the gravitational potential between "two" sources, thereby producing a different result.

including the famous *brane bending* mode [61]. Moreover, adding a second brane still increases the complexity, forcing one to take into account the related *radion* excitation [75]. However, after discussing these issues briefly at several places in chapter 2 and in chapter 5, we will argue that, fortunately, they should not alter our results, in the context of the applications that we consider, in any significant way when those results are taken over from the spin-0 to the spin-2 theory. This justifies our simplification.

Before finishing this section and then explaining in detail what we *will* discuss in this thesis, let us make one more remark on what we will *not* elaborate on. One of the most striking properties of the DGP model is its power to provide a mechanism for the accelerated expansion of the universe without the need of adding a cosmological constant [78, 79]. In particular, the DGP model is endowed with two branches for its vacuum solutions, namely the *normal branch* and the *self-accelerating branch*. While the first corresponds to a flat brane in the case of vanishing brane tension (or cosmological constant), the second is associated with a de Sitter brane even for vanishing cosmological constant. There is a vast amount of literature devoted to the subject of the self-accelerating branch and especially the question of its stability and the presence or absence of ghosts (see e.g. Ref. [80] or the review [68] and references therein). However, since these effects are due to the geometrical origin of the DGP model, it is necessary to include the full spectrum of degrees of freedom, and hence analyze the spin-2 theory, in order to capture them.[16] Thus, we will not add anything new to this rich subject in the present thesis.

1.1.2 Further Modification of the Laws of Gravity

We will investigate the gravitational laws of the present setup by calculating the gravitational potential energy between two static point sources localized on the opposite, parallel branes (in chapter 3). Thereby, we will find that the second brane enhances the effects of the DGP model by further weakening the 5D bulk gravity at certain distances. Furthermore, we will discover that the resulting gravitational potential gives rise to a new, (spatially) constant force in our universe that is potentially phenomenologically relevant. In particular, we will show that it is possible (i.e. not experimentally excluded) to choose such parameters r_c and R that there is a region where the gravitational force due to baryonic matter in our galaxy drops while the constant force due to matter on the parallel brane takes over. Hence, the matter on the distant brane would appear to us like "dark matter" without having to satisfy the other constraints that are usually attributed to DM in our universe (like having vanishing interactions with light and with itself). We will discuss how this force could explain the rotation curves in a certain class of galaxies without the need of invoking DM on our brane.

Typically, in the context of extra-dimensional models, the KK language is adopted, where the existence of the (geometrical) extra dimension is traded for

[16] In fact, the addition of a second brane can further increase the richness of this topic [75] (see also e.g. Ref. [76], where a possibility is explored to cancel the ghost in the self-accelerating branch by adding the second brane).

the presence of a tower of KK modes, seen by a 4D observer. Although such a viewpoint is usually used in the case of a compact extra dimension (since in that case one obtains a discrete mass spectrum), in section 3.1 we will also make use of this KK language and rederive our results obtained in the full 5D treatment. In this language, it is especially transparent how a subset of KK modes (belonging to the anti-symmetric mode functions) acts as repulsive gravity, thereby canceling part of the attractive potential and hence weakening the gravitational force. Furthermore, this equivalent viewpoint will serve as a cross-check for our main result.

We will also use the results of this investigation to address another issue that is deeply related to the modification of gravity at the opposite length scales, i.e. short distances. In particular, we wish to address the question what are the implications on the present scenario coming from black hole (BH) physics. For GR, or theories that behave like GR below some distance l_*, it has been shown [81–83] that BH physics (with a BH size smaller than l_*) puts a consistency bound on the short distance cutoff of GR (coupled to quantum fields), namely

$$\Lambda \lesssim \frac{M_{\rm P}}{\sqrt{N}}\,, \tag{1.5}$$

which is valid for a 4D observer, for whom $M_{\rm P}$ is the fundamental Planck scale. Here, Λ is the cutoff, and N is the number of particle species in the theory.[17] The physical meaning of expression (1.5) is that the parameter Λ^{-1} marks the lower bound on the scale of breakdown of semi-classical gravity. For example, the Hawking radiation from a BH of the size smaller than this scale cannot be treated as thermal, even approximately. This is a clear signal that GR requires a UV-completion at distances shorter than Λ^{-1}.

Furthermore, it has been demonstrated in the context of an ADD-type model (the model with *large extra dimensions* due to Arkani-Hamed, Dimopoulos, and Dvali [84]) that various setups with multiple branes, where a BH does not intersect all of the branes, are classically not static [85] (see also Refs. [86–88]). It was shown that there is a classical time scale until which the BH will "accrete" all of the other branes.[18] According to Ref. [85], in the language of species, this can be understood as a "democratization" process for the BH in the following sense: a semi-classical, thermal BH should evaporate into all species "democratically" (up to greybody factors). But as long as the BH does not intersect certain branes, it cannot evaporate into the species localized on them. Thus, the process of brane accretion restores that evaporation universality. In this view, the lack of time-independence in the setup is reflected by the lack of universal evaporation.

However, theories of the form considered in the present work differ from other extra-dimensional models (like the ADD model or the Randall–Sundrum model [89, 90]) in a very important aspect: they modify gravity at large distances, while coinciding with GR at short distance scales. Moreover, as opposed to the above-outlined "accretion" scenario, where the tension of the branes is responsible for the

[17] As can be seen from (1.5), in theories with a large number of species N, the maximal cutoff can be significantly lower than the Planck scale.

[18] In case the time scale is larger than the evaporation time, the BH will evaporate first.

attraction between the BH and the branes, in our setup the branes are tensionless. Nevertheless, we will show that there would be repulsion between a BH and the branes. We can, however, switch off that interaction by sending the distance between the branes to infinity. This is not possible in the ADD model because in that case we would need to send the compactification radius to infinity as well, which would make 4D gravity vanish. So how does our scenario fit into the aforementioned species picture? And what information do we receive from BH physics? We shall address these issues in section 3.4 and explore the implications for the bound on the number of species. This investigation beautifully illustrates how in gravity large distance scales are intricately connected to short distance physics, as we already alluded to in section 1.1.

1.1.3 Rise of the Casimir Force

The modified setup of two parallel DGP branes does not only give rise to a new gravitational law. It also reveals interesting quantum mechanical behavior. In particular, we will investigate the emergence of a Casimir effect in this scenario.

The fact that UV modes are being suppressed by the branes and the previously mentioned observation of the mirror images already indicate that the DGP model can provide a kind of "gravitational wave mirror". However, since the IR transparency phenomenon entails that the light modes are transparent, we expect that the explicit form of the Casimir force between two surfaces [91], if it arises, should be affected.

Our first goal of this investigation is to demonstrate that the Casimir effect can be derived at all, even in the absence of ideal boundary conditions (such as Dirichlet boundary conditions). Instead, we want to show that the DGP model comprises "effective" boundary conditions for the gravitational field.

Usually, it is questionable to consider the "gravitational Casimir effect", since boundary conditions for the gravitational field are not physical. In contrast to the electromagnetic field, that can be taken to vanish on perfect conducting plates (leading to the standard Casimir effect), gravity interacts very weakly with any material, which makes it difficult to realize a "gravitational wave mirror". However, as we intended to motivate above, the DGP model naturally provides such a setup that does not rely on ad hoc boundary conditions or speculative quantum gravity effects, as for example the proposal in Ref. [92]. Naturally, if such a Casimir effect exists for gravitons, its observation would be a strong indication for the quantum origin of the gravitational field, since the Casimir energy is due to vacuum fluctuations of the underlying quantum field.

Our second goal is to show that there are deviations from the standard result (i.e. the Casimir force for two perfectly conducting plates) due to the fact that the branes are transparent to the IR modes. In particular, we will show that there are two contributing (and opposite) effects. On the one hand, the presence of an IR region, where the soft modes do not "see" the branes, strengthens the Casimir force because those modes are removed from the discrete spectrum. On the other hand, the DGP branes provide only effective boundary conditions, so even the hard modes, those that are close to r_{c}^{-1}, "leak" out of the interior enclosed

by the two branes. We illustrate this by first considering a toy model where the soft modes are simply removed from the spectrum (see section 4.2.1) and then comparing to the case where the effective nature of the boundary conditions is restored (see section 4.2.2). This emergent Casimir force, and its deviation from the standard form, is another signature of the distinctive features of the DGP model. Hence, besides its theoretical importance, it can lead to new ways of experimentally probing the DGP model. Furthermore, an additional force between two branes, in the presence of localized kinetic terms, can have important implications for many brane-world scenarios, such as the brane inflation scenario [73] mentioned above, where the precise form of the attractive potential between the branes, driving inflation, is crucial.

Finally, let us stress that this effect is rather generic. As stated before, to derive our results we will use a prototype model that only involves a quantum scalar field with a localized kinetic term on a lower-dimensional surface. As we will explain in the beginning of chapter 4 (see also chapter 5), we expect that the results for bosonic fields with spins higher than zero will not change, except for numerical factors accounting for the additional degrees of freedom. Also, we will see that the qualitative result does not depend on whether we consider a 2D or a 5D system, as long as we are dealing with codimension-one branes. Therefore, such a Casimir effect would arise in a number of setups, including parallel two-dimensional surfaces in our 4D world. In fact, the feature of IR transparency exists for many surfaces, such as ordinary walls that act as dielectrics for the electromagnetic field. They are transparent to radio waves, but suppress waves with higher frequencies (since the effective kinetic terms of the photons are different in the vacuum and inside the wall).[19] Hence, this effect can be probed and investigated in any experiment where such surfaces are present.

It should be mentioned that delta-function potentials, as the localized curvature terms can be viewed, have been investigated in the literature on the Casimir effect for around 30 years (where they often go by the name of *semi-transparent potentials*), and it has been found that they lead to a modification of the Casimir effect.[20] The first paper that treated delta-function potentials in 3+1 dimensions was Ref. [94]. Later, Ref. [95] (see also Ref. [96] for further discussion) included such potentials in 1+1 dimensions, and Ref. [97] further clarified the situation in 3+1 dimensions (see also Refs. [98, 99] for additional results and an elucidating discussion concerning delta-function potentials in both 1+1 and 3+1 dimensions). However, in those papers delta-function potentials are coupled to the fields, rather than to their derivatives. Consequently, the resulting Casimir force, although different from the standard result (i.e. in the case of Dirichlet boundary conditions), is not equal to the one derived in the present work. Even though those delta-function potentials have been studied extensively since then, to the best of our knowledge,

[19] Note that this is reminiscent of the so-called *Dvali-Shifman mechanism*, proposed in Ref. [93], where the brane can also be considered a dielectric, while the bulk is a dual superconductor. In that case, the massless gauge field can actually be exactly localized on a brane because in that scenario the bulk is confining and hence does not allow the massless gauge field to escape there.

[20] Although, unfortunately, we were not aware of such work until the research that we published in Ref. [2] was completed.

the particular setup with derivative couplings, addressed in this work, (that is crucial for the aforementioned IR transparency phenomenon and hence the distinctive modified gravity behavior) has not yet been studied in the literature. Moreover, in the examples known to us, the derived Casimir force does not have a modified functional behavior, as we find in the present thesis, but just a modified overall strength.

As in the case of the calculation of the gravitational potential (see section 3.1.2), we will perform the calculation in the KK language. We will see that the masses of the KK modes get quantized in a specific way and discover how this mass quantization is eventually responsible for the Casimir force. Therefore, in this language the emergence of the Casimir force becomes quite transparent.

1.2 Dark Matter Superfluidity

In the second part of this thesis we discuss a DM model that does not originate from the modification of the structure of spacetime, but rather whose characteristic feature is to allow a phase transition to a Bose-Einstein condensate inside of galaxies in the 4D world. A model of that kind is given by

$$S = \int \mathrm{d}^4x \left(|\partial_\mu \Phi|^2 - m^2 |\Phi|^2 - \frac{\lambda}{2} |\Phi|^4 \right), \tag{1.6}$$

where a complex scalar field Φ with mass m exhibits quartic self-interactions with the coupling constant $\lambda > 0$. Even though this particular model has certainly been studied for a very long time, in all possible contexts, it can also be considered to belong to a subclass of DM models that have been proposed quite recently and which are dubbed *theory of DM superfluidity* [100–102] (for a recent set of lecture notes see Ref. [103]).[21] Although the theory of DM superfluidity—or rather the theory of a *certain kind* of superfluid [100]—approaches the missing mass problem by postulating a DM substance, it is still motivated by the observation that, effectively, gravitational dynamics are modified on galactic scales, and it attempts to explain the MOND empirical law (1.1). Hence, this theory provides an interesting example of a model that, even without modifying gravity, effectively changes Newton's law.[22]

[21] Note that the term "superfluidity" actually refers to the property of certain fluids that, due to their phonon excitations, a disturber traveling through it does not exhibit any friction if its velocity is below the fluid's sound speed. In this thesis we are not concerned with this frictionless motion but the capability of such fluids to form Bose-Einstein condensates and balance the gravitational attraction with the repulsive self-interaction. However, a substance that possesses such a capability also exhibits frictionlessness. Furthermore, in the existing literature the term "DM superfluid" is often used to distinguish the type of model where the phonon excitations play the relevant role from models that also allow for a Bose-Einstein condensation but where such collective excitations are absent. We will conform to such a terminology in this thesis.

[22] Although this is reminiscent of a scalar-tensor theory viewed in the Einstein frame (see e.g. Ref. [104] for an overview), it is in fact distinct from that. One major difference is that in the theory of superfluid DM the *same* degree of freedom that constitutes the more conventional DM is also responsible for an additional long-range force between baryons in a certain regime.

The theory of DM superfluidity can be thought of as itself being a subclass of the so-called *ultra-light DM models* (see e.g. Ref. [105] for a recent review), which have attracted much attention recently. One of their characteristic features is that they involve very light DM particles ($10^{-24}\,\mathrm{eV} < m < \mathrm{eV}$), which behave effectively as non-interacting, pressure-less DM on larger-than-galactic scales, while forming a condensate on smaller scales (giving rise to collective behavior). Thus, on cosmological scales ultra-light DM models reproduce the successful properties of the well-established DM models that belong to the CDM paradigm, where the DM is a perfect fluid that consists of non-relativistic, very weakly interacting (or non-interacting) particles. However, as mentioned previously (see section 1.1), for more than a decade this paradigm has been challenged by the appearance of discrepancies, often called *small-scale challenges* (see e.g. Refs. [39, 40, 46, 105]).

One of these discrepancies is the so-called *cusp-core problem*. N-body simulations of CDM suggest that the DM density distribution is given by the Navarro-Frank-White (NFW) profile [106],[23]

$$\rho_{\mathrm{NFW}}(r) = \frac{\rho_{\mathrm{c}}}{\frac{r}{r_{\mathrm{s}}}\left(1+\frac{r}{r_{\mathrm{s}}}\right)^2}\,, \tag{1.7}$$

where the characteristic density ρ_{c} and the scale radius r_{s} are phenomenological parameters that vary from halo to halo, but (according to numerical simulations) exhibit a tight relation, known as the mass-concentration relation (see e.g. Ref. [108]).[24] Whereas the profile (1.7) diverges in the central region (leading to a cusp), this is not supported by observations (mostly of low surface brightness (LSB) galaxies), which rather suggest that the central region looks like a (nearly flat) core. Other small-scale challenges include the *missing satellites problem*, where the number of subhalos in the Milky Way and other galaxies of the Local Group is much lower than predicted by simulations (in the CDM framework), and the *too big to fail problem*, which states that the most massive subhalos predicted by the aforementioned simulations should be able to host stars but apparently fail to do so. Furthermore, one of the most intriguing puzzles is the observation of several scaling relations, like the *radial acceleration relation* [109, 110] (that is closely related to the so-called *mass discrepancy acceleration relation* [111] and constitutes a generalization of the baryonic Tully-Fisher relation [112–114]—which is itself an extension of the well-known Tully-Fisher relation [115]). This relation suggests that the observed gravitational acceleration (which is due to both DM and baryonic matter) in a very large and diverse class of galaxies (including dwarf galaxies that are DM dominated) is very tightly related to the total baryonic mass (stars and gas) in those galaxies.

To explain this last-mentioned observation is one of the trademark successes of the MOND paradigm, and hence it is also successfully addressed by the DM super-

[23] Note, however, that several other density profiles have been suggested in the literature and claimed to describe certain types of galaxies even better than the NFW profile (see e.g. Ref. [107]).

[24] The parameter $c = R_{\mathrm{V}}/r_{\mathrm{s}}$ (where R_{V} is the virial radius) is known as the concentration parameter, whereas ρ_{c} depends on the halo mass if one integrates (1.7) up to the virial radius. Hence, the correlation between mass and concentration reflects the correlation between ρ_{c} and r_{s}.

fluidity model, which is designed to agree with the latter. The way to achieve this is to couple the Goldstone mode that is present in the superfluidity models to the baryons with a very particular coupling constant. Then, for large distances (beyond galactic scales) the substance behaves like ordinary CDM, while for galactic and sub-galactic scales the MOND phenomenology is recovered. The superfluidity models also address the cusp-core problem and another possible tension that we have not mentioned yet: the dynamical friction in some galaxies, derived in the CDM framework, might be too high to match observations (see e.g. Refs. [105, 116–119]).

Nevertheless, in the present thesis we will focus on the cusp-core problem. Therefore, we do not need to consider the more involved model of Refs. [100–102], but can work with the simplest DM superfluidity model given by (1.6), which in fact has been employed for this purpose long before the advent of its more intricate incarnation.[25] Thus, let us use the remainder of this section for a very brief historic overview and to explain how that model serves its purpose.

Among the earliest attempts to explain the observations of a "missing mass" were to postulate particles that interact with baryonic matter and with themselves mostly gravitationally. A majority of those models uses non-self-interacting particles. However, as mentioned before, such models lead to problematic predictions regarding the halo cores. Therefore, a possible "cure" is to consider self-interacting models [120, 121], which also improve the predictions on the abundance of dwarf galaxies. This approach has the appealing feature that DM behaves collisionless on larger scales, where the densities are low, but has a more favorable distribution in central, high-density regions.

A particular model that involves repulsive self-interactions, in addition to a sufficiently low DM particle mass, such that DM can undergo a phase transition to a Bose-Einstein condensate in the interior of galaxies, was considered in Ref. [122] and later slightly generalized in Ref. [123] (to include a complex rather than real scalar field). That model was exactly the model in (1.6). Unlike the aforementioned self-interacting scenarios, where the DM particle mass is rather high (of order GeV), this model possesses the useful feature of suppressed dynamical friction because it gives rise to a superfluid that can help to suppress dissipation in high-density, inner galactic regions. Even though this scenario has been claimed to be excluded on observational grounds in Ref. [123], in the latter work the rather drastic assumption has been employed that the whole galaxy is in thermal equilibrium (see also Ref. [124] for a more recent and improved discussion of that scenario).

Several related scenarios involving an ultra-light DM particle have been considered in the existing literature. Ref. [125] (see also Ref. [126]) has shown that in the presence of attractive interactions (gravitational or self-interactions) the superfluid core is prone to fragmentation unless the DM particles are extremely light, such that the "quantum pressure" (due to the Heisenberg uncertainty principle) dominates.[26] This latter principle is employed in the *Fuzzy Dark Matter* scenario [128]

[25] Of course, it is reasonable to assume that the cusp-core problem is related to at least some of the other puzzles (like the dynamical friction, which is sensitive to the DM density profile in the core), and hence this model could offer solutions to them as well.

[26] Models with axion-like particles (see e.g. the review [127]), having an attractive self-interaction, belong to this category.

(see also Refs. [118, 129] for a detailed phenomenological study of this model), with a particle mass of order $10^{-22}\,\mathrm{eV}$.

In the present thesis (in chapter 6) we will revisit the model (1.6) and analyze its observational viability, investigating a scenario where the galaxy is not completely in thermal equilibrium.[27] In particular, we will discuss the stability of the emerging superfluid core against perturbations and explore the constraints on this scenario, taking into account bounds from the gravitational (Jeans) instability and from the upper limit on the self-interaction strength. In the previously existing literature, such an upper limit has frequently been derived from the so-called *Bullet Cluster constraint* and widely applied to DM models, including the ones with ultra-light DM particles. We will argue that this bound has to be modified in this latter case because the DM particles occupy a highly degenerate phase space, which leads to an enhanced interaction rate. Applying this new bound properly, we will demonstrate that the outlined superfluid DM scenario is capable of producing a flat, thermalized galactic core, provided that the superfluid core breaks into droplets. For their size to be of order kiloparsec, the DM mass has to satisfy $m \lesssim 10^{-17}\,\mathrm{eV}$.

1.3 Outline

The contents of this thesis is organized as follows. The first part (Part I) deals with large distance modified gravity, in particular the DGP model. Chapter 2 contains both a review of the standard DGP model (with a single brane), including the derivation of the 4D metric perturbation (section 2.1.1), as well as the gravitational force law on the brane (section 2.1.2), and original material, setting up the investigation of the double-brane DGP model. The latter includes a derivation of the propagator in section 2.2.1 and the translation to the KK language in section 2.2.2. This chapter also discusses the well-known concept of the graviton resonance (section 2.3.1) and the potentially slightly less-known mechanism of "mirror images" in the DGP model (section 2.3.2).

In the ensuing chapter 3 we study the classical effects of the modified DGP system with two branes. For this, we derive the gravitational potential energy both in the 5D description (section 3.1.1) and using the KK decomposition (section 3.1.2). We then use the novel force law to discuss a possible application in DM phenomenology in section 3.2. Next, we show how the system behaves for large brane separations (section 3.3) and then make use of this behavior in the discussion about the cutoff of semi-classical gravity in the presence of a large number of particle species (section 3.4). We conclude that chapter with a summary in section 3.5.

The next chapter 4 deals with a quantum mechanical consequence of the present setup in the form of the Casimir effect. First, in section 4.1, we quantize the system and explain how to regularize and renormalize the vacuum energy within the dimensionally reduced description, showing how a discrete spectrum of modes arises. Then, we set out to derive the Casimir effect. We start with a derivation in

[27] In the context of the more involved theory of DM superfluidity such a scenario has already been discussed in Ref. [102].

1+1 dimensions, since some of the analytical expressions can only be obtained in this simplified system. For this, we discuss the effect of the IR transparency region on the Casimir force (section 4.2.1) and explain how the effective nature of the boundary conditions, provided by the DGP branes, further modifies the final result (section 4.2.2). This is done by deriving approximate analytical expressions. The result is then further justified and refined by a numerical analysis in section 4.2.3. In section 4.3 we finally treat the 5D system, obtaining most of the results numerically. We then summarize and discuss our findings in section 4.4.

The research reported on in Part I of the present thesis is summarized and concluded in chapter 5, where we also discuss the experimental viability of the DGP model, the implications of our results, and the possible extensions of our work.

In the second part (Part II) of this thesis, we study superfluid DM (chapter 6). We start with a review of the particular model, including the derivation of the DM density distribution in the presence of gravity (section 6.1). Then, we discuss several possibilities of how the formation of superfluid cores in galaxies and clusters can proceed (section 6.2). The next section 6.3 contains the derivation of the modified Bullet Cluster bound on the DM interaction strength in the case of highly degenerate, ultra-light particles. We conclude this investigation with the analysis and display of the full parameter space of the present scenario (section 6.4) and a discussion of the results (section 6.5).

Some additional and more detailed material, which is vital for the investigation of the DGP model in Part I, is delegated to the appendix, starting with the discussion of the propagator for arbitrary (and not just stationary) sources (in appendix A). The actual calculation of the mode functions, necessary for the KK description, and derivation of the mass quantization equation is performed in appendix B. Various additional numerical cross-checks on the validity of the approximate solution of the modified force law can be found in appendix C. Finally, appendix D contains the evaluation of a particular Bessel function sum that is crucial for the analytical calculation of the 5D Casimir energy in the limit $r_c \to \infty$.

Part I

Modified Gravity

2

Fundamentals of the DGP Model With One and Two Branes

In this chapter we shall derive and collect basic results in the DGP framework that we will use in subsequent chapters. In the first section we will review the original DGP model in some depth. However, since the literature on the DGP model has grown immensely in the past two decades (see e.g. just the more theoretically focused Refs. [22, 25–29, 53, 55, 59, 61, 63, 64, 66, 70, 71, 75–79, 130–137] and many more), it is beyond the scope of this thesis to discuss the model (and its *decoupling limit*) exhaustively. Also, as we will explain below, the results derived in this thesis all follow from very basic features of the DGP model, which are even present if the graviton (spin-2 particle) would be replaced by a scalar (spin-0 particle). Since we then do not require the mastery of all the intricacies of the DGP model, it would be misplaced to discuss the latter in this thesis. In particular, we will not discuss the issue of the brane bending mode (or radion stabilization), since this is a feature of the gauge theory of a spin-2 particle, not of the spin-0 particle. Rather, we will mostly focus on the graviton propagator and the properties of the gravitational potential between two static sources in the DGP model.

On the other hand, we will derive some (to the best of our knowledge) new expressions for the propagator and the fields in the presence of a second DGP brane. The second section of this chapter is devoted to these derivations. Furthermore, it will be useful to discuss both the 5D language and the dimensionally reduced KK formulation, so we will derive and compare various expressions in both languages. This too is allocated to the second section.

We conclude this chapter with a section on the phenomenon of infrared transparency, which is a key feature of the DGP model, related to most of its salient properties.

Note that a major part of section 2.2.2 is a verbatim reproduction of Refs. [1, 2],

and a minor part of section 2.3.2 uses verbatim material from Ref. [1].

2.1 Spin-2 Field With One Brane

Let us begin with the review of the DGP model in the presence of a single 3-brane, which was the setup introduced originally in Ref. [64]. The action is given by[1]

$$S = -\frac{M_*^3}{2}\int \mathrm{d}^5X\,\sqrt{G}\mathcal{R}_{(5)} - \frac{M_{\mathrm{P}}^2}{2}\int \mathrm{d}^4x\,\sqrt{|g|}\mathcal{R}_{(4)}\,. \tag{2.1}$$

The 5D coordinates are denoted by X^A. To work with the theory (2.1), a convenient foliation is chosen: the 5D bulk is foliated with 4D (timelike) hypersurfaces with constant y, where the 3-brane (i.e. the 3+1-dimensional brane that constitutes "our" universe) is the hypersurface at $y = 0$.[2] The coordinates on those hypersurfaces are given by x^μ. Thus, the coordinates in the chosen foliation read $X^A \doteq (x^\mu, y)$. The bulk metric in these coordinates is denoted $G_{AB}(x^\mu, y)$, and the (5D) Ricci scalar is given by $\mathcal{R}_{(5)}$. Hence, the first term in (2.1) is the usual (5D) Einstein-Hilbert action, where M_* is the fundamental (i.e. five-dimensional) Planck mass. The basis vectors respecting this foliation are given by

$$Y^A \equiv \left.\frac{\partial X^A}{\partial y}\right|_{x^\mu=\mathrm{const}} \quad \text{and} \quad e^A_\mu \equiv \left.\frac{\partial X^A}{\partial x^\mu}\right|_{y=\mathrm{const}}\,.$$

To further specify the foliation, we could fix the "lapse" and "shift" functions of the y-coordinate, i.e. specify how the vector Y^A is oriented with respect to the normal vector l^A (that is orthogonal to the hypersurfaces). Although we can choose the lapse and shift functions arbitrarily (see e.g. Ref. [138]), we will keep the lapse function undetermined for the moment, in order to have more gauge freedom, which we want to use for simplifications later. Then, the simplest choice is to take $Y^A \propto l^A$, thereby setting the shift function to zero. With this choice, the metric takes the form

$$G_{AB} = \begin{pmatrix} \widetilde{g}_{\mu\nu} & 0 \\ 0 & -N^2 \end{pmatrix},$$

where N is the lapse function and $\widetilde{g}_{\mu\nu}$ is the induced metric, satisfying

$$\widetilde{g}_{\mu\nu} = G_{AB}e^A_\mu e^B_\nu\,.$$

The metric determinants are related via

$$\sqrt{G} = \sqrt{|\widetilde{g}|}N\,. \tag{2.2}$$

[1] Notice that we choose here a slightly different convention than for the action (1.2), in light of the anticipated inclusion of the matter sector.

[2] Note that by choosing this foliation, the position of the brane is fixed (in this coordinate system). In other words, we reduce some of the gauge redundancy associated with the bulk diffeomorphism invariance by choosing a gauge where the brane is located at $y = 0$ (see Ref. [61] or e.g. Ref. [59] for more details). In this gauge (or coordinate system), the brane breaks the translational invariance.

From the point of view of the 4D observer on the $(y = 0)$-hypersurface,

$$g_{\mu\nu}(x^\mu) \equiv \tilde{g}_{\mu\nu}(x^\mu, y = 0)$$

is just "our" 4D spacetime metric. Hence, the second term in (2.1) is the 4D Einstein-Hilbert action (with the 4D Ricci scalar $\mathcal{R}_{(4)}$), which is added to the theory. Note that in this model the associated Planck mass $M_{\rm P}$ is the one observed in our world and in general independent of M_*.

Of course, (2.1) should be supplemented with the corresponding action for all the other fields in the theory. In particular, if one views the 4D Einstein-Hilbert action as induced by quantum corrections, one has to add the worldvolume theory (i.e. the SM fields and possibly additional fields from physics beyond the SM, localized on the 3-brane) that leads to those quantum corrections. We will specify those additional actions when they are needed.

Note that we do not include a tension (which the brane localizing the non-gravitational fields could in general possess) to the 4D worldvolume theory, following the original proposal. One possible reason for that would be that the induced (by quantum corrections) vacuum energy cancels it. For the most part, we will not enter into this discussion in the present thesis. However, we will provide additional comments on this issue in chapter 5.

2.1.1 Four-Dimensional Metric Perturbation

Equations of Motion

We now want to find the equations of motion for the metric (i.e. the Einstein field equations), in the presence of some localized fields on the 3-brane. Mostly, we follow here the original derivation in Ref. [64] (but see also e.g. Refs. [59, 137]). We can write the appropriate action as

$$S = -\frac{M_*^3}{2}\int \mathrm{d}^5X\,\sqrt{G}\mathcal{R}_{(5)} + \int \mathrm{d}^4x\,\mathrm{d}y\,\sqrt{|g|}\delta(y)\left(-\frac{M_{\rm P}^2}{2}\mathcal{R}_{(4)} + \mathcal{L}_{\rm SM}\right), \tag{2.3}$$

where $\mathcal{L}_{\rm SM}$ includes all the non-gravitational fields on the worldvolume (although we choose to call them SM fields, the Lagrangian could be more general).

Varying (2.3) with respect to the metric leads to

$$\delta S = -\frac{M_*^3}{2}\int \mathrm{d}^5X\,\sqrt{G}\mathcal{G}^{(5)}_{AB}\delta G^{AB} + \frac{1}{2}\int \mathrm{d}^4x\,\mathrm{d}y\,\sqrt{|g|}\delta(y)\Big(-M_{\rm P}^2\mathcal{G}^{(4)}_{\mu\nu} + T_{\mu\nu}\Big)\delta g^{\mu\nu}\,, \tag{2.4}$$

where

$$\mathcal{G}^{(5)}_{AB} = \mathcal{R}^{(5)}_{AB} - \frac{1}{2}\mathcal{R}_{(5)}G_{AB} \quad \text{and} \quad \mathcal{G}^{(4)}_{\mu\nu} = \mathcal{R}^{(4)}_{\mu\nu} - \frac{1}{2}\mathcal{R}_{(4)}g_{\mu\nu}$$

denote the 5D and 4D Einstein tensor, respectively, and

$$T_{\mu\nu} \equiv 2\frac{\partial\mathcal{L}_{\rm SM}}{\partial g^{\mu\nu}} - g_{\mu\nu}\mathcal{L}_{\rm SM}$$

is the worldvolume energy-momentum tensor.[3] The integrand in the second term of (2.4) can be written as (keeping in mind the present delta-function)

$$\begin{aligned}\Big(-M_{\rm P}^2\mathcal{G}^{(4)}_{\mu\nu}+T_{\mu\nu}\Big)\delta\widetilde{g}^{\mu\nu} &= \Big(M_{\rm P}^2\mathcal{G}^{\mu\nu}_{(4)}-T^{\mu\nu}\Big)\delta\widetilde{g}_{\mu\nu}\,,\\ &= \Big(M_{\rm P}^2\mathcal{G}^{\mu\nu}_{(4)}-T^{\mu\nu}\Big)\delta\Big(G_{AB}e^A_\mu e^B_\nu\Big)\,,\\ &= \Big(-M_{\rm P}^2\mathcal{G}^{(4)}_{AB}+T_{AB}\Big)\delta G^{AB}\,,\end{aligned}$$

where in the last line we made use of the fact that the basis vectors e^A_μ are not affected by the variation (since they only depend on the chosen foliation) and wrote the "transverse" tensors (having no component orthogonal to the 3-brane) in the 5D coordinates. Since in our 4+1 coordinate system (x^μ, y) we have $e^A_\mu \doteq \delta^A_\mu$, we can also write

$$\Big(-M_{\rm P}^2\mathcal{G}^{AB}_{(4)}+T^{AB}\Big)\equiv\Big(-M_{\rm P}^2\mathcal{G}^{\mu\nu}_{(4)}+T^{\mu\nu}\Big)e^A_\mu e^B_\nu \doteq \Big(-M_{\rm P}^2\mathcal{G}^{\mu\nu}_{(4)}+T^{\mu\nu}\Big)\delta^A_\mu\delta^B_\nu\,.$$

Then, the Einstein field equations read

$$M_*^3\mathcal{G}^{(5)}_{AB}N=\delta(y)\Big(-M_{\rm P}^2\mathcal{G}^{(4)}_{\mu\nu}+T_{\mu\nu}\Big)\delta^\mu_A\delta^\nu_B\,, \tag{2.5}$$

where we also made use of (2.2).[4]

Linearized Theory

Since we are interested in the linearized theory, we expand (2.5) around Minkowski spacetime, using

$$G_{AB}=\eta_{AB}+h_{AB}\,, \tag{2.6}$$

where h_{AB} is the 5D metric perturbation. Up to first order in h_{AB}, the Einstein tensor, in any dimension D, reads

$$\mathcal{G}^{(D)}_{ab}=\frac{1}{2}\Big[\partial_b\partial_c h^c_a+\partial_a\partial_c h^c_b-\partial_a\partial_b h^{(D)}-\Box_{(D)}h_{ab}-\eta_{ab}\Big(\partial_c\partial_d h^{cd}-\Box_{(D)}h^{(D)}\Big)\Big]\,, \tag{2.7}$$

where

$$h^{(D)}\equiv h^a_a\,,\quad \Box_{(D)}\equiv\partial_a\partial^a\,,$$

are the D-dimensional trace of h_{ab} and the D-dimensional d'Alembertian, respectively, and the indices take values in D spacetime dimensions. The general coordinate transformation invariance of the full (5D) theory translates to the gauge redundancy

$$h_{AB}\to h_{AB}+\partial_A\xi_B+\partial_B\xi_A \tag{2.8}$$

[3] We dropped here the part of the variation that can be expressed as a variation of quantities on the spacetime boundary. Note that since these quantities involve derivatives of the metric, one has to include Gibbons-Hawking-York boundary terms to obtain a well-posed variational principle (see e.g. Ref. [138]). We will assume that those boundary terms are present and not enter into these subtleties here.

[4] The factor N on the left-hand side of (2.5) will become unity, to leading order in h_{AB}, once we go to the linearized theory, using (2.6), since $N\simeq 1-\frac{1}{2}h_{yy}$.

of the linearized theory, where $\xi^A(X^A)$ can have an arbitrary coordinate dependence. The transformation (2.8) implies

$$h_{\mu\nu} \to h_{\mu\nu} + \partial_\mu \xi_\nu + \partial_\nu \xi_\mu \tag{2.9}$$

for the 4D metric perturbation. It is easy to check that (2.7) is invariant under (2.8) in $D = 5$ and under (2.9) in $D = 4$. Hence, as expected, the equations of motion (2.5) are invariant under the gauge transformation (2.8) (see also footnote 4). We can use this redundancy to transform to the de Donder gauge[5]

$$\partial_B h^{AB} - \frac{1}{2}\partial^A h^{(5)} = 0\,, \tag{2.10}$$

in which the 5D Einstein tensor reduces to

$$\mathcal{G}^{(5)}_{AB} = -\frac{1}{2}\Box_{(5)}\Big(h_{AB} - \frac{1}{2}\eta_{AB}h^{(5)}\Big)\,.$$

Notice that since $h^{(5)} = h - h_{yy}$, where we defined

$$h \equiv \eta^{\mu\nu}h_{\mu\nu}\,, \tag{2.11}$$

the gauge fixing condition (2.10) implies

$$\partial_\nu h^{\mu\nu} - \frac{1}{2}\partial^\mu h = -\Big(\partial_y h^{\mu y} + \frac{1}{2}\partial^\mu h_{yy}\Big)$$

for the 4D metric perturbation. Hence, the 4D Einstein tensor takes the more cumbersome form

$$\begin{aligned}\mathcal{G}^{(4)}_{\alpha\beta} = &-\frac{1}{2}\Box\Big(h_{\alpha\beta} - \frac{1}{2}\eta_{\alpha\beta}h\Big)\\ &-\frac{1}{2}\Big[\partial_\alpha\partial_y h^y_\beta + \partial_\beta\partial_y h^y_\alpha + \partial_\alpha\partial_\beta h_{yy} - \eta_{\alpha\beta}\Big(\partial_\mu\partial_y h^{\mu y} + \frac{1}{2}\Box h_{yy}\Big)\Big]\,,\end{aligned} \tag{2.12}$$

where

$$\Box \equiv \Box_{(4)}\,.$$

Since in the present DGP setup all of the energy-momentum that sources gravity is localized on the 3-brane (the right-hand side of (2.5) vanishes for $A \neq \alpha$ and/or $B \neq \beta$), the αy- and yy-components lead to the equations

$$\begin{aligned}\Box_{(5)}h_{\mu y} &= 0\,,\\ \Box_{(5)}(h_{yy} + h) &= 0\,.\end{aligned}$$

Thus, we can find the solutions[6]

$$h_{\mu y} = 0 \quad \text{and} \quad h_{yy} = -h\,.$$

[5]Note that we have already fixed some part of the gauge above. In particular, we set the shift function to zero, and hence $h_{\mu y} = 0$. Thus, one has to check if this is consistent with the de Donder gauge choice. We will do that by keeping $h_{\mu y}$ arbitrary for the moment and see later that it can indeed be set to zero.

[6]Note that this is, of course, not the most general solution, unless we specify some special boundary conditions. In fact, a more careful analysis, and not choosing this particular solution, would reveal that h_{yy} is associated with the so-called *brane bending mode*, which is responsible for shifting the brane in the presence of matter (see e.g. Refs. [59, 61, 75, 137]). However, for our purposes we do not have to go into these subtleties.

Using these, (2.12) simplifies to

$$\mathcal{G}^{(4)}_{\alpha\beta} = -\frac{1}{2}(\Box h_{\alpha\beta} - \partial_\alpha\partial_\beta h)\,,$$

and hence the (inhomogeneous) Einstein field equations (2.5) read

$$M_*^3\Box_{(5)}(h_{\mu\nu} - \eta_{\mu\nu}h) = -\delta(y)\Big[M_{\rm P}^2(\Box h_{\mu\nu} - \partial_\mu\partial_\nu h) + 2T_{\mu\nu}\Big]\,. \tag{2.13}$$

Going to momentum space (with respect to the worldvolume coordinates), this equation can be expressed as[7]

$$\begin{aligned} &M_*^3\Big(\overline{h}_{\mu\nu}(k,y) - \eta_{\mu\nu}\overline{h}(k,y)\Big) \\ &\qquad = A(k,y)\Big[M_{\rm P}^2\Big(k^2\overline{h}_{\mu\nu}(k,y=0) - k_\mu k_\nu\overline{h}(k,y=0)\Big) - 2\overline{T}_{\mu\nu}(k)\Big]\,, \end{aligned} \tag{2.14}$$

where k^2 is the worldvolume 4-momentum squared,[8] the barred quantities are the Fourier transforms, e.g.

$$\overline{h}_{\mu\nu}(k,y) = \int \mathrm{d}^4x\, \mathrm{e}^{\mathrm{i}k_\alpha x^\alpha} h_{\mu\nu}(x,y)\,,$$

and

$$A(k,y) \equiv \int \frac{\mathrm{d}k^5}{2\pi}\frac{\mathrm{e}^{\mathrm{i}k^5 y}}{(k^5)^2 - k^2}\,. \tag{2.15}$$

From this, we see that the metric perturbation on the brane (in momentum space),

$$h^0_{\mu\nu} \equiv \overline{h}_{\mu\nu}(k, y=0)\,,$$

satisfies the following equations of motion

$$k^2 h^0_{\mu\nu} - k_\mu k_\nu h^0 - m^2(k)(h^0_{\mu\nu} - \eta_{\mu\nu}h^0) = \frac{2}{M_{\rm P}^2}\overline{T}_{\mu\nu}\,, \tag{2.16}$$

where

$$h^0 \equiv \overline{h}(k, y=0)$$

and

$$\begin{aligned} m^2(k) &\equiv \frac{M_*^3}{M_{\rm P}^2 A(k, y=0)}\,, \\ &= -\frac{2\mathrm{i}k}{r_{\rm c}}\,, \end{aligned} \tag{2.17}$$

with $k \equiv \sqrt{k^2}$. The last line of the previous expression follows from expression (A.6) that is derived in appendix A (and the definition (1.3)). Here we can observe that in the DGP model the metric perturbation on the brane acquires a

[7] For example, we can multiply the equation by $\mathrm{e}^{-\mathrm{i}k^5 y}$, then integrate over y and finally revert back to the y-position space (see also appendix A).

[8] Note that in our notation $T_{\mu\nu}(x)$ already denotes a quantity that is only defined at $y = 0$, and hence we can suppress this extra-dimensional coordinate.

(4-momentum dependent) mass term. The mass term, $m^2(k)$, can be imaginary or real, depending on whether the source is time-dependent or static, and hence whether the metric perturbation is propagating or not. Although we will only consider time-independent sources in this thesis (static point sources or the vacuum), for completeness, we discuss the propagator structure in generality and calculate (2.17) in appendix A. We can solve (2.16) in the standard way: take the trace and insert back the expression for h^0, which leads to

$$(k^2 - m^2(k))h^0_{\mu\nu}(k) = \frac{2}{M_{\rm P}^2}\left[\overline{T}_{\mu\nu}(k) - \frac{1}{3}\left(\eta_{\mu\nu} - \frac{k_\mu k_\nu}{m^2(k)}\right)\overline{T}(k)\right]. \tag{2.18}$$

This has the solution

$$h_{\mu\nu}(x, y=0) = \frac{2}{M_{\rm P}^2}\int \mathrm{d}^4k\, \mathrm{e}^{-\mathrm{i}k_\alpha x^\alpha}\frac{1}{k^2 - m^2(k)}\left[\overline{T}_{\mu\nu}(k) - \frac{1}{3}\left(\eta_{\mu\nu} - \frac{k_\mu k_\nu}{m^2(k)}\right)\overline{T}(k)\right] \tag{2.19}$$

in position space.[9]

2.1.2 Gravitational Potential Energy

From (2.18), written in the slightly more convenient form

$$h^0_{\mu\nu}(k) = \frac{2}{M_{\rm P}^2}\frac{1}{k^2 - m^2(k)}\left[\frac{1}{2}(\eta_{\mu\alpha}\eta_{\nu\beta} + \eta_{\mu\beta}\eta_{\nu\alpha}) - \frac{1}{3}\eta_{\alpha\beta}\left(\eta_{\mu\nu} - \frac{k_\mu k_\nu}{m^2(k)}\right)\right]\overline{T}^{\alpha\beta}(k)\,, \tag{2.20}$$

we can immediately read off the graviton propagator, which is just the quantity (up to the normalization factor) contracted with $\overline{T}^{\alpha\beta}(k)$,[10]

$$\overline{D}_{\mu\nu,\alpha\beta}(k) = \frac{1}{k^2 - m^2(k)}\left[\frac{1}{2}(P_{\mu\alpha}P_{\nu\beta} + P_{\mu\beta}P_{\nu\alpha}) - \frac{1}{3}P_{\alpha\beta}P_{\mu\nu}\right], \tag{2.21}$$

with

$$P_{\mu\nu} = \eta_{\mu\nu} - \frac{k_\mu k_\nu}{m^2(k)}\,. \tag{2.22}$$

Note that in (2.20) the tensors $P_{\mu\nu}$ that are contracted with the energy-momentum tensor reduce to $\eta_{\mu\nu}$ because the (worldvolume) energy-momentum tensor is conserved. The latter is a consequence of the 5D energy-momentum conservation, $\partial_\mu T^{\mu\nu} + \partial_y T^{y\nu} = 0$, and the fact that we only consider energy-momentum tensors that are localized on the brane and do not have components orthogonal to it ($T^{y\nu} = 0$).

We see that in the DGP model the metric perturbation (and the propagator) has the following two interesting properties: first, the tensor structure is the one for a massive spin-2 field (note the factor 1/3 as opposed to 1/2 in standard GR),

[9] In the literature, sometimes the canonically normalized perturbation is used, $h_{\mu\nu} \to \frac{2}{M_{\rm P}}h_{\mu\nu}$.

[10] Equation $h^0_{\mu\nu}(k) = \frac{2}{M_{\rm P}^2}\overline{D}_{\mu\nu,\alpha\beta}(k)\overline{T}^{\alpha\beta}(k)$ translates to $h_{\mu\nu}(x,0) = \frac{2}{M_{\rm P}^2}\int \mathrm{d}^4x'\, D_{\mu\nu,\alpha\beta}(x-x')\times$ $\times T^{\alpha\beta}(x')$ in position space. We suppress here the y-dependence of the propagator, since we are only considering propagation along the brane in this section.

leading to the vDVZ-discontinuity [56, 57] (see the discussion below). Second, the pole structure is very distinctive. The mass is momentum-dependent and leads to the fact that the graviton on the brane is a resonance [66, 70, 71], i.e. a continuum of states rather than a normalizable zero-mode (see also section 2.3.1).

Let us calculate the gravitational potential energy between two static point masses, located on the brane. In this case, the energy-momentum tensor is given by

$$T^{\mu\nu}(x) = \delta_0^\mu \delta_0^\nu \Big(m_1 \delta^{(3)}(\vec{x}) + m_2 \delta^{(3)}(\vec{x} - \vec{r}) \Big) \,,$$

where m_i are the masses, separated by the distance $r \equiv |\vec{r}|$. Then, the vacuum energy in the presence of the sources (and hence the potential energy between them) is given by (see e.g. Ref. [139])

$$\begin{aligned} V &= \left(\int \mathrm{d}x^0 \right)^{-1} \frac{1}{2} \frac{1}{M_\mathrm{P}^2} \int \mathrm{d}^4x_1 \, \mathrm{d}^4x_2 \, T^{\mu\nu}(x_1) D_{\mu\nu,\alpha\beta}(x_1 - x_2) T^{\alpha\beta}(x_2) \,, \\ &= \left(\int \mathrm{d}x^0 \right)^{-1} \frac{1}{2} \frac{1}{M_\mathrm{P}^2} \int \frac{\mathrm{d}^4k}{(2\pi)^4} \overline{T}^{\mu\nu}(-k) \overline{D}_{\mu\nu,\alpha\beta}(k) \overline{T}^{\alpha\beta}(k) \,. \end{aligned}$$

As noted above, for conserved energy-momentum the momentum-dependent part of the tensor structure in (2.21) drops out, and hence

$$V = \left(\int \mathrm{d}x^0 \right)^{-1} \frac{1}{2M_\mathrm{P}^2} \int \frac{\mathrm{d}^4k}{(2\pi)^4} \frac{\overline{T}_{\mu\nu}(-k)\overline{T}^{\mu\nu}(k) - \frac{1}{3}\overline{T}(-k)\overline{T}(k)}{k^2 - m^2(k)} \,. \tag{2.23}$$

Inserting the energy-momentum tensor for the static point sources, for which

$$\overline{T}_{\mu\nu}(-k)\overline{T}^{\mu\nu}(k) = \overline{T}(-k)\overline{T}(k) = \int \mathrm{d}x^0 \, 2\pi\delta(k^0) m_1 m_2 \Big(\mathrm{e}^{\mathrm{i}\vec{k}\cdot\vec{r}} + \text{c.c.} \Big)$$

(after dropping the self-energy terms), we obtain

$$V = -\frac{2}{3} \frac{m_1 m_2}{M_\mathrm{P}^2} \int \frac{\mathrm{d}^3k}{(2\pi)^3} \frac{\mathrm{e}^{\mathrm{i}\vec{k}\cdot\vec{r}}}{|\vec{k}|^2 + m^2(k)|_{k^0=0}} \,,$$

with

$$m^2(k)|_{k^0=0} = \frac{2|\vec{k}|}{r_\mathrm{c}} \,,$$

using (2.17). We can now solve this integral and find

$$V = -\frac{1}{3} \frac{m_1 m_2}{\pi^2 M_\mathrm{P}^2 r} F_\mathrm{DGP}(r) \,, \tag{2.24}$$

where

$$\begin{aligned} F_\mathrm{DGP}(r) &\equiv \sin\left(\frac{2r}{r_\mathrm{c}}\right) \mathrm{Ci}\left(\frac{2r}{r_\mathrm{c}}\right) + \cos\left(\frac{2r}{r_\mathrm{c}}\right) \left[\frac{\pi}{2} - \mathrm{Si}\left(\frac{2r}{r_\mathrm{c}}\right) \right] , \qquad (2.25) \\ &\simeq \begin{cases} \dfrac{\pi}{2} + \left(\mathcal{O}(1) + 2\ln\dfrac{r}{r_\mathrm{c}} \right) \dfrac{r}{r_\mathrm{c}} + \mathcal{O}\left(\dfrac{r^2}{r_\mathrm{c}^2} \right) , & r \ll r_\mathrm{c} \,, \\ \dfrac{1}{2}\dfrac{r_\mathrm{c}}{r} + \mathcal{O}\left(\dfrac{r_\mathrm{c}^2}{r^2} \right) , & r \gg r_\mathrm{c} \,, \end{cases} \end{aligned}$$

and $\mathrm{Si}(z)$ and $\mathrm{Ci}(z)$ are the sine integral and the cosine integral, respectively. We see that for short distances (relative to the cross-over scale), we recover the 4D gravitational potential energy, $\propto \frac{m_1 m_2}{M_{\rm P}^2}\frac{1}{r}$, while for large distances we obtain the 5D Newton's law, $\propto \frac{m_1 m_2}{M_*^3}\frac{1}{r^2}$.

Note, however, that in the short distance limit the above result has a factor of 4/3, which is different from the standard result in GR, where the numerical factor in the gravitational potential is unity (recall that $M_{\rm P}^2 = (8\pi G)^{-1}$). This difference comes from the fact that the factor in front of the second term in the numerator of (2.23) is 1/3 rather than 1/2 (as for a massless graviton). Even though one could absorb the above factor of 4/3 in the definition of the Planck mass (or equivalently, in the gravitational coupling constant), this redefinition would lead to a wrong result in situations where photons are involved because the trace of the energy-momentum tensor is zero for the Maxwell Lagrangian, and hence it does not contribute to the second term of the numerator of expression (2.23). This is what is known as the vDVZ discontinuity: a finite measurement is apparently able to tell us if the graviton mass is identically zero or not.

The situation is even more transparent if one goes to the zero-mass limit and decomposes the five degrees of freedom of the massive graviton into two degrees of freedom of a massless spin-2 field,[11] two degrees of freedom of a massless spin-1 field and one degree of freedom of a massless spin-0 field. Then, one can see that the scalar field couples to the trace of the matter energy-momentum tensor and hence increases the gravitational potential between sources for which this quantity is non-vanishing (see e.g. Ref. [59]). This additional, gravitational contribution is sometimes called *fifth force* in the literature.

However, for small graviton masses, the linear approximation cannot be trusted below some distance scale, known as the Vainshtein radius $r_{\rm V}$ [58], because the (classical) expansion parameter in massive gravity is $r_{\rm V}/r$ instead of $r_{\rm g}/r$, as in massless gravity, where $r_{\rm g}$ is the Schwarzschild radius. Since $r_{\rm V} \gg r_{\rm g}$ (for a typical system), non-linearities in massive gravity become important much earlier than non-linearities in GR.[12] In terms of the fundamental degrees of freedom, it has been realized [55] that the scalar field degree of freedom is strongly coupled (i.e. its self-interaction dominates over its kinetic term) inside $r_{\rm V}$ and actually does not contribute (relevantly) to the gravitational potential. Therefore, the vDVZ discontinuity only appears if one incorrectly attempts to compute the potential in the massive gravity case by using the one-graviton exchange amplitude. Hence, the existence of the Vainshtein radius has the consequence that the leading behavior of gravity inside the 4D regime (below $r_{\rm c}$) is not just Einsteinian but interpolates between 4D GR for $r \ll r_{\rm V}$ (mediated by two tensorial degrees of freedom) and a 4D scalar-tensor gravitational theory for $r \gg r_{\rm V}$ (mediated by two tensorial and one scalar degree of freedom).

The aforementioned state of affairs is well known and will not be discussed

[11] We will show later that the graviton in DGP is rather quasi-massive, since it corresponds to a resonance. However, the decomposition in terms of degrees of freedom goes through.

[12] The precise form of $r_{\rm V}$ depends on the particular massive gravity theory. For example, in the case of the DGP model it is given by $r_{\rm V} \sim (r_{\rm g} r_{\rm c}^2)^{1/3}$, where $r_{\rm g}$ is the Schwarzschild radius of the spherically symmetric system.

further in the present thesis. Our focus lies on the non-trivial pole structure (the momentum-dependent mass) of the propagator, which is directly responsible for the distinctive behavior of the gravitational potential (in situations where the linearized theory is applicable). Therefore, in order to trace back the results to the pole structure as clearly as possible (and also for the sake of simplicity), in the remainder of this thesis (Part I), we will consider a simplified scalar field prototype model, which will be introduced in the next section. In particular, since we will only study certain energy-momentum tensors (of static point sources and of the vacuum), we will adopt the viewpoint that a scalar field theory with just a scalar degree of freedom is an excellent prototype theory to study physics resulting from the non-trivial pole structure in the DGP model. However, we have to keep in mind that for an actual problem in nature the result will get modified. As long as we consider just the regimes $r \ll r_{\mathrm{V}}$ (and can verify that a Vainshtein screening mechanism, as described above, is indeed operational) or $r \gg r_{\mathrm{V}}$, but not the transition between them, our result will capture the correct qualitative behavior, up to order-one numerical coefficients. We will return to this issue when we will discuss the validity of our results, in more detail, in chapter 5.

Also, note that the situation outlined above leads to some ambiguity in the overall numerical coefficient of the Newton potential, depending on whether we want to reproduce the standard factor of unity (multiplying Gm_1m_2/r) for an exchange of a massless tensor, a massless tensor and a massless scalar (although we saw that this option would contradict experiment for distances below the Vainshtein radius because the scalar decouples there), or just a massless scalar. For example, Ref. [64] seems to normalize the gravitational potential energy mediated by just a scalar to 1/2. We will discuss the choice of our convention, in detail, in section 3.1.1.

Another comment is in order here. As was indicated above, a careful treatment of the decomposition of the 5D graviton into the tensor, vector, and scalar modes, taking into account the gauge redundancy, would reveal that the scalar mode is associated with the "brane bending" [61] (see also Refs. [140, 141]). However, since the immediate results in this thesis, as just explained, do not depend on the particular gauge structure of the spin-2 theory, we shall not have anything more to say about this topic (except some brief, additional comments in section 3.4.1 and chapter 5).

2.2 Spin-0 Field With Two Branes

As explained in the previous section, in the remainder of this thesis we will consider a scalar field theory that exhibits some crucial properties of the (linearized) DGP model (2.1), in particular the pole structure of the propagator, but lacks the more complicated gauge structure, which is not essential for our discussion. Such a scalar field theory is modeled by

$$S = \int \mathrm{d}^4x\,\mathrm{d}y \left\{ \frac{1}{2}(\partial_A\Phi)^2 + \frac{1}{2} r_{\mathrm{c}}\delta(y)(\partial_\mu\Phi)^2 \right\}. \tag{2.26}$$

Here, $\Phi(x^\mu, y)$ is a real, massless, 5D scalar field, which has an additional 4D kinetic term, localized on the brane, with the coupling strength r_c.[13] If $r_\mathrm{c} \propto \frac{M_\mathrm{P}^2}{M_*^3}$, which then quantifies the relative strengths of the scalar field propagators on the brane and the bulk, respectively, then this prototype model imitates the gravitational behavior of the model (2.1), for the class of sources considered in this thesis.

We will show in the following chapters that this model (for the sake of brevity, we will refer to it as the DGP model in the following) possesses further, phenomenologically interesting implications if one adds a second (parallel) 3-brane to the setup. The two branes are separated by a distance R along the fifth dimension. For concreteness, we will assume that the coupling strength is identical on both branes, although we will later also consider generalizations of this (see section 3.3). Thus, the model that we will study in the present thesis is

$$S = \int \mathrm{d}^4x\,\mathrm{d}y \left\{ \frac{1}{2}(\partial_A \Phi)^2 + r_\mathrm{c}\left[\delta\left(y+\frac{R}{2}\right) + \delta\left(y-\frac{R}{2}\right)\right]\frac{1}{2}(\partial_\mu\Phi)^2 + J(x^\mu, y)\Phi \right\}, \tag{2.27}$$

where we also included the source term $J(x^\mu, y)$ and placed the branes symmetrically around the origin for later convenience.

From now on, all quantities are understood as expressions in the presence of two branes. However, to avoid notational clutter, we will not use special notation for that. In those cases where we wish to express the single-brane quantities, we will indicate that explicitly.

We would like to pause here for a moment in order to briefly discuss the difference between the prototypical spin-0 theory and the full spin-2 theory when it comes to adding a second brane. Such an extension increases the complexity of the model in the case of the spin-2 gauge theory because it can lead to the appearance of an additional mode, the *radion*, due to the separation of the branes. The status of the radion mode depends on the nature of the branes and the bulk, in particular on the presence or absence of the corresponding cosmological constants. Such a mode could in principle destabilize the brane separation. However, in Ref. [75] it was shown that in the case considered in this thesis, i.e. a tensionless brane (and provided that we deal with the normal branch) without a bulk cosmological constant, there is no physical radion.[14] Hence, the results obtained in this thesis should not get affected if we extrapolate our findings in the spin-0 setup to the full spin-2 case (except the order-one modifications, coming from taking into account the contribution from all five degrees of freedom, as mentioned before).

2.2.1 Scalar Field Propagator

Let us derive the propagator for the action (2.27). This action leads to the equation of motion

$$\left[\Box - \partial_y^2 + r_\mathrm{c}\delta\left(y+\frac{R}{2}\right)\Box + r_\mathrm{c}\delta\left(y-\frac{R}{2}\right)\Box\right]\Phi = J(x^\mu, y)\,. \tag{2.28}$$

[13] In other words, r_c quantifies the strength of the derivative coupling to the delta-function.

[14] We comment on the more general case of a non-vanishing brane tension in chapter 5.

If the source is static, we can look for static solutions (we discuss the general, non-static case in appendix A). For this, we can first solve

$$\Big[\Delta+\partial_y^2+r_c\delta\Big(y+\frac{R}{2}\Big)\Delta+r_c\delta\Big(y-\frac{R}{2}\Big)\Delta\Big]G(\vec{x},\vec{x'};y,y')=\delta^{(3)}(\vec{x}-\vec{x'})\delta(y-y')\,, \tag{2.29}$$

where Δ is the Laplace operator and $G(\vec{x},\vec{x'};y,y')$ is the Green's function. Note that the operator on the left-hand side is not translationally invariant along the y-direction, but it is translationally invariant along the brane-direction. Hence, the above equation can be written as

$$\Big[\Delta+\partial_y^2+r_c\delta\Big(y+\frac{R}{2}\Big)\Delta+r_c\delta\Big(y-\frac{R}{2}\Big)\Delta\Big]G(\vec{x};y,y')=\delta^{(3)}(\vec{x})\delta(y-y')\,.$$

We can Fourier transform this, with respect to the coordinates $\vec{x}$, to get

$$\Big[|\vec{k}|^2-\partial_y^2+r_c\delta\Big(y+\frac{R}{2}\Big)|\vec{k}|^2+r_c\delta\Big(y-\frac{R}{2}\Big)|\vec{k}|^2\Big]\overline{G}(|\vec{k}|;y,y')=-\delta(y-y')\,,$$

where

$$\overline{G}(|\vec{k}|;y,y')=\int \mathrm{d}^3x\,\mathrm{e}^{-\mathrm{i}\vec{k}\vec{x}}G(\vec{x};y,y')\,.$$

Next, we can also Fourier transform with respect to the coordinate of the extra dimension y, using

$$\overline{G}(|\vec{k}|;y,y')=\int\frac{\mathrm{d}k^5}{2\pi}\,\mathrm{e}^{\mathrm{i}k^5y}\widetilde{G}(|\vec{k}|;k^5,y')\,,$$

where k^5 is the momentum in the fifth dimension. We then find the formal solution

$$\widetilde{G}(|\vec{k}|;k^5,y')=-\frac{\mathrm{e}^{-\mathrm{i}k^5y'}+r_c|\vec{k}|^2\Big(\overline{G}(|\vec{k}|;-\frac{R}{2},y')\mathrm{e}^{\mathrm{i}k^5\frac{R}{2}}+\overline{G}(|\vec{k}|;\frac{R}{2},y')\,\mathrm{e}^{-\mathrm{i}k^5\frac{R}{2}}\Big)}{|\vec{k}|^2+(k^5)^2}\,.$$

Transforming back to the y-coordinates and using

$$\int\frac{\mathrm{d}k^5}{2\pi}\frac{\mathrm{e}^{\mathrm{i}k^5(y+a)}}{|\vec{k}|^2+(k^5)^2}=\frac{\mathrm{e}^{-|\vec{k}||y+a|}}{2|\vec{k}|}\,,\quad(\text{with } a\in\mathbb{R})\,, \tag{2.30}$$

we get

$$\begin{aligned}\overline{G}(|\vec{k}|;y,y')=\frac{\mathrm{e}^{-|\vec{k}||y-y'|}}{2|\vec{k}|}&-\frac{r_c|\vec{k}|^2\overline{G}(|\vec{k}|;-\frac{R}{2},y')}{2|\vec{k}|}\mathrm{e}^{-|\vec{k}|\left|y+\frac{R}{2}\right|}\\&-\frac{r_c|\vec{k}|^2\overline{G}(|\vec{k}|;\frac{R}{2},y')}{2|\vec{k}|}\mathrm{e}^{-|\vec{k}|\left|y-\frac{R}{2}\right|}\,.\end{aligned}$$

We can now solve for the coefficients $\overline{G}(|\vec{k}|;-\frac{R}{2},y')$ and $\overline{G}(|\vec{k}|;\frac{R}{2},y')$ and arrive at

$$\begin{aligned}\overline{G}(|\vec{k}|;y,y')=&-\frac{\mathrm{e}^{-|\vec{k}||y-y'|}}{2|\vec{k}|}-\frac{r_c}{2}\frac{r_c|\vec{k}|\mathrm{e}^{-|\vec{k}|R}\Big(E(y,-y')+E(-y,y')\Big)}{(2+r_c|\vec{k}|)^2-r_c^2|\vec{k}|^2\,\mathrm{e}^{-2|\vec{k}|R}}\\&+\frac{r_c}{2}\frac{(2+r_c|\vec{k}|)\Big(E(y,y')+E(-y,-y')\Big)}{(2+r_c|\vec{k}|)^2-r_c^2|\vec{k}|^2\,\mathrm{e}^{-2|\vec{k}|R}}\,,\end{aligned} \tag{2.31}$$

where

$$E(z,z') \equiv \mathrm{e}^{-|\vec{k}|\left(\left|z-\frac{R}{2}\right|+\left|z'-\frac{R}{2}\right|\right)} . \tag{2.32}$$

In the case of a single brane, located at the origin ($R \to 0$), the above propagator reduces to

$$\overline{G}^{(1\mathrm{B})}(|\vec{k}|;y,y') = -\frac{\mathrm{e}^{-|\vec{k}||y-y'|}}{2|\vec{k}|} + \frac{r_\mathrm{c}}{2}\frac{\mathrm{e}^{-|\vec{k}|(|y|+|y'|)}}{2+r_\mathrm{c}|\vec{k}|} , \tag{2.33}$$

where we also re-scaled $r_\mathrm{c} \to r_\mathrm{c}/2$, so that this limit reproduces the correct action (2.26).[15] Of course, (2.33) coincides with the expression found in Ref. [71] (up to different normalization conventions, as explained in section 2.1.2).

2.2.2 Kaluza-Klein Decomposition

It is possible to re-express the theory in (2.27) in the so-called Kaluza-Klein language, where one expands (symbolically)

$$\Phi(x^\mu,y) = \sum\!\!\!\!\!\!\int \mathrm{d}m\, \psi_m(y)\phi_m(x^\mu) ,$$

with $\psi_m(y)$ the *mode functions* and $\phi_m(x^\mu)$ the 4D *KK modes*, and integrates over the extra dimension. Usually, such a decomposition is performed if the extra dimension is compact, which then leads to the replacement of the extra dimension for an infinite (discrete) tower of massive KK modes. In the present case the extra dimension is infinite, and hence the KK modes exhibit a continuous spectrum. Nevertheless, performing the calculation in the KK language is not only a useful cross-check to the fully 5D calculation (as seen in section 3.1) but also adds an interesting new perspective (see chapter 4): when we regularize the system, by compactifying the extra dimension on a ring, the masses become discrete (quantized) and lead directly to the Casimir energy. Hence, the result is an immediate consequence of the particular KK mass quantization. In this section, we will perform the KK decomposition both in an infinite extra dimension and on a ring. While the former is simpler and more directly related to the original (single-brane) DGP model, the latter is needed for the calculation of the Casimir force in chapter 4. Of course, we will see that performing the appropriate limit in the compactified case will bring us back to the infinite-dimension case, as it should.

Infinite Extra Dimension

We can expand the field Φ in the following way:

$$\Phi(x^\mu,y) = \sum_{\alpha=1}^{2}\int_0^\infty \mathrm{d}m\, \psi_{m,\alpha}(y)\phi_{m,\alpha}(x^\mu) .$$

The mode functions (or wave functions) $\psi_{m,\alpha}(y)$ constitute a complete basis of the y-space. Since the system is symmetric around the origin, we have divided the

[15] Note that just placing two branes on top of each other, without re-scaling r_c, effectively doubles the coupling strength.

mode functions into even ($\alpha = 1$) and odd ($\alpha = 2$). We can render the Lagrangian in (2.27) diagonal in the KK modes $\phi_{m,\alpha}(x^\mu)$ if the mode functions satisfy the equation

$$\left\{\partial_y^2 + m_\alpha^2\left[1 + r_\mathrm{c}\,\delta\left(y + \frac{R}{2}\right) + r_\mathrm{c}\,\delta\left(y - \frac{R}{2}\right)\right]\right\}\psi_{m,\alpha}(y) = 0\,, \tag{2.34}$$

which implies the orthonormality condition

$$\int_{-\infty}^{\infty} \mathrm{d}y\,\psi_{m,\alpha}(y)\psi_{m',\alpha'}(y)\left[1 + r_\mathrm{c}\,\delta\left(y + \frac{R}{2}\right) + r_\mathrm{c}\,\delta\left(y - \frac{R}{2}\right)\right] = \delta(m - m')\delta_{\alpha\alpha'}\,. \tag{2.35}$$

Using this, the 5D action reduces to

$$S = \int \mathrm{d}x^4 \sum_{\alpha=1}^{2} \int_0^\infty \mathrm{d}m \left\{-\frac{1}{2}\phi_{m,\alpha}(x^\mu)\left(\Box + m^2\right)\phi_{m,\alpha}(x^\mu) + \phi_{m,\alpha}(x^\mu)J_{m,\alpha}(x^\mu)\right\}, \tag{2.36}$$

with[16]

$$J_{m,\alpha}(x^\mu) = \int \mathrm{d}y\, J(x^\mu, y)\psi_{m,\alpha}(y)\,. \tag{2.37}$$

We can determine the basis $\{\psi_{m,\alpha}(y)\}$ by solving (2.34). This is done in appendix B.1.

From the action (2.36), we derive the equation of motion

$$\left(\Box + m^2\right)\phi_{m,\alpha}(x^\mu) = J_{m,\alpha}(x^\mu)\,. \tag{2.38}$$

We can now further proceed to derive the Green's function in the KK language. Since we will later be interested in the static source

$$J(x^\mu, y) = g\left[\delta^{(3)}(\vec{x})\delta\left(y + \frac{R}{2}\right) + \delta^{(3)}(\vec{x} - \vec{r})\delta\left(y - \frac{R}{2}\right)\right],$$

the 4D source (see (2.37))

$$J_{m,\alpha}(x^\mu) = g\left[\psi_{m,\alpha}\left(-\frac{R}{2}\right)\delta^{(3)}(\vec{x}) + \psi_{m,\alpha}\left(\frac{R}{2}\right)\delta^{(3)}(\vec{x} - \vec{r})\right] \tag{2.39}$$

will be static as well. Thus, we can look for the solution of

$$\left(\Delta - m^2\right)G_m(\vec{x} - \vec{x'}) = \delta^{(3)}(\vec{x} - \vec{x'})\,,$$

leading to the (4D) Green's function

$$\begin{aligned} G_m(\vec{x} - \vec{x'}) &= -\int \frac{\mathrm{d}^3\vec{k}}{(2\pi)^3}\frac{\mathrm{e}^{\mathrm{i}\vec{k}\cdot(\vec{x}-\vec{x'})}}{|\vec{k}|^2 + m^2}\,, \\ &= -\frac{1}{4\pi r}\mathrm{e}^{-mr}\,, \end{aligned} \tag{2.40}$$

with $r = |\vec{x} - \vec{x'}|$, as usual.

[16] Note that $J_{m,\alpha}(x^\mu)$ is *not* a KK mode of $J(x^\mu, y)$, which would rather be $\tilde{J}_{m,\alpha}(x^\mu) \equiv \int \mathrm{d}y\,\psi_{m,\alpha}(y)[1 + r_\mathrm{c}\delta(y + R/2) + r_\mathrm{c}\delta(y - R/2)]J(x^\mu, y)$.

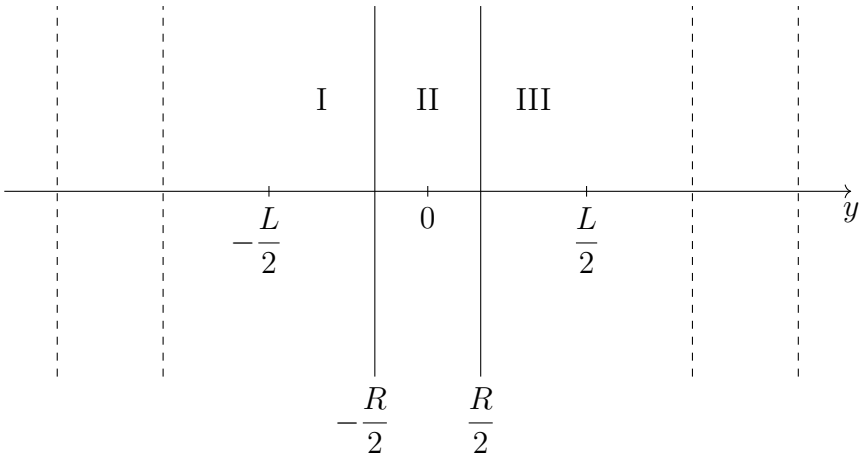

Figure 2.1: The setup: Periodic space (with period L) along the extra dimension y, with two DGP branes (solid lines). The branes (with suppressed transverse dimensions) are repeated (dashed lines) after the period. I, II and III are the regions we need to match in order to find the field solution.

Compact Extra Dimension

For the derivation in chapter 4, it will prove useful to introduce an IR regulator for the system by compactifying the extra dimension, using periodic boundary conditions. We take the finite size of the extra dimension to be L. Later, we will remove the regulator and end up with an infinite space. Focusing on the extra dimension and suppressing the transverse dimensions, the system is illustrated by Figure 2.1.

We proceed in a very similar way as in the previous derivation. Now, we can decompose the 5D scalar field as

$$\Phi(x^\mu, y) = \sum_{\alpha=1}^{2} \sum_{m} \psi_{m,\alpha}(y)\phi_{m,\alpha}(x^\mu)\,,$$

where the mode functions $\psi_{m,\alpha}(y)$ again span a complete basis of the y-space, satisfying the same equation (2.34) as before, but now they are subject to the periodic boundary condition. We derive the appropriate mode functions in appendix B.2. Using that they satisfy the orthonormality condition

$$\int_{-\frac{L}{2}}^{\frac{L}{2}} \mathrm{d}y\, \psi_{m,\alpha}(y)\psi_{m',\alpha'}(y)\Big[1 + r_\mathrm{c}\,\delta\Big(y + \frac{R}{2}\Big) + r_\mathrm{c}\,\delta\Big(y - \frac{R}{2}\Big)\Big] = \delta_{m,m'}\delta_{\alpha,\alpha'}\,, \tag{2.41}$$

the 5D action then reduces to

$$S = \int \mathrm{d}^4x \sum_{\alpha=1}^{2} \sum_{m} \frac{1}{2}\Big[\big(\partial_\mu\phi_{m,\alpha}(x)\big)^2 - m_\alpha^2\phi_{m,\alpha}^2(x)\Big]\,. \tag{2.42}$$

Note that we dropped here the source term, since we will only consider the vacuum, for the application to the Casimir effect.

The information about the extra dimension and the brane configuration is now encoded in the discrete masses. By solving for $\psi_{m,\alpha}(y)$, we found (see appendix B.2) that the masses have to satisfy the following quantization equation:

$$\tan\left(\frac{m_\alpha L}{2}\right) = -\frac{m_\alpha r_\mathrm{c}}{2} \times \begin{cases} \dfrac{1+\cos\left(m_\alpha R\right)}{1+\frac{m_\alpha r_\mathrm{c}}{2}\sin\left(m_\alpha R\right)}\,, & \text{for } \alpha = 1 \text{ (even)}\,, \\ \dfrac{1-\cos\left(m_\alpha R\right)}{1-\frac{m_\alpha r_\mathrm{c}}{2}\sin\left(m_\alpha R\right)}\,, & \text{for } \alpha = 2 \text{ (odd)}\,. \end{cases} \tag{2.43}$$

Note that we only have one mode with zero mass, the even zero-mode, since the odd zero-mode vanishes, $\psi_{0,2}(y) = 0$.

We have thus traded the extra dimension for a KK tower of massive Klein-Gordon fields, satisfying the equation

$$\left(\Box + m_\alpha^2\right)\phi_{m,\alpha}(x) = 0\,. \tag{2.44}$$

2.3 Infrared Transparency

The IR transparency phenomenon, outlined in section 1.1.1, i.e. the fact that massive KK modes can only be exchanged efficiently at short distances (below r_c), while the light modes (lighter than $\sim r_\mathrm{c}^{-1}$) can also propagate at long distances, is responsible for a number of interesting features in the DGP model. Not only can the gravitational behavior (see (2.25)) be understood as a consequence of this phenomenon but also other properties can be traced back to it. We will outline two of them in the following sections, since they provided a motivation to investigate a third consequence—the impact on the Casimir effect—that is a major part of this thesis. We will illustrate this phenomenon using the original setup with a single brane.

2.3.1 Resonance Graviton

Five-Dimensional Language

We saw in section 2.1.2 that the pole structure of the graviton propagator is given by

$$D(k) \equiv \frac{1}{k^2 - m^2(k)}\,.$$

For a freely propagating wave (on the brane), $m^2(k)$ is given by $-\mathrm{i}k\Gamma$ (see (2.17)), where $\Gamma \sim r_\mathrm{c}^{-1}$ can be interpreted as a resonance width [71]. For short wavelengths, $|k| \gg \Gamma$, the width Γ effectively goes to zero, and the above propagator describes a stable, massless particle, propagating in four dimensions. However, it is only completely stable in the limiting case of $\Gamma = 0$, which corresponds to $r_\mathrm{c} \to \infty$ and hence the situation where the bulk gravity is decoupled. For finite r_c, the propagator corresponds to a continuum of states, where long wavelengths contribute in the propagator as $D(k) \propto 1/k$ and hence mediate a 5D Newton force.

This can be made even more explicit by using a Källén-Lehmann spectral representation, where the propagator is decomposed as (cf. (A.10))

$$\frac{1}{r_{\rm c}k^2+2{\rm i}k}=\int_0^\infty\frac{{\rm d}s}{2\pi}\rho(s)\frac{1}{k^2-s+{\rm i}\varepsilon}\,,$$

with the spectral function

$$\rho(s)=\frac{4}{r_{\rm c}}\frac{1}{\sqrt{s}}\frac{r_{\rm c}}{4+sr_{\rm c}^2}\,.$$

Since $\rho(s)$ is continuous in s, this demonstrates that the DGP propagator represents a continuum of massive states (as to be expected, since the extra dimension is infinite). Moreover, we can see that for large $r_{\rm c}$ (as compared to 4D distances r), this spectral function is sharply peaked around $s=0$, and in particular

$$\rho(s)\stackrel{r_{\rm c}\to\infty}{\longrightarrow}\text{constant}\times\delta(s)\,.$$

Thus, for distances $r\ll r_{\rm c}$ the gravitational force is effectively mediated by a single massless graviton (we ignore the additional vector and scalar modes in this discussion), leading to a 4D Newton's law. For distances $r\gg r_{\rm c}$, however, this graviton "decays" into a continuous tower of massive gravitons, leading to a 5D force law.

Kaluza-Klein Language

We can understand the same physics, as outlined above, directly using the KK language. We have shown that the (massive) propagators of the tower of KK modes (derived for static sources) are given by (2.40). The analog of (2.39) for two point masses on the brane (separated by distance $\vec{r}$), in the presence of a single brane at the origin, can be obtained by sending R to zero, which leads to

$$J^{(1{\rm B})}_{m,\alpha}(x^\mu)=g\Big[\psi^{(1{\rm B})}_{m,\alpha}(0)\delta^{(3)}(\vec{x})+\psi^{(1{\rm B})}_{m,\alpha}(0)\delta^{(3)}(\vec{x}-\vec{r})\Big]\,.$$

In order to find the mode function $\psi^{(1{\rm B})}_{m,\alpha}(0)$, we just take the $R\to0$ limit of the relevant expressions in appendix B.1, noting that the odd functions vanish at the origin, and re-scale $r_{\rm c}\to r_{\rm c}/2$ as before (to end up with the correct action (2.26)). Hence,

$$\psi^{(1{\rm B})}_{m,\alpha}(0)=\delta_{\alpha,1}\sqrt{\frac{4}{\pi}}\Big(4+r_{\rm c}^2m^2\Big)^{-1/2}\,,$$

as was first obtained in Ref. [70].

Thus, the potential energy between two point sources on the brane is

$$\begin{aligned}V^{(1{\rm B})}_{\rm KK}(r)&=\sum_\alpha\int_0^\infty{\rm d}m\,\frac{1}{2}\int{\rm d}^3x\,{\rm d}^3x'\,J^{(1{\rm B})}_{m,\alpha}(\vec{x})G_m(\vec{x}-\vec{x'})J^{(1{\rm B})}_{m,\alpha}(\vec{x'})\,,\\&=-\frac{g^2}{\pi^2r}\int_0^\infty{\rm d}m\,\frac{{\rm e}^{-mr}}{4+r_{\rm c}^2m^2}\,.\end{aligned}$$

We see that for distances $r \ll r_c$ the denominator (i.e. the mode functions) cut off the integral long before the exponential becomes relevant, which leads to a 4D $(1/r)$-potential. On the other hand, for $r \gg r_c$ the denominator is frozen, while the exponential cuts off the integral, leading to a 5D $(1/r^2)$-potential.

Hence, in the KK language, the massive modes "conspire" in such a way as to reproduce the resonance-graviton behavior.

2.3.2 Gravitational Mirror Images

Our second example involves a feature of the DGP brane that is apparent to a 5D observer and which can also be traced back to the IR transparency phenomenon. The discussion in this section follows a similar one in Ref. [71] and is additionally based on an argument presented to us by Gia Dvali.

The propagator for the DGP model between two static point masses at y and y' along the extra dimension, in the presence of the brane at the origin, is given by (see section 2.2.1 for the derivation)

$$\overline{G}^{(1B)}(|\vec{k}|; y, y') \sim -\frac{e^{-|\vec{k}||y-y'|}}{|\vec{k}|} + r_c \frac{e^{-|\vec{k}|(|y|+|y'|)}}{2 + r_c|\vec{k}|}\,, \tag{2.45}$$

where we suppressed the overall numerical coefficient, since we only care about the pole structure, but not the contribution of the various degrees of freedom, for the following argument. We can approximate (2.45) in the regime $r \ll r_c$ (and hence $kr_c \gg 1$) as

$$\overline{G}^{(1B)}(|\vec{k}|; y, y') \sim -\frac{e^{-|\vec{k}||y-y'|}}{|\vec{k}|} + \frac{e^{-|\vec{k}|(|y|+|y'|)}}{|\vec{k}|} - 2\frac{e^{-|\vec{k}|(|y|+|y'|)}}{r_c|\vec{k}|^2}\,.$$

Then, the potential energy between two point sources m_1 and m_2 at y and y' is

$$V^{(1B)}(r; y, y') \sim -\frac{m_1 m_2}{M_*^3}\left(\frac{1}{r^2 + |y-y'|^2} - \frac{1}{r^2 + (|y| + |y'|)^2} + \frac{2}{r r_c}\arctan\frac{r}{|y| + |y'|}\right) \tag{2.46}$$

(see also section 3.1.1). Although this result gives us the potential energy between two point sources, we can read off from it the gravitational potential due to one point source, evaluated at the location of the other (probe) source, in the presence of a brane because of the following reason: for a static point source with mass m_1 at $(\vec{r}, y)$, the solution for the scalar field (evaluated at the point $(\vec{x}, y')$) is

$$\Phi(\vec{x}, y') \sim \frac{m_1}{M_*^{3/2}} \int d^3\vec{k}\, e^{i\vec{k}\cdot(\vec{x}-\vec{r})} \overline{G}^{(1B)}(|\vec{k}|; y, y')\,.$$

But since our scalar field Φ is essentially the graviton (see the discussion in section 2.1.2), the gravitational potential is $M_*^{-3/2}\Phi$ (recall that Φ is canonically normalized), which is the same as $V^{(1B)}(r; y, y')/m_2$ (from (2.46)). Hence, expression

(2.46), divided by m_2, can be viewed as the gravitational potential of a point mass m_1 at location $(\vec{r}, y)$, evaluated by a (probe) point mass m_2 at $(\vec{x} = \vec{0}, y')$.

We see that the resulting potential differs from a mere $\left(-\frac{m_1}{M_*^3}\frac{1}{r^2+|y-y'|^2}\right)$-potential quite dramatically, due to the presence of the DGP brane. The situation is similar to the so-called image problem in classical electrostatics, so we can use that intuition to interpret the present setup. There, we consider the situation of a point charge in the presence of a perfectly conducting plate. The (positive) point charge induces a negative charge on the plate, and the resulting potential is the same as if a mirror image charge had been introduced on the opposite side of the plate.

Similarly, the potential in the DGP scenario has a form as if the brane introduced a negative (anti-gravitating) mass on the opposite side of the brane (opposite to the probe mass). For probe masses at $y' \leq 0$ (with the source m_1 at positive y) the "image" mass cancels the 5D potential, while for probe masses at $y' > 0$ the image mass enhances the attraction between m_1 and m_2.

However, there is an important difference to the situation in the electrostatics case. In the DGP scenario, if the point masses are located at opposite sides of the brane, there is still an attractive (but 4D) potential left (since the last term in (2.46) scales as either $r_c^{-1}/(|y| + |y'|)$ or r_c^{-1}/r, depending on if $|y| + |y'| \gg r$ or $|y| + |y'| \ll r$, respectively). In this sense, the DGP brane "screens" 5D gravity.

Hence, we can conclude that if we consider a single point mass in the bulk near the brane, the brane will have a repulsive force on the point mass (by effectively generating an "anti-gravitating" mirror image on the opposite side).

3

Modification of the DGP Gravitational Force Law

In this chapter, we want to explore how Newton's law gets modified in a DGP scenario where a second DGP brane is present. In particular, we wish to investigate how the potential energy (2.24) between two static point sources on the *same* brane changes, but also derive the gravitational force between two sources on *different* branes. We will see that the second brane has the effect of further screening gravity, even the already weakened gravity as deduced in the original single-brane case. We will show that this has interesting phenomenological implications.

As explained in section 2.1.2, the "true" gravitational force is due to the exchange of the massive graviton, and hence it will introduce an additional Vainshtein scale to the problem. However, as we will argue in chapter 5, the full gravitational force will only differ from our result (i.e. in the relevant region) by an order-one numerical factor.

Furthermore, we discuss the present setup in the context of the cutoff of semi-classical gravity, which differs from the Planck scale in the presence of a large number of particle species.

The contents of this chapter is based on Ref. [1] and is mostly a verbatim reproduction, although modifications, adjustments and extensions have been made. Also, the order of the presentation of the material has been changed and (hopefully) helpful comments have been added.

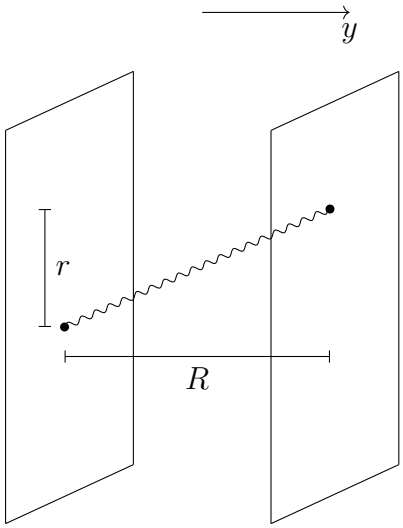

Figure 3.1: Potential energy between two static point sources on different, parallel branes, mediated by the scalar field.

3.1 Gravitational Potential Energy Between Static Point Masses

Let us start with calculating the gravitational potential energy between two static point sources, localized on the opposite branes, as shown in Figure 3.1. We will begin with the full 5D calculation and then perform an analogous computation in the KK decomposition.

3.1.1 Five-Dimensional Description

For time-independent sources, $J(\vec{x}, y)$, the potential energy is given by

$$V = \frac{1}{2}\int \mathrm{d}^3x\,\mathrm{d}y\,\mathrm{d}^3x'\,\mathrm{d}y'\,J(\vec{x},y)G(\vec{x}-\vec{x'};y,y')J(\vec{x'},y')\,.$$

Using

$$J(\vec{x},y) = g\Big[\delta^{(3)}(\vec{x})\delta\Big(y+\frac{R}{2}\Big)+\delta^{(3)}(\vec{x}-\vec{r})\delta\Big(y-\frac{R}{2}\Big)\Big] \tag{3.1}$$

and the (Fourier transform of the) propagator (2.31), the energy reduces to (again dropping the self-energy terms)

$$\begin{aligned} V &= g^2\int\frac{\mathrm{d}^3k}{(2\pi)^3}\mathrm{e}^{\mathrm{i}\vec{k}\cdot\vec{r}}\,\overline{G}\Big(|\vec{k}|;-\frac{R}{2},\frac{R}{2}\Big)\,,\\ &= g^2\int\frac{\mathrm{d}^3k}{(2\pi)^3}\mathrm{e}^{\mathrm{i}\vec{k}\cdot\vec{r}}\left(-\frac{2}{|\vec{k}|}\frac{\mathrm{e}^{-|\vec{k}|R}}{(2+r_\mathrm{c}|\vec{k}|)^2-r_\mathrm{c}^2|\vec{k}|^2\,\mathrm{e}^{-2|\vec{k}|R}}\right),\\ &= -\frac{g^2}{\pi^2}\frac{1}{r}\int_0^\infty \mathrm{d}|\vec{k}|\frac{\sin(|\vec{k}|r)\,\mathrm{e}^{-|\vec{k}|R}}{(2+r_\mathrm{c}|\vec{k}|)^2-r_\mathrm{c}^2|\vec{k}|^2\,\mathrm{e}^{-2|\vec{k}|R}}\,, \end{aligned} \tag{3.2}$$

where $r \equiv |\vec{r}|$.

We see already from (2.27), with (3.1), that if the field Φ is to mimic the graviton, the correct coupling constant should be $g \propto M_*^{-3/2} = \sqrt{r_c}/M_P$ (for unit-mass point sources). We fix the numerical coefficient such that

$$g^2 = \frac{r_c}{2M_P^2}\,. \tag{3.3}$$

A comment on this point should be in order here. We already explained in section 2.1.2 that the exact normalization depends on if we want to reproduce the standard Newton's law for an exchange of tensor degrees of freedom or/and an exchange of a scalar degree of freedom. Moreover, as will become clear in section 3.2, the presence of a second brane provides us with an additional choice of normalization. We can either reproduce the standard Newton's law for point sources on the same brane if their 4D separation is much smaller than a characteristic distance scale ρ, to be introduced below, (i.e. $r \ll \rho$) or for the opposite case ($r \gg \rho$). The normalization (3.3) corresponds to the choice that the scalar field (would-be graviton) mediates the standard Newton force between static point sources on our brane that are close enough ($r \ll \rho$).

The resulting integral in (3.2) cannot be solved exactly, but we can extract the leading-order behavior for the three interesting regimes to be specified shortly. Let us rewrite (3.2) as

$$V(r,R) = -\frac{g^2}{4\pi^2}\frac{1}{r r_c} J\,, \tag{3.4}$$

where

$$J = \int_0^\infty \mathrm{d}x\, \frac{\sin x\, \mathrm{e}^{-\frac{R}{r}x}}{\frac{r}{r_c} + x + \frac{1}{4}\frac{r_c}{r}x^2\left(1 - \mathrm{e}^{-2\frac{R}{r}x}\right)}\,. \tag{3.5}$$

Note that in the present discussion we are solely interested in the situation where $r, R < r_c$ because r_c is already at least of the order of the Hubble size (see the discussion in chapter 5). Hence, we want to approximate the potential energy for the regime $r \ll r_c$ and $R \ll r_c$.

Since the exponential cuts off the above integral at r/R, we can approximate it as

$$J \simeq \int_0^{\frac{r}{R}} \mathrm{d}x\, \frac{\sin x}{\frac{r}{r_c} + x + \frac{1}{2}\frac{\rho^2}{r^2}x^3}\,, \tag{3.6}$$

where we have introduced the new length scale

$$\rho \equiv \sqrt{R r_c} \tag{3.7}$$

because it will emerge in the result. In the regime $r \gg R$, we can further rewrite

$$J \simeq \int_0^\infty \mathrm{d}x\, \frac{\sin x}{\frac{r}{r_c} + x + \frac{1}{2}\frac{\rho^2}{r^2}x^3}\,. \tag{3.8}$$

For $r \gg \rho$, the last term in the denominator of (3.8) is never dominant in the relevant integration region ($x \lesssim 1$), and hence we can approximate

$$J \simeq \int_0^\infty \mathrm{d}x\, \frac{\sin x}{\frac{r}{r_c} + x} = F_{\mathrm{DGP}}\left(\frac{r}{2}\right) + \mathcal{O}(1)\mathrm{e}^{-\sqrt{2}\frac{r}{\rho}}\,, \qquad r \gg \rho\,, \tag{3.9}$$

with $F_{\rm DGP}(r)$ given by (2.25). Thus, in this regime the potential energy is approximately the same as the one found in the original DGP setup [64].[1] Since we are only interested in the regime $r \ll r_{\rm c}$, the above expression reduces to

$$F_{\rm DGP}\Big(\frac{r}{2}\Big) \simeq \frac{\pi}{2} + \Big(\mathcal{O}(1) + \ln\frac{r}{r_{\rm c}}\Big)\frac{r}{r_{\rm c}} + \mathcal{O}\Big(\frac{r^2}{r_{\rm c}^2}\Big)\,, \qquad r \ll r_{\rm c}\,.$$

For $r \ll \rho$, the last term in the denominator of (3.8) cannot be neglected. However, now we can approximate

$$\begin{aligned} J &\simeq \int_0^\infty {\rm d}x\, \frac{\frac{\sin x}{x}}{1 + \frac{1}{2}\frac{\rho^2}{r^2}x^2} + \mathcal{O}\Big(\frac{r}{r_{\rm c}}\Big) + \mathcal{O}\Big(\frac{R}{r_{\rm c}}\Big)\,, \\ &= \frac{\pi}{2}\Big(1 - {\rm e}^{-\sqrt{2}\frac{r}{\rho}}\Big) + \mathcal{O}\Big(\frac{r}{r_{\rm c}}\Big) + \mathcal{O}\Big(\frac{R}{r_{\rm c}}\Big)\,, \\ &\simeq \frac{\pi}{\sqrt{2}}\frac{r}{\rho} + \mathcal{O}\Big(\frac{r^2}{\rho^2}\Big) + \mathcal{O}\Big(\frac{r}{r_{\rm c}}\Big) + \mathcal{O}\Big(\frac{R}{r_{\rm c}}\Big)\,, \qquad r \ll \rho\,. \end{aligned} \tag{3.10}$$

Since an asymptotic expansion of the integral (3.5) is not available, which would justify the approximations (3.9) and (3.10) analytically, we use numerical means to show in appendix C.1 that the approximations are nevertheless reliable in the stated regimes. We also verify numerically (in the same appendix C.1) that the corrections to the leading-order terms, given above, are correct.

Finally, in the region $r \ll R$, we can approximate $\sin x \simeq x$ in the numerator of (3.6) and (using `Mathematica`) find[2]

$$\begin{aligned} J &\simeq \int_0^{\frac{r}{R}} {\rm d}x\, \frac{x}{\frac{r}{r_{\rm c}} + x + \frac{1}{2}\frac{\rho^2}{r^2}x^3}\,, \\ &\simeq \frac{\pi}{\sqrt{2}}\frac{r}{\rho}H\Big(\frac{R}{r_{\rm c}}\Big) + \mathcal{O}\Big(\frac{r^3}{R^3}\Big) \times \mathcal{O}\Big(\frac{R}{r_{\rm c}}\Big)\,, \qquad r \ll R\,, \end{aligned} \tag{3.11}$$

where

$$H\Big(\frac{R}{r_{\rm c}}\Big) \equiv 1 - \frac{1}{\pi\sqrt{2}}\Big(\mathcal{O}(1) + \ln\frac{R}{r_{\rm c}}\Big)\sqrt{\frac{R}{r_{\rm c}}} + \Big(\text{subleading orders of } \frac{R}{r_{\rm c}}\Big)\,. \tag{3.12}$$

[1] This is not surprising, since for two point sources that are separated by a large distance r, their bulk separation becomes less important and thus the system with two branes behaves like a single-brane system. Note, however, that $F_{\rm DGP}(r/2) = F_{\rm DGP}(r)|_{r_{\rm c}\to 2r_{\rm c}}$ because two branes, with coupling $r_{\rm c}$, on top of each other have effectively twice the coupling strength.

[2] The subleading terms in this expression were extracted numerically. However, we can understand some of their features from the following consideration. Note that in going from (3.5) to (3.11), we omitted terms with positive (possible fractional) powers of r/R (and additional powers of $R/r_{\rm c}$), which are subleading in this regime. What is the next-to-leading power of r/R? On physical grounds, we know that the force *along the brane* should go to zero for $r \to 0$. Also, we can see from (3.5) explicitly that $\frac{\partial}{\partial r}(J/r) \to 0$ for $r \to 0$. Hence, we know that the leading correction (in r/R) to (3.11) has to vanish faster than quadratic. From this argument, it follows that the (magnitude of the) force in the regime $r \ll R$ is bounded by the (magnitude of the) force in regime $R \ll r \ll \rho$ and will approach zero eventually. However, to determine how fast it will approach zero, we resort to a numerical analysis (see appendix C.1), which shows that the leading correction in (3.11) is cubic in r/R (with a coefficient of order $R/r_{\rm c}$).

We can now state the asymptotic behavior of the potential energy in the three specified regimes. For $r, R \ll r_c$,

$$V(r,R) = -\frac{1}{8\pi^2 M_P^2}\frac{1}{r}J$$
$$\simeq -\frac{1}{16\pi M_P^2} \times \begin{cases} \text{(I)} & \frac{1}{r} + \frac{2}{\pi}\Big(\mathcal{O}(1) + \ln\frac{r}{r_c}\Big)\frac{1}{r_c} + \mathcal{O}(1)\frac{1}{r}e^{-\sqrt{2}\frac{r}{\rho}}\,, & \rho \ll r\,, \\ \text{(II)} & \frac{\sqrt{2}}{\rho} - \frac{r}{\rho^2} + \frac{1}{r}\Big(\mathcal{O}\Big(\frac{r^3}{\rho^3}\Big) + \mathcal{O}\Big(\frac{r}{r_c}\Big) + \mathcal{O}\Big(\frac{R}{r_c}\Big)\Big)\,, & R \ll r \ll \rho\,, \\ \text{(III)} & \frac{\sqrt{2}}{\rho}H\Big(\frac{R}{r_c}\Big) + \frac{1}{r}\mathcal{O}\Big(\frac{r^3}{R^3}\Big) \times \mathcal{O}\Big(\frac{R}{r_c}\Big)\,, & r \ll R\,, \end{cases} \tag{3.13}$$

with ρ and $H\left(\frac{R}{r_c}\right)$ as defined in (3.7) and (3.12), respectively.

Thus, we see that for regions (II) and (III) the potential is proportional to $1/\sqrt{R}$, and it is weaker than the $(\frac{1}{r^2+R^2})$-potential that we would get without the DGP branes (but for sources that are still separated by R along the extra dimension), since $1/(r_c\rho) \ll 1/(r^2+R^2)$. It is also weaker than the potential in the case when only one of the two branes is removed (which has been first obtained in Ref. [71]). From (2.46), we see that such a potential would be given by

$$V^{(1B)}(r;R,0) \propto -\frac{1}{M_*^3}\frac{1}{r r_c}\arctan\frac{r}{R} \sim -\frac{1}{M_P^2} \times \begin{cases} \frac{1}{R}\,, & r \ll R\,, \\ \frac{1}{r}\,, & r \gg R\,, \end{cases} \tag{3.14}$$

with $r, R \ll \rho$. In Ref. [71] it was argued that the DGP brane acts as a kind of anti-gravity and reduces 5D gravity to 4D gravity (see also section 2.3.2). Now we find in the present work that two branes enhance this effect and further weaken gravity.

Relating to the discussion of section 2.3.2, we can infer that the effect of the branes is to introduce even stronger repulsive (anti-gravitating) image point masses. Hence, if we would consider a point mass on our brane, then the parallel brane (if it would be empty of sources) would be repelled.[3] This repulsion in our double-brane setup would be even greater than the repulsion between a brane and a point source in empty space in the original DGP setup.

3.1.2 Kaluza-Klein Description

The gravitational potential energy can be derived in the Kaluza-Klein language. The advantage of this calculation is that we can gain more insight into the system and compare the results in both languages.

[3] Of course, strictly speaking, in our present construction the branes are boundaries and hence do not respond to dynamics. However, we can switch gears and consider a situation where the mechanism that localizes a point mass on the brane dominates over the mechanism which fixes the branes to particular spacetime points.

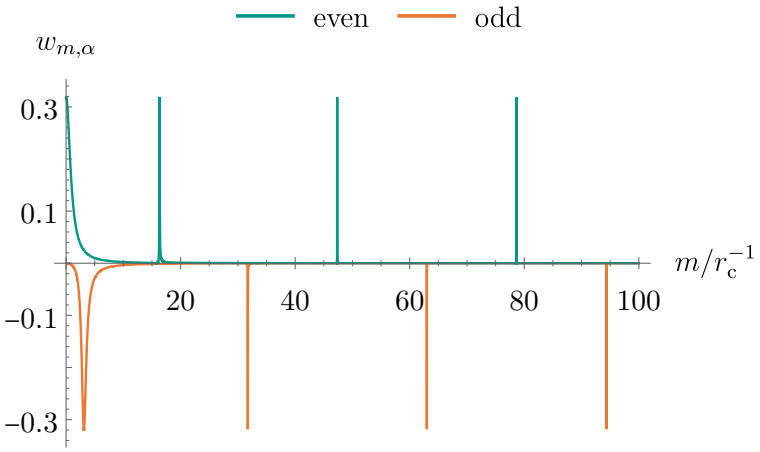

Figure 3.2: Wave profiles (given by (3.17)), with m in units of r_c^{-1} and $r_c/R = 5$. The wave profiles are non-vanishing only for certain values of m, separated by $\sim R^{-1}$ (see (3.18)). The even modes contribute to the attractive potential, while the odd modes contribute repulsively.

The potential energy between the two sources is

$$\begin{aligned} V_{\mathrm{KK}}(r,R) &= \sum_\alpha \int_0^\infty \mathrm{d}m\, \frac{1}{2} \int \mathrm{d}^3x\, \mathrm{d}^3x'\, J_{m,\alpha}(\vec{x}) G_m(\vec{x}-\vec{x'}) J_{m,\alpha}(\vec{x'})\,, \\ &= -\frac{g^2}{4\pi r} \sum_\alpha \int_0^\infty \mathrm{d}m\, w_{m,\alpha} \mathrm{e}^{-mr}\,, \end{aligned} \tag{3.15}$$

where we have used (see section 2.2.2)

$$J_{m,\alpha}(x^\mu) = g\left[\psi_{m,\alpha}\left(-\frac{R}{2}\right)\delta^{(3)}(\vec{x}) + \psi_{m,\alpha}\left(\frac{R}{2}\right)\delta^{(3)}(\vec{x}-\vec{r})\right], \tag{3.16}$$

the propagator (2.40), and defined the "wave profile"

$$\begin{aligned} w_{m,\alpha} &\equiv \psi_{m,\alpha}\left(-\frac{R}{2}\right)\psi_{m,\alpha}\left(\frac{R}{2}\right), \\ &= \begin{cases} \dfrac{1}{\pi}\left[1+\left(r_c m + \tan\left(\dfrac{mR}{2}\right)\right)^2\right]^{-1}, & \alpha = \text{even}\,, \\ -\dfrac{1}{\pi}\left[1+\left(r_c m - \cot\left(\dfrac{mR}{2}\right)\right)^2\right]^{-1}, & \alpha = \text{odd}\,, \end{cases} \end{aligned} \tag{3.17}$$

which has been plotted in Figure 3.2.

We observe that the wave profiles quickly tend to zero, except for distinct "peaks" (of height $1/\pi$) at certain values of m. The smaller R/r_c, the wider the peaks are apart. These distinct peaks result from the fact that the wave profiles have to satisfy certain matching conditions at the branes, and it makes sense that for less distant branes there are also less modes (or peaks) in a certain m-interval.

Hence, the modes that contribute effectively to the potential are discrete. For $m \gg r_{\rm c}^{-1}$, only those modes contribute for which

$$\begin{aligned} &\text{even:} \qquad \left|\tan\left(\frac{mR}{2}\right)\right| \gg 1 \Rightarrow m \sim \frac{\pi}{R}(2n-1)\,, \\ &\text{odd:} \qquad \left|\cot\left(\frac{mR}{2}\right)\right| \gg 1 \Rightarrow m \sim \frac{2\pi}{R}n\,, \end{aligned} \tag{3.18}$$

with $n \in \mathbb{N}$. Of course, the Yukawa-suppression factor in (3.15) determines which of those discrete modes eventually survive and contribute to the resulting potential.

Another interesting observation is that the even wave profile invariably contributes positively (and hence to the attractive gravitational potential), while the odd wave profile always contributes negatively (and hence adds a repulsive part to the gravitational potential).

Now we want to see how these wave profiles conspire together, so that the potential turns out to be the same as in the 5D description. Unfortunately, in the KK picture it is very difficult to approximate the integral (3.15) in all but the case (I).

We have to solve

$$V_{\rm KK}(r,R) = -\frac{g^2}{4\pi^2}\frac{1}{r r_{\rm c}}(J_{\rm even} - J_{\rm odd})\,, \tag{3.19}$$

with

$$J_{\rm even} = \int_0^\infty {\rm d}x\, \frac{{\rm e}^{-\frac{r}{r_{\rm c}}x}}{1+\left[x+\tan\left(\frac{1}{2}\frac{R}{r_{\rm c}}x\right)\right]^2}\,, \tag{3.20a}$$

$$J_{\rm odd} = \int_0^\infty {\rm d}x\, \frac{{\rm e}^{-\frac{r}{r_{\rm c}}x}}{1+\left[x-\cot\left(\frac{1}{2}\frac{R}{r_{\rm c}}x\right)\right]^2}\,. \tag{3.20b}$$

Let us first consider case (I): both integrals are cut off at $r_{\rm c}/r$. The result of the integrals crucially depends on the interplay between the two terms in the square-bracket of the denominator. In $J_{\rm even}$, the tangent is always sub-dominant, so

$$J_{\rm even} \sim \int_0^{\frac{r_{\rm c}}{r}} {\rm d}x\, \frac{1}{1+x^2} = \arctan\frac{r_{\rm c}}{r} \sim \frac{\pi}{2} - \frac{r}{r_{\rm c}} + \mathcal{O}\left[\left(\frac{r}{r_{\rm c}}\right)^3\right]. \tag{3.21}$$

In $J_{\rm odd}$, the two terms in the square-bracket become of the same order for $x \sim x_*$, with

$$x_* \equiv \sqrt{2}\frac{\rho}{R}\,. \tag{3.22}$$

But in the case (I), $x_* \gg r_{\rm c}/r$, so the cotangent always dominates, and we find

$$J_{\rm odd} \sim \frac{1}{4}\frac{R^2}{r_{\rm c}^2}\int_0^{\frac{r_{\rm c}}{r}} {\rm d}x\, x^2 = \frac{1}{12}\frac{R}{r}\frac{\rho^2}{r^2}\,. \tag{3.23}$$

Hence, the leading contribution to the potential comes from $J_{\rm even}$, and we recover the same result (for the leading order) as in the 5D description.

Now, let us turn to case (II). In J_{even}, the tangent is still sub-dominant. However, in J_{odd} the story changes. Now $x_* \ll r_c/r$, and hence for $x \sim x_*$, the terms in the square-bracket cancel each other, and the integrand has a finite contribution in that integration interval. We were not able to approximate the result analytically, but numerical calculations show that, in the leading approximation (where we take $e^{-\frac{r}{r_c}x} \cong 1$), J_{odd} goes to the same value as J_{even}. Hence, up to (at least) second order, the corresponding first peaks (see Figure 3.2) cancel each other and the resulting potential energy vanishes.

If we examine (3.20a) and (3.20b) more closely (taking into account the Yukawa-suppression factor), we find that the first peak of J_{even} and J_{odd}, respectively, together contribute the same leading factor ρ^{-1} that we found in the 5D calculation. We can interpret this result as if those modes that contribute to the repulsive potential (belonging to the first odd peak) counteract the modes that contribute to the attractive potential (belonging to the first even peak) and thus weaken gravity.

In case (III), the square-brackets in the denominators go to zero multiple times, so many of the peaks contribute to the result. A numerical analysis again shows that we recover the leading behavior of (3.11).

3.2 Force Along the Brane

Although the potential (3.13) is R-dependent, the sources in our scenario are, per construction, localized on the brane, so nothing can move into the bulk (except the graviton itself). Stated differently, every force that is orthogonal to the brane is compensated by the force that is responsible for localizing the matter on the brane. Hence, in the following section, we will be interested in the force along the r-direction.

We find

$$\begin{aligned} F_{\text{r}} &\equiv -\frac{\partial V(r,R)}{\partial r} \\ &\simeq -\frac{1}{16\pi M_{\text{P}}^2} \times \begin{cases} \text{(I)} & \dfrac{1}{r^2} + \mathcal{O}\Big(\dfrac{1}{r\rho}\Big) e^{-\sqrt{2}\frac{r}{\rho}} + \mathcal{O}\Big(\dfrac{1}{r r_c}\Big), & \rho \ll r\,, \\ \text{(II)} & \dfrac{1}{\rho^2} + \dfrac{1}{\rho^2}\mathcal{O}\Big(\dfrac{r}{\rho}\Big) + \dfrac{1}{r^2}\mathcal{O}\Big(\dfrac{R}{r_c}\Big), & R \ll r \ll \rho\,, \\ \text{(III)} & \dfrac{1}{R^2}\mathcal{O}\Big(\dfrac{r}{R}\Big) \times \mathcal{O}\Big(\dfrac{R}{r_c}\Big), & r \ll R\,. \end{cases} \end{aligned} \tag{3.24}$$

The exact force (i.e. the numerical solution) is shown in Figure C.2 (or rather its modulus in units of $G/(2R^2)$), where we also plotted the analytical approximations in the corresponding regimes, given in (3.24).

We see that the following picture emerges. Let us assume that we are an observer who can be approximated by a static point source with mass m, living on "our" brane at $y = 0$. Now imagine there is a different static point source with mass M, located on the parallel brane, at the location $y = R$ and $\vec{r} = 0$. We start on our brane at $\vec{r} = 0$ and probe the gravitational force along the spatial

dimensions of our world. If we started increasing the worldvolume distance r, we would measure a linearly growing force, which would be suppressed by $\mathcal{O}\left(\frac{r}{R}\right)$ (with respect to regime (II)), as long as we stayed within the region $r \ll R$. However, if we measured again at $R \ll r \ll \rho$, we would determine the constant force $F_{\rm r} = -\frac{GMm}{2\rho^2}$. Finally, for $r \gg \rho$, we would measure the same (or rather 1/2) 4D force $F_{\rm r} = -\frac{GMm}{2r^2}$ as if the second point source were located on our brane and there were no extra dimensions.

We would like to emphasize that this force behaves differently than both the standard 5D force and the 4D force found in the original single-brane setup [71]. In particular, the emergence of regime (II), giving rise to the spatially constant force, is a special feature of the present double-brane scenario. Let us explicitly compare the newly discovered force to the following two other scenarios involving 3-branes embedded in a 5D spacetime. One scenario is that a point source is located outside our 3-brane along the extra dimension, but it is located either in empty space or on a brane that does not contain a DGP term (responsible for quasi-localizing gravity). Note that we should still assume that we live on a 3-brane because otherwise it would not be reasonable to consider the force along the r-direction, since nothing would keep us on a hypersurface with fixed y. Moreover, without brane localization, our world would be truly five-dimensional, which is experimentally ruled out. We also assume that our brane is a DGP brane (i.e. containing a localized curvature term) in this scenario, which we therefore call *1B*.

The second scenario is similar to the first but additionally assumes that *our* brane does not contain a DGP term. This is, of course, also observationally excluded because we know that gravity behaves four-dimensional, but let us consider this scenario for illustrative purposes, anyway. We call this second scenario *0B*.

In scenario 0B, if two point sources were separated by a distance R along the extra dimension, then the potential would be given by $\propto -\frac{1}{M_*^3}\frac{1}{r^2+R^2}$, and the force along our brane would be[4]

$$F_{\rm r}^{(0{\rm B})} \propto -\frac{1}{M_*^3}\frac{r}{\left(r^2+R^2\right)^2}\,. \tag{3.25}$$

In scenario 1B, which was considered in Ref. [71], with two point sources again separated by a distance R along the extra dimension, the potential is (see (2.46)) $\propto -\frac{1}{M_{\rm P}^2}\frac{1}{r}\arctan\frac{r}{R}$, leading to a force along our brane of the form

$$F_{\rm r}^{(1{\rm B})} \propto -\frac{1}{M_{\rm P}^2}\left(\frac{\arctan\frac{r}{R}}{r^2} - \frac{\frac{R}{r}}{r^2+R^2}\right). \tag{3.26}$$

Both forces, $F_{\rm r}^{(0{\rm B})}$ and $F_{\rm r}^{(1{\rm B})}$, have a linear regime (for $r \ll R$) and a regime (for $r \gg R$) where they approach the 5D ($\propto -1/r^3$) and 4D ($\propto -1/r^2$) Newton's law, respectively, with the transition scale at $r \sim R$. However, they lack the spatially constant regime exhibited by the force (3.24), which is present if both branes contain a DGP term. We display the three scenarios, just discussed, in Figure 3.3. The forces are given in units of $(M_{\rm P}R)^{-2}$ and are additionally normalized such that

[4]We neglect here, and in the following discussion, the prefactors involving π's and other numerical constants.

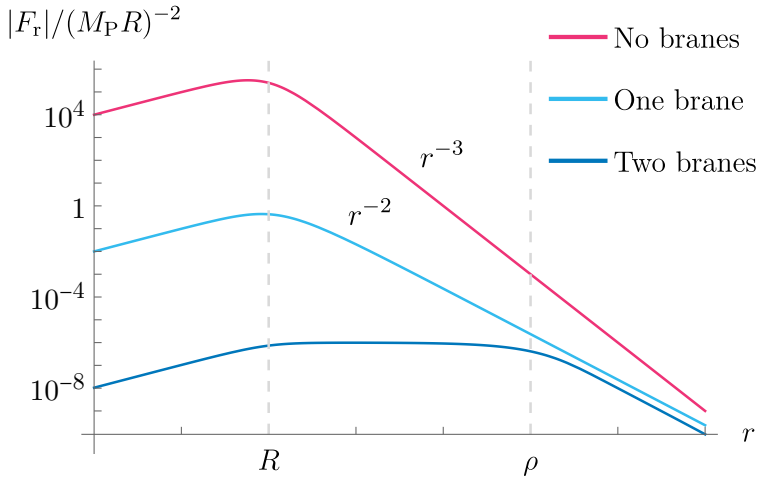

Figure 3.3: Log-log plot of the forces $F_r^{(0B)}$ (magenta), $F_r^{(1B)}$ (light blue), and F_r (dark blue), given in (3.25), (3.26), and (3.24), respectively. The forces are plotted in units of $(M_P R)^{-2}$ and are normalized such that their numerical coefficient in the linear regime (III) is unity. Thus, all three forces are given by $\frac{r}{r_c}$ for $r \ll R$, but the scaling with r_c/R is different, namely $F_r^{(0B)} \propto (r_c/R) F_r^{(1B)} \propto (r_c/R)^2 F_r$. The functions are plotted for $r_c/R = 10^6$. We see that $F_r^{(0B)}$ and $F_r^{(1B)}$ change to an (r^{-3})- and an (r^{-2})-behavior, respectively, at $r \sim R$. This behavior extends to region (I) ($\rho \ll r \ll r_c$). In contrast, the force F_r, found in the case of two parallel DGP branes, exhibits a constant regime (II) ($R \ll r \ll \rho$), before it assumes the same (r^{-2})-behavior as $F_r^{(1B)}$, in region (I).

they all have the same numerical prefactor (unity) in the linear regime, which is done for clarity of presentation (these factors are almost invisible in the log-log plot, anyway, and they depend on how we normalize the standard Newton force). We clearly see that all three forces have a linear regime, but whereas the other two forces change immediately (at R) to the 4D and 5D regimes, "our" force has a constant region (whose size depends on the ratio r_c/R). The forces have constant offsets, with respect to each other, in this log-log plot because they satisfy the relation $F_r^{(0B)} \sim (r_c/R) F_r^{(1B)} \sim (r_c/R)^2 F_r$. This is as expected, since our double-brane force is weaker than the original DGP force, which is itself weaker than the 5D force, as we already pointed out in section 3.1.1.

Now, it is intriguing that in the scenario with two DGP branes, a spatially constant attractive force emerges, beyond the length scale R. Let us entertain the possibility for a moment that this force could compensate the decreasing force (as we increase r) originating from the baryonic matter on our brane (in our present scenario, this baryonic matter would constitute a galaxy, centered around $\vec{r} = 0$). Then, one might hope that such a scenario could explain the fact that the gravitational force being exerted from, say, the interior of our galaxy, is stronger than the baryonic mass distribution would imply (as discussed in section 1.1), without the need of postulating the presence of DM on our brane.

In the regime $R \ll r \ll \rho$, the mass M of the source on the second brane has to be much larger than the enclosed baryonic matter on our brane, so that the constant force can compete with the baryonic Newton force. In other words, one

is forced to take

$$M \sim M_{\rm b}(r_*)\left(\frac{\rho}{r_*}\right)^2 \gg M_{\rm b}(r_*)\,, \tag{3.27}$$

where $M_{\rm b}(r_*)$ denotes the enclosed baryonic mass at the radius r_*, at which the baryonic Newton force starts to decrease. One also has to assume $r_* \gtrsim R$ (in the following, we will consider the lower bound in order to maximize the size of the region where the constant force dominates), so that the constant force does not spoil the observations that are compatible with the usual baryonic Newton force for $r \lesssim r_*$.

In this scenario, the constant force would dominate at the outer galactic region, and the angular velocities of orbiting objects would go like $v(r) \propto \sqrt{r}\sqrt{GM}/\rho$. Although this behavior is not observed in more massive galaxies, where the rotation curves tend to become flat, there exist claims in the literature that in LSB galaxies the circular velocities at large radii scale as $\propto \sqrt{r}$ [142] or even $\propto r$ [143] (see also e.g. Refs. [144, 145]).

Note that for the validity of the above-outlined scenario we have to check if the Newton force between the baryonic matter on our brane and the observer would not be modified by the parallel brane in a severe way. For this, we can again approximate the baryonic matter as a point mass and calculate the potential energy, as given in (3.30), where r is the distance between the point sources. The integral one has to evaluate is even more involved than the one we considered previously. Hence, the analysis is carried out numerically and displayed in appendix C.2. We see (from Figure C.5) that the Newton force is unchanged for $r \ll \rho$ (regimes (II) and (III)).[5] For $\rho \ll r \ll r_{\rm c}$, the force crosses over to an equivalent Newton force with one half its value. This can be understood by noting that, in this region, the observer is at such a large distance that the two branes appear to lie on top of each other, and hence $r_{\rm c} \to 2r_{\rm c}$ (see also footnote 2 in appendix C). Since after r_* ($\ll \rho$) the Newton force falls off, the proposed scenario remains valid. Figure 3.4 summarizes the above statement, by comparing the "baryonic" force to the "dark" force (which is due to the point source on the parallel brane). We fixed the mass of the "baryonic" point source to be

$$M_{\rm b} = \frac{M}{2}\left(\frac{R}{\rho}\right)^2 = \frac{M}{2}\frac{R}{r_{\rm c}}\,, \tag{3.28}$$

where M is the mass of the "dark" point source on the parallel brane, such that the asymptote of the "dark" force in regime II is equal to the "baryonic" force at $r = R$. We see from Figure 3.4 that in this scenario, for $r \ll R$ (the interior of our galaxy), the usual baryonic force is much larger than the dark force. However, for $r \gtrsim R$, the constant dark force takes over.

[5] Although we actually plotted there not the force but the quantity $\propto rV_{\rm b}(r)$, the force will also stay unchanged across R (see also Figure 3.4). One should contrast this to the "dark" force, discussed before, where the force in r-direction does change its scaling across R, although the potential does not change its leading behavior in this region. The difference is due to the fact that, up to leading order, $V_{\rm b}$ depends on r in that region, while the leading term in V does not (and hence deriving with respect to r removes this term).

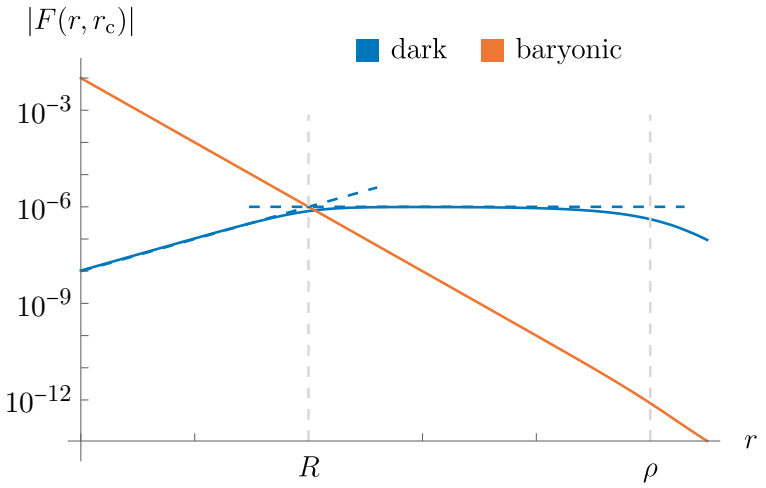

Figure 3.4: Log-log plot of the (norm of the) force along the brane, as a function of r (in units of R). The "dark" force (due to a point source with mass M on the parallel brane), expressed in units of $(GMm)/(2R^2)$ (which is just $-f$ from (C.2)), is plotted as the blue solid curve. The blue dashed curves are its asymptotes in regimes (III) and (II), given by $\frac{r}{r_c}$ and $\frac{R}{r_c}$, respectively. The orange curve shows the "baryonic" force (due to a point source on our brane), expressed in the same units. The "baryonic" force is obtained numerically from (C.3), with $F_b = -\frac{\partial}{\partial r} V_b$ (cf. footnote 1 in appendix C). Note that we reintroduced the point source masses and took $M_b = MR/(2r_c)$ (see (3.28)). We did not plot the asymptote $\sim 1/r^2$ because, in the regime $r \ll \rho$, it is indistinguishable from F_b. The point mass that gives rise to F_b is chosen such that both forces are of the same order at $r = R$. We chose the ratio $r_c/R = 10^6$.

It should be emphasized that the above distance-independent force was derived for a *point* source at the second brane. Thus, it could be interesting to take an extended source and investigate how the asymptotic circular velocities would be affected. It has been pointed out [146] that there is a substantial diversity in the rotation curves in LSB galaxies. This diversity might be explained by varying mass distributions on the parallel brane. Since in the present scenario only the parallel brane would contain this "dark" matter distribution, the latter does not have to be weakly interacting, but could even form a highly localized density distribution.

Let us estimate, very crudely, the values of the involved length scales, such that the above-outlined scenario can be valid. If we wish the distance-independent force to be operational at $r \gtrsim 1\,\text{kpc}$, we should choose $R \sim 1\,\text{kpc}$. If we then want this regime to hold up to at least $r \gtrsim 10^2\,\text{kpc}$, we should take

$$\rho \gtrsim 10^2\,\text{kpc}$$

because for $r \gtrsim \rho$ the potential drops and the angular velocities would start to decrease. Since there is the constraint $r_c \gtrsim H_0^{-1} \sim 10^6\,\text{kpc}$, where H_0 is the *Hubble constant*, from cosmological observations [147] (see also the discussion in chapter 5), we actually require $\rho \gtrsim 10^3\,\text{kpc}$, which is significantly larger than the size of the galaxy. This constraint, however, does not necessarily imply that the constant force should extend to galaxy cluster scales because our analysis shows that the constant force gets corrections as r approaches ρ. For example, from Figure 3.4,

we see that this force starts to deviate from its constant behavior for $r \gtrsim 10^2\,\mathrm{kpc}$ if we take $\rho = 10^3\,\mathrm{kpc}$. A more detailed investigation is needed in order to establish the exact behavior of this new force at those large scales. Moreover, the results have to be compared to predictions made by the standard CDM scenario and to observations. Such an analysis has to be postponed to future work.

Let us finally note that if the above scenario is valid, we have to ask the question why the mass on the parallel brane is so tightly related to the mass in the "baryonic" galaxy, as seen from (3.27). This question should then be addressed in the investigation of galaxy formation.

3.3 Decoupling the Second Brane

We now want to consider two static point sources on our brane (but still in the presence of the parallel brane). For convenience, we will position our brane at $y = 0$, while the parallel brane is shifted to $y = R$ (so the distance between the branes remains R), by performing an appropriate shift of coordinates. Also, since both sources are now located at $y' = y = 0$, we only need the expression $\overline{G}(|\vec{k}|; 0, 0)$ (that we get after shifting the coordinates in (2.31)), which reads

$$\overline{G}(|\vec{k}|; 0, 0) = -\frac{1}{|\vec{k}|}\frac{2 + r_\mathrm{c}|\vec{k}|}{(2 + r_\mathrm{c}|\vec{k}|)^2 - r_\mathrm{c}^2|\vec{k}|^2\,\mathrm{e}^{-2|\vec{k}|R}} + r_\mathrm{c}\frac{\mathrm{e}^{-2|\vec{k}|R}}{(2 + r_\mathrm{c}|\vec{k}|)^2 - r_\mathrm{c}^2|\vec{k}|^2\,\mathrm{e}^{-2|\vec{k}|R}}\,. \tag{3.29}$$

The potential energy is

$$V(r) = g^2 \int \frac{\mathrm{d}^3\vec{k}}{(2\pi)^3}\,\mathrm{e}^{\mathrm{i}\vec{k}\cdot\vec{r}}\,\overline{G}(|\vec{k}|; 0, 0)\,. \tag{3.30}$$

In the limit $R \to \infty$, the propagator becomes

$$\overline{G}(|\vec{k}|; 0, 0)|_{R\to\infty} = -\frac{1}{|\vec{k}|}\frac{1}{2 + r_\mathrm{c}|\vec{k}|}\,, \tag{3.31}$$

which is the same as in the case with only one single brane. This can be seen by comparing to (2.33), with $y = y' = 0$. Hence, for $R \to \infty$, we find the same result for the potential energy as in Ref. [64]:

$$V(r)|_{R\to\infty} = -\frac{g^2}{2\pi^2}\frac{1}{r r_\mathrm{c}}F_\mathrm{DGP}(r)\,, \tag{3.32}$$

where $F_\mathrm{DGP}(r)$ is again given by (2.25).[6] Thus, we find that a second brane, together with its induced kinetic term, has no influence on gravity in our world if the brane is far away.

[6] If one doubts that (3.31) is a good approximation because values for $k \to 0$ enter the integral in (3.30), one can take the full propagator $\overline{G}(|\vec{k}|; 0, 0)$ and approximate the resulting potential energy. We find that in the regime $r, r_\mathrm{c} \ll R$ (for an arbitrary hierarchy between r and r_c) the potential approaches indeed (3.32). For the regime $r \ll R \ll r_\mathrm{c}$, the Newtonian limit ($r \ll r_\mathrm{c}$) of (3.32) is recovered. Also note that the numerical prefactor of (3.32) can differ, due to a different normalization, which can be absorbed in the coupling g (see also the comment below (3.3)).

In the previous discussion, we considered identical induced kinetic terms on the two branes, by taking an equal length scale r_c for them. However, we can reproduce an equivalent conclusion if we consider the theory

$$S = \int \mathrm{d}^4x\,\mathrm{d}y \left\{ \frac{1}{2}(\partial_A \Phi)^2 + [r_c\delta(y) + \tilde{r}_c\delta(y-R)]\frac{1}{2}(\partial_\mu \Phi)^2 + J(x^\mu, y)\Phi \right\}, \quad (3.33)$$

where, in general, $r_c \neq \tilde{r}_c$. Performing the same steps that led to (2.31), we now find

$$\overline{G}(|\vec{k}|;0,0) = \frac{1}{|\vec{k}|}\frac{2+\tilde{r}_c|\vec{k}| - \tilde{r}_c|\vec{k}|\,\mathrm{e}^{-2|\vec{k}|R}}{(2+\tilde{r}_c|\vec{k}|)(2+r_c|\vec{k}|) - r_c\tilde{r}_c|\vec{k}|^2\,\mathrm{e}^{-2|\vec{k}|R}}\,, \quad (3.34)$$

which again reduces to (3.31) in the limit $R \to \infty$.[7]

3.4 Consistency With Black Hole Physics and Interpretation in Terms of Particle Species

In this last section, we want to use our findings to discuss some implications for the present system, imposed by the consistency with BH physics. Although the existence of BHs (and their exact form) in the DGP setup has not yet been conclusively established,[8] the following discussion will be based on the assumption that, for distances $r \ll r_c$, there should exist BHs in the DGP model that have the same properties as the standard 4D BHs in GR.

3.4.1 Classically Static Configuration

In Ref. [85], several scenarios (in the context of the ADD model) have been investigated where a BH, seemingly, could not evaporate into the species localized on one or more branes because its size was smaller than the distance to those branes. It has been found that all of those scenarios corresponded to time-dependent configurations. It was shown that a (classically) static configuration was only reached, after the BH has accreted all the branes (or had evaporated altogether) and henceforth could evaporate into all species. This was interpreted as a "democratic transition" from a "Non-Einsteinian" BH (meaning that it is not the usual time-independent, universally evaporating BH, derived from GR) to a time-independent, semi-classical BH.

Now we want to apply that investigation to our present setting. Let us consider a BH that is localized on "our" brane, in the presence of a parallel brane that has some species localized on it, which are not localized on our brane. In the situations of Ref. [85], the tension of the branes was the key property in deriving the gravitational interaction between the branes and the BH and discovering the "accretion" mechanism. However, in our scenario, the branes are tensionless, so one might naively suspect that they would not interact with a BH on our brane.

[7] It is simpler to derive this propagator from (2.29) (with the shifted branes and unequal cross-over scales) if one immediately fixes the first source at $y' = 0$.

[8] For some discussions, see Refs. [130, 133].

But we showed in section 2.3.2 that the branes in our scenario, due to their DGP term, would react to a present mass source, such as a BH, by repelling it. Thus, unless we treat the branes as fixed boundaries, our configuration would be also time-dependent.

It goes beyond the scope of this thesis to investigate if a static configuration can be reached and to determine the time scale. However, the fact that the second brane does not influence us if it is very far away (see section 3.3) suggests that there is at least the trivial static configuration where the second brane is sent to infinity. In this case, there could be a situation where a BH on our brane cannot evaporate into the species on the parallel brane.

This result differs from the one in the ADD case, and it seemingly tells us that in the DGP scenario a BH that does not evaporate universally into all species does not have the tendency to "democratize" its evaporation.

However, it is subtle to adopt such an interpretation. For the authors of Ref. [85] to interpret the evolution towards time-independence (the accretion of the branes) as the evolution towards democratization, driven by the presence of the localized species on the distant branes, it was crucial to note the following relation: since in a general coordinate invariant setup the branes have a dynamical origin (they are domain walls, instead of being merely boundary conditions), they must have a tension, which then will excite particles (even without additionally localized bulk fields). Hence, an attraction between a BH and the branes is always accompanied by the presence of localized species on the latter. In our setup, however, the branes were originally introduced as boundaries, and hence they can be tensionless.

Thus, our result could indicate that in the DGP brane-world an interpretation in terms of species has its limits. Alternatively, the species picture could be trying to tell us that our construction of two distant DGP branes is not consistent. For example, it might be the case that it is not possible to localize different species on the two branes in such a way.

Another possibility is that this apparently qualitatively different behavior than in Ref. [85] is an artifact of our simplified scalar field prototype theory. As mentioned in the beginning of section 2.1, the general coordinate invariance in the DGP model, and in particular its translational invariance along the extra dimension, is best observed if one does not fix the position of the brane/s but employs the full gauge redundancy to transform between different positions. This, in turn, is associated with the brane bending mode. Hence, if one analyzes the full spin-2 theory, it is conceivable that the brane bending mode will restore a similar behavior in the present setup as the one observed in Ref. [85]. Such an investigation is beyond the scope of this thesis.

3.4.2 Dependence of the Cross-Over Scale on the Number of Species

As explained in section 1.1.2, in theories that tend to GR in the IR, consistency with BH physics requires a bound on the cutoff of semi-classical gravity. This bound

depends on the number of particle species in the theory.[9] Now, in our scenario, the situation is somewhat different. We consider a model that goes to GR at short distances but not at large distances. However, it is possible to derive a similar bound in our case if one assumes the existence of ordinary BHs. Furthermore, postulating the equality of the cutoffs for a 5D and a 4D observer, leads to an interesting relation between the cross-over scale and the number of species. In the following, we will reproduce the derivation given in Ref. [136].

If the existence of the standard 4D BH with Schwarzschild radius

$$r_{\rm g} = \frac{M}{M_*^3 r_{\rm c}} = \frac{M}{M_{\rm P}^2}\,,$$

for length scales $r < r_{\rm c}$, is assumed, one can derive the same bound for a 4D observer as in (1.5),

$$\Lambda \lesssim \frac{M_{\rm P}}{\sqrt{N}}\,,$$

where Λ is the cutoff of semi-classical gravity and N is the number of localized species on the brane. Let us, for definiteness, consider the case that we can have a semi-classical BH of a size all the way down to $\sqrt{N}/M_{\rm P}$. Then, the highest possible cutoff will be

$$\Lambda_{\rm max} = \frac{M_{\rm P}}{\sqrt{N}}\,.$$

Although, in principle, this cutoff could be independent of the cutoff for the 5D bulk observer (who only sees one species), the authors in Ref. [136] explore the possibility that they are the same, so $\Lambda_{\rm max} = M_*$. Since $r_{\rm c} \equiv M_{\rm P}^2/M_*^3$, this leads to

$$N = r_{\rm c} M_*\,. \tag{3.35}$$

If we accept the relation (3.35), we see that, for fixed M_* in the bulk, the number of localized particles is

$$N = \frac{M_{\rm P}^2}{M_*^2}\,, \tag{3.36}$$

and hence, from this point of view, is responsible for the strength of gravity on the brane.

On the other hand, we saw in our discussion in section 3.3 that if the second brane is separated far enough, then no matter how strong gravity is on that brane, it will not affect the gravitational laws in our world. Hence, the above assumption of the equality of 5D and 4D cutoffs of semi-classical gravity leads to an interesting observation: even if there is a very high number of species in the theory (but localized on a different brane), it does not alter the cutoff of semi-classical gravity in our universe. This is, again, an implication that differs from the situation in models where there is a normalizable zero-mode of the graviton.

[9] A similar relation as (1.5) can also be derived on perturbative grounds, using that the graviton propagator will get radiative corrections from the N fields [28, 148]. However, we want to emphasize that the perturbative argument is, in fact, a naturalness argument, since the radiative corrections could cancel each other, whereas the non-perturbative (BH) argument leads to a consistency limit.

3.5 Summary and Discussion

We have investigated the modification of the original DGP setup [64] due to the addition of a second 3-brane with a localized curvature term, parallel to the brane where our SM fields are localized. We have shown that the potential energy between two static point masses exhibits similar properties as in the original DGP setup, but it also acquires a qualitatively different behavior. By calculating the potential energy between two point masses on different branes, in the regime where the cross-over scale r_c is much bigger than the 4D distance r and the brane separation R, we found that a new length scale emerges, namely $\rho = \sqrt{Rr_c}$. For $\rho \ll r$, the (leading contribution of the) potential energy goes like $1/r$, while for $r \ll \rho$, it scales as $1/\sqrt{R}$. Thus, we found that in the presence of the branes, 5D gravity is screened. Although a screening was already observed in Ref. [71] for one brane, we established that the addition of the second brane weakens gravity still further, so it behaves even weaker (for $r \ll \rho$) than four-dimensional.

Taking into account higher-order contributions to the potential, we found a linear r-dependence in the region $R \ll r \ll \rho$. Hence, if we consider the force along the 3-brane, there is a spatially constant attractive force between the point masses. This constant force, being exerted from matter sources on the parallel brane, can lead to circular velocities of objects, orbiting e.g. the center of our galaxy, that do not decrease but rather slightly increase. This might be phenomenologically interesting for LSB galaxies, as it suggests that an explanation of the observed rotation curves might be possible without introducing DM on our brane. It may be worthwhile to consider extended sources on both branes and to investigate, in a future work, how the potential energy behaves and hence what rotation curves can be obtained. Moreover, much work remains to be done in order to derive the cosmological implications and the viability, on all relevant scales, of a scenario where DM (with the standard CDM properties) on our brane is replaced by matter distributions (with potentially much different behavior than in the standard CDM paradigm) on a parallel brane.

We derived the potential energy in two different ways: we calculated it in five dimensions and derived an expression in terms of KK modes, after performing the dimensional reduction. In the KK picture, we showed that the even modes contribute only to the attractive potential, while the odd modes contribute only to the repulsive part, and thus weaken gravity.

Finally, we have considered the limiting case where the second brane is sent far away ($R \gg r_c$). In this case, the laws of gravity on our brane behave like in the original DGP scenario and are not influenced by the presence of another brane. If one assumes the existence of BHs at distances $r \ll r_c$ and adopts a species-viewpoint, this result is interesting for the following reasons. A BH on our brane will just evaporate into species localized on our brane. The strength of the gravitational potential and the cutoff of semi-classical gravity in our universe are not altered by the (possibly large) number of species on the distant brane. This suggests that either the usual bound on the number of species has limited applicability for a DGP-type model or that the species-viewpoint points to an inconsistency in our

assumed construction of two DGP branes, including the potential inconsistency of neglecting the brane bending mode for this discussion.

To gain more insight, one could investigate, in a future work, how a classically static configuration (where the second brane is at a finite distance) might be achieved in the presence of the branes and their repulsive nature. Would the BH also attempt to accrete the other brane, as in Ref. [85]?

4

The Casimir Effect

In this chapter, we will show that the DGP branes give rise to (effective) boundary conditions for the gravitational field and hence lead to the (gravitational) Casimir effect. We will also see that the Casimir force is modified with respect to the standard result that is derived for Dirichlet boundary conditions on parallel plates. We will continue to work with the simplified theory (2.27), which describes only one propagating (scalar) degree of freedom, instead of the five propagating degrees of freedom (scalar, vector and tensor) of the full-fledged DGP theory (or rather its generalization with two branes). However, the standard Casimir effect is qualitatively the same for all bosonic fields (see e.g. Ref. [149] for spin-0 and spin-1 and Refs. [150, 151] for spin-2), with the different numbers of degrees of freedom just affecting the numerical factor of the result. As we will show, the modification of our derived Casimir effect is entirely due to the special mass quantization that results from the presence of the branes. Hence, we do not expect differences for higher-spin fields, besides the usual factors accounting for the differing degrees of freedom (see also section 4.4 for more commentary on this issue).

In the present chapter, we will work (exclusively) in the KK picture, since it is elucidating to observe how the Casimir effect follows from the particular structure of the quantized masses of the KK modes. For the derivation, it will prove useful to work with the regularized system, as depicted in Figure 2.1, and only at the end send the size of the extra dimension to infinity. In the next section, we will derive the vacuum energy of this system.

This chapter is based on Ref. [2] and is, to a large extent, a verbatim reproduction, with minor modifications.

4.1 Vacuum Energy

As shown in section 2.2.2, the KK modes satisfy (2.44), with masses given by the solution of the transcendental equation (2.43). Using a finite 3-volume on the brane, with size V, and periodic boundary conditions,[1] the solutions to (2.44) can be quantized in the standard way, leading to

$$\widehat{\phi}_{m,\alpha} = \frac{1}{\sqrt{V}} \sum_{\vec{k}} \frac{1}{\sqrt{2\omega_{m,\alpha}(\vec{k})}} \left(\widehat{a}_{m,\alpha}(\vec{k}) \mathrm{e}^{-\mathrm{i}\left(\omega_{m,\alpha}(\vec{k})t - \vec{k}\cdot\vec{x}\right)} + \widehat{a}^{\dagger}_{m,\alpha}(\vec{k}) \mathrm{e}^{\mathrm{i}\left(\omega_{m,\alpha}(\vec{k})t - \vec{k}\cdot\vec{x}\right)} \right),$$

with

$$\omega_{m,\alpha}(\vec{k}) = \sqrt{|\vec{k}|^2 + m_\alpha^2}\,, \qquad k_i = \frac{2\pi n_i}{V^{1/3}}\,, \quad n_i = 0, \pm 1, \ldots \tag{4.1}$$

and the canonical commutation relations

$$\left[\widehat{a}_{m,\alpha}(\vec{k}), \widehat{a}^{\dagger}_{m',\alpha'}(\vec{k'}) \right] = \delta_{\vec{k},\vec{k'}} \delta_{m,m'} \delta_{\alpha,\alpha'}\,, \quad \text{(all others zero)}\,.$$

The Hamiltonian is then given by

$$\widehat{H} = \sum_{\alpha} \sum_{m} \sum_{\vec{k}} \omega_{m,\alpha}(\vec{k}) \left(\widehat{a}^{\dagger}_{m,\alpha}(\vec{k}) \widehat{a}_{m,\alpha}(\vec{k}) + \frac{1}{2} \right),$$

and the vacuum energy per unit 3-volume (i.e. the vacuum energy density measured by a brane-observer) is

$$E = \frac{1}{V} \langle 0 | \widehat{H} | 0 \rangle = \frac{1}{V} \sum_{\alpha} \sum_{m} \sum_{\vec{k}} \frac{\omega_{m,\alpha}(\vec{k})}{2}\,.$$

Let us now go to the limit of an infinitely large 3-brane ($V \to \infty$). Then, we can replace

$$\frac{1}{V} \sum_{\vec{k}} \leftrightarrow \int \frac{\mathrm{d}k_1\, \mathrm{d}k_2\, \mathrm{d}k_3}{(2\pi)^3}$$

and find

$$E = \frac{1}{4\pi^2} \sum_{\alpha} \sum_{m} \int_0^\infty \mathrm{d}k\, k^2 \omega_{m,\alpha}(\vec{k})\,.$$

Of course, this quantity is divergent because we are integrating over all momenta and summing over the full KK tower of masses. In order to regularize this expression, we will use the scheme of cutoff regularization (there is a vast amount of literature on different regularization schemes; see e.g. Ref. [149]) and introduce the exponential cutoff

$$\exp\left[-\omega_{m,\alpha}(\vec{k}) \frac{a}{\pi} \right].$$

Thus, we are cutting off the high frequencies at the frequency $\sim a^{-1}$. We can interpret this in an analogous way to the standard calculation of the vacuum energy

[1] We use here the box normalization on the 3-brane just for clarity and will take the limit of the infinite-size box shortly.

between two conducting plates in the presence of an electromagnetic field. There, the plates are not expected to provide Dirichlet boundary conditions for the photon at frequencies much larger than the plasma frequency of the plates. Here, we also expect the effective Lagrangian (2.27) to be valid only for distances larger than a. Therefore, the regularized vacuum energy is

$$E^{\text{reg}} = \frac{1}{4\pi^2} \sum_{\alpha} \sum_{m} \int_0^\infty \mathrm{d}k \, k^2 \omega_{m,\alpha}(\vec{k}) \mathrm{e}^{-\omega_{m,\alpha}(\vec{k})\frac{a}{\pi}} \,. \tag{4.2}$$

By construction, expression (4.2) is cutoff dependent and will blow up for $a \to 0$. However, since this singular behavior has nothing to do with the presence of the branes, but comes from the fact that the vacuum energy is divergent, we will renormalize the energy by subtracting the vacuum energy of a system without branes. Note, however, that such a subtraction does not remove the divergence completely. We will find in section 4.2.3, using numerical methods, that the renormalized energy in 2D still has a non-vanishing, logarithmic a-dependence. Also, in the 5D system an a-dependence remains. However, this divergent part is independent of the separation distance of the branes. Hence, the Casimir force is finite and cutoff independent.[2]

Now, in the system *without* the branes we can again decompose the 5D scalar field into massive KK modes, using just $\cos(my)$ and $\sin(my)$ as mode functions. The periodic boundary conditions will then lead to

$$m_0 = \frac{2\pi n}{L} \,, \quad n = 0, 1, 2, \ldots \tag{4.3}$$

Note that here, unlike in the setup *with* branes, the masses of the even and the odd modes are equal (and again, only the even modes have a zero-mode because $\sin(0) = 0$).[3] Further notice that the masses m_0 can also be recovered from (2.43) in the limit $r_{\text{c}} \to 0$, as it should be.

Thus, the (regularized) vacuum energy in the absence of branes is given by

$$E_0^{\text{reg}} = E^{\text{reg}}|_{m \to m_0} \,. \tag{4.4}$$

Then, the Casimir energy of the DGP system is

$$E_{\text{C}} \equiv \lim_{\substack{a \to 0 \\ L \to \infty}} \left(E^{\text{reg}} - E_0^{\text{reg}} \right) , \tag{4.5}$$

where we removed the short distance cutoff a and sent the size of the extra dimension to infinity (which is usually the case in the DGP model). We expect

[2]Note that there exists extensive literature that deals with improved regularization and renormalization techniques, such that those kinds of remaining divergences are removed. In the context of delta-function potentials, one can also find discussions of the physical origin of such divergences (see e.g. Refs. [97, 99]). Since we are only interested in the observable Casimir force, where these divergences drop out, it is beyond the scope of this thesis to discuss this further.

[3]The reason that in the dimensionally reduced system every mode (except the even zero-mode) is twofold degenerate, is that the original 5D setup (without branes) had a conserved fifth momentum, due to the translational invariance in y-direction, which translates to an O(2)-invariance in the reduced system.

expression (4.5) to be finite, since the Casimir effect is known to be an IR effect and therefore should be independent of high energy physics. We will now calculate this expression and show that this is indeed the case (note, however, the comment below (4.2)).

4.2 Casimir Effect in 1+1 Dimensions

Since evaluating expression (4.2) is quite involved, we will first consider a simplified version in order to isolate the relevant features, before tackling the full problem.

Let us consider our setup in 1+1 dimensions, i.e. with just the "extra" dimension and time. In this case, the 3-branes become 0-branes (i.e. just points in the y-direction) and there are no transverse dimensions on the branes. This situation is described by the action

$$S_{\text{2D}} = \int \mathrm{d}t\,\mathrm{d}y\,\frac{1}{2}\Big\{\dot{\Phi}^2 - (\partial_y\Phi)^2 + r_{\text{c}}\Big[\delta\Big(y+\frac{R}{2}\Big) + \delta\Big(y-\frac{R}{2}\Big)\Big]\dot{\Phi}^2\Big\}\,, \tag{4.6}$$

where $\dot{(\cdot)}$ denotes time-derivatives.

Now we decompose

$$\Phi(t,y) = \sum_{\alpha=1}^{2}\sum_{m}\psi_{m,\alpha}(y)\phi_{m,\alpha}(t)\,,$$

where $\psi_{m,\alpha}(y)$ are the same mode functions as before, satisfying (2.34). Then, the dimensionally reduced action reads

$$S_{\text{2D}} = \int \mathrm{d}t\,\sum_{\alpha}\sum_{m}\frac{1}{2}\Big(\dot{\phi}^2_{m,\alpha}(t) - m_\alpha^2\phi^2_{m,\alpha}(t)\Big)\,. \tag{4.7}$$

The KK fields are now just harmonic oscillators, with the frequencies given by the solutions of (2.43). Following the same steps as in section 4.1, we find the Hamiltonian

$${}^{(\text{2D})}\widehat{H} = \sum_{\alpha=1}^{2}\sum_{m>0} m_\alpha\Big(\widehat{a}^\dagger_{m,\alpha}\widehat{a}_{m,\alpha} + \frac{1}{2}\Big)\,.$$

Note that in the 2D case the Hamiltonian does not contain the zero-mode (with $m_1 = 0$) because it is constant and hence drops out ($\dot{\phi}_{0,1} = 0$).

The vacuum energy is given by

$${}^{(\text{2D})}E = \langle 0|{}^{(\text{2D})}\widehat{H}|0\rangle = \sum_{\alpha=1}^{2}\sum_{m>0}\frac{m_\alpha}{2}\,,$$

and after regularizing we get

$${}^{(\text{2D})}E^{\text{reg}} = \sum_{\alpha=1}^{2}\sum_{m>0}\frac{m_\alpha}{2}\mathrm{e}^{-m_\alpha\frac{a}{\pi}}\,, \tag{4.8}$$

which is much simpler than (4.2). However, since the masses m_α cannot be determined exactly, we can calculate (4.8) only either approximately or numerically. We will do the former in the next two sections and the latter in the section after that.

4.2.1 Infrared Transparent and Opaque Regions—Sharp Transition Approximation

In this thesis, we are interested in the parameter space covering $R \lesssim r_\mathrm{c}$ (cf. section 3.1.1). If we especially consider the limit $R \ll r_\mathrm{c}$, we find that (2.43) allows two different regimes. We can rewrite it as

$$-\frac{2\sin\left(\frac{m_\alpha L}{2}\right)}{m_\alpha r_\mathrm{c}} = \begin{cases} 2\cos\left[\dfrac{m_\alpha}{2}(L-R)\right]\cos\left(\dfrac{m_\alpha R}{2}\right), & \text{for } \alpha = 1 \text{ (even)}, \\ -2\sin\left[\dfrac{m_\alpha}{2}(L-R)\right]\sin\left(\dfrac{m_\alpha R}{2}\right), & \text{for } \alpha = 2 \text{ (odd)}. \end{cases} \tag{4.9}$$

For $m_\alpha r_\mathrm{c} \ll 1$, the left-hand side of (4.9) blows up, and hence we find solutions for (since the right-hand side lies in the interval $[-2, 2]$)

$$m_\alpha = \frac{2\pi n}{L}, \quad n = 1, 2, 3, \ldots \qquad \left(m_\alpha \ll r_\mathrm{c}^{-1}\right). \tag{4.10a}$$

For $m_\alpha r_\mathrm{c} \gg 1$, the left-hand side of (4.9) vanishes, which leads to

$$m_1 = \begin{cases} \dfrac{\pi n}{L-R} \\ \dfrac{\pi n}{R} \end{cases}, \quad n = 1, 3, 5, \ldots \qquad \text{(even modes)}, \qquad \left(m_\alpha \gg r_\mathrm{c}^{-1}\right). \tag{4.10b}$$

$$m_2 = \begin{cases} \dfrac{\pi n}{L-R} \\ \dfrac{\pi n}{R} \end{cases}, \quad n = 2, 4, 6, \ldots \qquad \text{(odd modes)}, \qquad \left(m_\alpha \gg r_\mathrm{c}^{-1}\right).$$

Note, however, that the upper solutions of the even and odd parts of (4.10b) are only valid for $n \gg (L-R)/r_\mathrm{c}$.

We see that the system has an *infrared transparent regime* (for $m \ll r_\mathrm{c}^{-1}$), where the modes do not "see" the branes and hence have the same frequency as in a (periodic) box of size L. The system also has an *opaque regime* (for $m \gg r_\mathrm{c}^{-1}$), where the branes act effectively as Dirichlet boundary conditions for the modes, and hence the latter acquire frequencies as expected for such a configuration. The system is depicted in Figure 4.1.[4]

Now, let us first ignore the fact that there is a transition region at $m \sim r_\mathrm{c}^{-1}$ and consider a "toy model" where we artificially construct boundary conditions for the scalar field in such a way that the modes with $m \leq r_\mathrm{c}^{-1}$ are "free", i.e. they do not have to fulfill any boundary conditions at the location of the branes, while all heavier modes, $m > r_\mathrm{c}^{-1}$, have to satisfy Dirichlet boundary conditions there (so the branes act as "perfect conductors" for the scalar field[5]). Then, the (regularized) energy for a system with such a *sharp* transition is given by

$${}^{(2\mathrm{D})}E_\mathrm{s}^\mathrm{reg} = \underbrace{\sum_{n=1}^{n_\mathrm{max}} \frac{2\pi n}{L} \mathrm{e}^{-\frac{2an}{L}}}_{\Sigma_1^\mathrm{s}} + \underbrace{\frac{1}{2}\sum_{n=n_\mathrm{min}+1}^{\infty} \frac{\pi n}{L-R} \mathrm{e}^{-\frac{an}{L-R}}}_{\Sigma_2^\mathrm{s}} + \underbrace{\frac{1}{2}\sum_{n=1}^{\infty} \frac{\pi n}{R} \mathrm{e}^{-\frac{an}{R}}}_{\Sigma_3^\mathrm{s}}, \tag{4.11}$$

[4] This is, of course, just a slightly different way to view Figure 2.1.

[5] We can see explicitly that the field amplitudes vanish at $y = \pm\frac{R}{2}$, for $mr_\mathrm{c} \gg 1$, from the expressions for the mode functions (B.10) and (B.11).

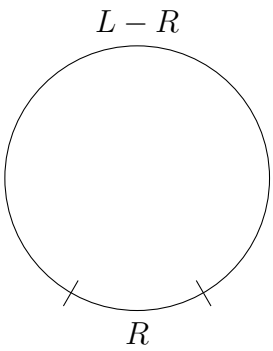

Figure 4.1: A ring (with circumference L) with two branes (perpendicular lines), separated by R. For "transparent" branes, one expects the frequencies to obey $m = (2\pi n)/L$, with $n \in \mathbb{N}$. For Dirichlet boundary conditions at the branes, one expects $m = \pi n/(L-R)$ and $m = \pi n/R$, with $n \in \mathbb{N}$. Both solutions are the limiting cases of (2.43) for $m \ll r_{\mathrm{c}}^{-1}$ and $m \gg r_{\mathrm{c}}^{-1}$, respectively.

with

$$n_{\max} = \frac{1}{2\pi}\frac{L}{r_{\mathrm{c}}} \quad \text{and} \quad n_{\min} = \frac{1}{\pi}\frac{L-R}{r_{\mathrm{c}}}\,. \tag{4.12}$$

If we perform the summations and then expand around $a = 0$ and $1/L = 0$, we find

$$\Sigma_1^{\mathrm{s}} = \frac{L}{4\pi r_{\mathrm{c}}^2} + \frac{1}{2r_{\mathrm{c}}} - \frac{La}{6\pi^2 r_{\mathrm{c}}^3} + \mathcal{O}\Big(\frac{a}{r_{\mathrm{c}}^2}\Big) + \mathcal{O}\Big(\frac{a}{Lr_{\mathrm{c}}}\Big)\,, \tag{4.13a}$$

$$\Sigma_2^{\mathrm{s}} = \frac{\pi L}{2a^2} - \frac{\pi R}{2a^2} - \frac{L}{4\pi r_{\mathrm{c}}^2} + \frac{R}{4\pi r_{\mathrm{c}}^2} - \frac{1}{4r_{\mathrm{c}}} + \frac{La}{6\pi^2 r_{\mathrm{c}}^3} + \mathcal{O}\Big(\frac{1}{L}\Big) + \mathcal{O}\Big(\frac{a}{r_{\mathrm{c}}^2}\Big)\,, \tag{4.13b}$$

$$\Sigma_3^{\mathrm{s}} = \frac{\pi R}{2a^2} - \frac{\pi}{24R} + \mathcal{O}\Big(\frac{a^2}{R^3}\Big)\,. \tag{4.13c}$$

To renormalize expression (4.11), we again subtract the vacuum energy of a system in the absence of branes,

$${}^{(2\mathrm{D})}E_0^{\mathrm{reg}} = \sum_{n=1}^{\infty} \frac{2\pi n}{L} \mathrm{e}^{-\frac{2an}{L}} = \frac{\pi L}{2a^2} + \mathcal{O}\Big(\frac{1}{L}\Big) + \mathcal{O}\Big(\frac{a^2}{L^3}\Big)\,. \tag{4.14}$$

Then, it follows that

$$\begin{aligned} {}^{(2\mathrm{D})}E_{\mathrm{C}}^{\mathrm{s}} &= \lim_{\substack{a\to 0\\ L\to\infty}} \Big({}^{(2\mathrm{D})}E_{\mathrm{s}}^{\mathrm{reg}} - {}^{(2\mathrm{D})}E_0^{\mathrm{reg}}\Big)\,, \\ &= -\frac{\pi}{24R} + \frac{1}{4r_{\mathrm{c}}} + \frac{R}{4\pi r_{\mathrm{c}}^2}\,. \end{aligned} \tag{4.15}$$

Thus, we find that, after removing the regulators a and L, the resulting Casimir energy has three finite and cutoff-independent terms. The first term is identical to what one would get if calculating the standard Casimir energy between two conducting plates (Dirichlet boundary conditions), separated by a distance R in 1+1 dimensions. However, we see that the inclusion of an IR transparency region

leads to two new contributions, which modify the Casimir energy. The first new contribution (second term in (4.15)) increases the Casimir energy by a constant. However, note that the sign of this term depends on whether the first mode in the opaque region is even or odd. In the present situation, the constant is positive because the first mode entering Σ_2^{s} in (4.11) is odd. Had we organized the system according to a different prescription—modes with $m < r_{\mathrm{c}}^{-1}$ are "free" and modes with $m \geq r_{\mathrm{c}}^{-1}$ are "bound"—the first mode to enter the summation would have been the even one. In this case, the constant contribution would be negative, $-\frac{1}{4r_{\mathrm{c}}}$.

Since we are ultimately interested in the Casimir force, which is given by

$$F_{\mathrm{C}} \equiv -\frac{E_{\mathrm{C}}}{\partial R}\,, \tag{4.16}$$

the more important, novel contribution is the last term in (4.15). Here, the sign turns out to be independent of the particular separation of the free and bound modes (i.e. independent of whether the first mode is even or odd) and is always positive. Thus, the Casimir force, in the presence of an IR transparency region, is

$${}^{(2\mathrm{D})}F_{\mathrm{C}}^{\mathrm{s}} = -\frac{{}^{(2\mathrm{D})}E_{\mathrm{C}}^{\mathrm{s}}}{\partial R} = -\frac{\pi}{24R^2} - \frac{1}{4\pi r_{\mathrm{c}}^2}\,. \tag{4.17}$$

Hence, it is amplified as compared to the standard Casimir force without an IR transparency region.

This result can be interpreted in the following way: usually (that is, in the case where the branes provide ideal Dirichlet boundary conditions), we can "fit" only those wavelengths λ into the system shown in Figure 4.1 that are fractions of $2R$ and $2(L-R)$, and hence

$$\lambda = \begin{cases} 2\dfrac{R}{n}\,, & (\text{inside the branes})\,, \\ 2\dfrac{L-R}{n}\,, & (\text{outside the branes})\,, \end{cases} \tag{4.18}$$

where $n \in \mathbb{N}$. However, we have to exclude wavelengths that lie below the validity distance of the theory, by introducing the cutoff a and hence excluding wavelengths $\lambda \lesssim a$. One then finds in the limit $L \to \infty$ (which turns the "outside"-modes continuous) and $a \to 0$ that due to the fact that the "inside"-modes are discrete (and hence reduced in number) there is an attractive force between the plates (branes). The fact that this effect is independent of the short distance cutoff a is said to indicate that the Casimir effect is an IR effect.

Now we found the following modification to this situation. If we remove all the ("outside") wavelengths from (4.18) for which $n \lesssim 2(L-R)/r_{\mathrm{c}}$, such that all wavelengths $\lambda \gtrsim r_{\mathrm{c}}$ do not "see" the boundary conditions at the branes anymore[6], we diminish the number of allowed modes in our brane system even further. Hence, the (magnitude of the) Casimir force is increased by a constant (proportional to the size of the "exclusion window").

We summarize the relevant distance scales in Figure 4.2.

[6]Thus, the wavelengths with $\lambda \gtrsim r_{\mathrm{c}}$ are given by $\lambda = L/n$. In the continuous limit $L \to \infty$, these wavelengths are not constrained at all.

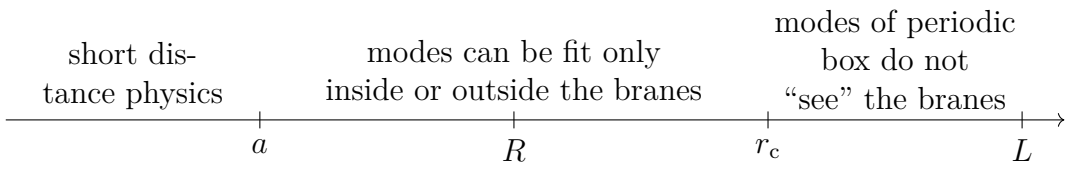

Figure 4.2: Different scales of the system and their relevance for the Casimir effect.

4.2.2 Taking Into Account the Transition Region—Leaking Branes

In order to analyze our more realistic model, where the branes do not just alternate between being perfect conductors (for $m > r_c^{-1}$) and being invisible (for $m < r_c^{-1}$) but have the DGP-like behavior, we have to study more closely the region $m \sim r_c^{-1}$. In this case, the right-hand side of (4.9) is an oscillating function, and hence the solutions for m_α are not available exactly. However, working in the limit $R \ll r_c < L$, we can derive leading corrections to the results (4.10a) and (4.10b), which improve the accurateness of the result as we approach $m \sim r_c^{-1}$. In this limit, the "inside"-modes, $m \propto n/R$, of the regime $mr_c \gg 1$ are already good approximate solutions, so we can focus on the "outside"-modes, $m \propto n/(L-R)$, there.

Even Modes

For the correction of the even modes in the opaque region, we can expand (4.9), using $m(L-R) = \pi n + \epsilon$ (for $|\epsilon| \ll 1$), and find $\epsilon \sim 2(L-R)/(\pi n r_c)$, as long as $n \lesssim 2L/(\pi R)$.

Similarly, for the IR region, we expand with the ansatz $mL = 2\pi n + \epsilon$ (for $|\epsilon| \ll 1$) and find $\epsilon \sim -4\pi n r_c/L$.

Thus, in the leading approximation, we obtain

$$m_1 = \begin{cases} \dfrac{2\pi n}{L} - \dfrac{4\pi n}{L}\dfrac{r_c}{L}\,, & \text{for } n \ll n_{\max}\,, \\ \underbrace{\dfrac{\pi n}{L-R} + \dfrac{2}{\pi n}\dfrac{1}{r_c}}_{m_1^c}\,, & \text{for } n_{\min} \ll n \ll n_*\,, \\ \dfrac{\pi n}{R}\,, \end{cases} \quad \begin{array}{l} (\text{for } n \in \mathbb{N})\,, \\ \\ (\text{for odd integers } n)\,, \end{array} \tag{4.19}$$

with $n_{\max}$ and $n_{\min}$ again given by (4.12). Note that the form of the correction of m_1^c is only valid up to $n \sim n_*$, with

$$n_* \equiv \frac{2}{\pi}\frac{L-R}{R}\,. \tag{4.20}$$

Odd Modes

The leading correction of the odd modes in the opaque region has a more subtle form than for the even modes. It turns out that it first grows (with n) and then decreases again, with the turning point set by a new scale. We can see this as

follows. We rewrite (4.9), using $m(L-R) = \pi n + \beta$ (for $|\beta| \ll \pi n$),[7] and find $\beta \sim 2\arctan[f(n)]$, as long as $n \lesssim 2L/(\pi R)$. The argument of the arctan is given by

$$f(n) = \frac{R}{2L}\frac{n\pi}{\left(\frac{n}{n_\rho}\right)^2 - 1}\,, \tag{4.21}$$

where

$$n_\rho = \sqrt{2}\frac{L-R}{\pi\rho} \quad \text{and} \quad \rho = \sqrt{R r_\mathrm{c}}\,. \tag{4.22}$$

Notice that first (for $n \lesssim n_\rho$) the correction grows linearly with n (since $\beta \propto -nR/L$) and later (for $n \gtrsim n_\rho$) decreases again ($\beta \propto L/(n r_\mathrm{c})$). At the turning point, at $n \sim n_\rho$, the mass (leading term) is $m \sim \rho^{-1}$, and thus we have found a new characteristic scale, ρ. Interestingly, ρ is the same scale that played a prominent role for the behavior of the gravitational force in chapter 3.

Finally, for the IR region, we expand with the ansatz $mL = 2\pi n + \epsilon$ (for $\epsilon \ll 1$) and find $\epsilon \sim -4(\pi n)^3 R^2 r_\mathrm{c}/L^3$.

Then, in the leading approximation, we obtain

$$m_2 = \left\{\begin{array}{ll} \dfrac{2\pi n}{L} - 4(\pi n)^3\dfrac{R^2 r_\mathrm{c}}{L^4}\,, & \text{for } n \ll n_\mathrm{max}\,, \quad (\text{for } n \in \mathbb{N})\,, \\ \underbrace{\dfrac{\pi n}{L-R} + \dfrac{2}{L-R}\arctan[f(n)]}_{m_2^\mathrm{c}}\,, & \text{for } n_\mathrm{min} \ll n \ll n_*\,, \\ \dfrac{\pi n}{R}\,, & \end{array}\right\} \begin{array}{l} \\ \\ (\text{for even} \\ \text{integers } n)\,, \end{array} \tag{4.23}$$

with

$$m_2^\mathrm{c} \simeq \begin{cases} m_{2,a}^\mathrm{c} \equiv \dfrac{\pi n}{L-R} - \dfrac{\pi n}{L-R}\dfrac{R}{L}\,, & n \ll n_\rho\,, \\ m_{2,b}^\mathrm{c} \equiv \dfrac{\pi n}{L-R} + 2\dfrac{L-R}{\pi n L r_\mathrm{c}}\,, & n \gg n_\rho\,. \end{cases} \tag{4.24}$$

Again, the form of the correction of m_2^c is only valid up to $n \sim n_*$, with n_* given in (4.20).

Validity of the Approximations

Note that the corrections that we derived in (4.19) and (4.23) improve the solutions for m_α, as we approach the transition region from the IR transparent and the opaque regimes, respectively, but they are not valid at $m \sim r_\mathrm{c}^{-1}$. Here, we cannot write down an asymptotic expansion for m_α. However, if we extend the validity region of the solutions in (4.19) and (4.23) all the way to $m \sim r_\mathrm{c}^{-1}$, we will only introduce an error to the vacuum energy that is of the order of r_c^{-1}. We can see this by looking at (4.9). For $m \sim r_\mathrm{c}^{-1}$, the solutions will obviously be modified. However, the number of modes that solve this equation is still proportional to the

[7] Note that this time we do not assume β to be much smaller than 1. However, we still require it to be much smaller than πn, since we are looking for a correction to the leading term of m_2.

number of times the left-hand side and the right-hand side crosses zero. In the limit $L > r_c \gg R$, this is of the order L/r_c, which is independent of R. Hence, the contribution to the energy, from that region, is

$$\left(\sim \frac{1}{r_c} + \sim \frac{1}{L}\right)\frac{L}{r_c} = \mathcal{O}(1)\frac{L}{r_c^2} + \mathcal{O}(1)\frac{1}{r_c}\,, \tag{4.25}$$

which deviates by $\mathcal{O}(1)$ factors from the true result. The first term cancels from the two sums Σ_1^s and Σ_2^s, as can be seen explicitly in (4.11),[8] but the second term will contribute to the energy. Hence, correcting the masses around r_c^{-1}, would just change the r_c^{-1}-part of the vacuum energy by an $\mathcal{O}(1)$ numerical factor. Since this constant term will drop out in the expression of the Casimir force, we can safely use the expansions (4.19) and (4.23) for $n \ll n_*$ ($m_\alpha \ll R^{-1}$). Although the corrections lose their validity as we approach $m_\alpha \sim R^{-1}$, they are suppressed as $\sim R/r_c$. Thus, in this section, we will consider the above expressions to be good approximate solutions (up to corrections R/r_c) of (2.43) for the full range of masses. However, we will see in the next section, by performing a numerical analysis, that the corrections for $n \gtrsim n_*$ will in fact also contribute, since they do not fall off fast enough at the lower limit.

We further observe that the relevant correction to the Casimir energy (due to the "leakage") comes from the region $R < \lambda < r_c$. There, the correction of the even modes goes like $1/n$ and hence does not vanish fast enough, leading to a logarithmic contribution to the energy. The correction of the odd modes also has a contribution $1/n$ (for $n \gg n_\rho$), however, more importantly, it has an additional contribution that peaks around $n \sim n_\rho$, where $m_2 \sim \rho^{-1}$. Hence, the energy will get a contribution ρ^{-1}, as we will explain below.

Corrected Casimir Energy

Let us now study the new contributions to (4.11) in detail. If we use the (corrected) even mass from (4.19) for the IR transparency region and plug it into Σ_1^s, we find that (4.13a) acquires the additional contribution

$$-\frac{1}{4\pi r_c} + \dots$$

where the ellipses denote terms vanishing in the limit $a \to 0$, $L \to \infty$. However, as we explained before, the precise numerical factor of the term $\sim 1/r_c$ is only numerically calculable and not the one given above. The correction of the odd mass in the IR transparency region, (4.23), is much smaller than for the even modes. Since we did not expand the even masses up to that order, we have to use the leading approximation for the odd modes if we want a consistent error estimate for Σ_1^s.[9] Hence, there is no additional contribution to Σ_1^s from the odd modes. Thus, the energy from the IR transparency region is modified according to

$$\Sigma_1^s \to \Sigma_1 = \Sigma_1^s + \mathcal{O}(1)\frac{1}{r_c} + \dots \tag{4.26}$$

[8] This is just an "artifact" from the fact that we split the sum there.

[9] If we would take into account this correction, Σ_1 would now contain a term $\propto R^2/r_c^3$.

We see that, as expected, the correction of the IR transparency modes due to the non-sharp transition at $m \sim r_\mathrm{c}^{-1}$ only modifies the r_c^{-1}-term of the energy.

Next, we consider the correction of Σ_2^s coming from the even modes. We cannot just plug in the correction that we found in (4.19) and sum up to infinity because the correction is only valid up to $n \sim n_*$. Hence, we have to divide the sum into two parts,[10]

$$\frac{1}{2}\sum_{\substack{n=n_\mathrm{min}+2\\(\text{odd } n)}}^{n_*} m_1^\mathrm{c} \mathrm{e}^{-m_1^\mathrm{c}\frac{a}{\pi}} + \frac{1}{2}\sum_{\substack{n=n_*+2\\(\text{odd } n)}}^{\infty} \frac{\pi n}{L-R}\mathrm{e}^{-\frac{an}{L-R}}\,.$$

Thus, the correction to Σ_2^s will come entirely from the first part. Unfortunately, it cannot be summed exactly. However, we can find an asymptotic expansion around $a = 0$ for this sum (we have used `Mathematica` for this). The new contribution is

$$-\frac{1}{2\pi r_\mathrm{c}}\ln\frac{R}{2r_\mathrm{c}} + \ldots$$

For the correction of Σ_2^s resulting from the odd modes, we again have to note that the correction that we found in (4.23) is only valid up to $n \sim n_*$. Furthermore, because it is the rather complicated function $\sim \arctan f$, an asymptotic expansion of the sum, involving this correction, is not available. Therefore, we will split the sum even further and use the two approximate expressions, given in (4.24), in the respective regions. Hence, we have to evaluate the sums

$$\underbrace{\frac{1}{2}\sum_{\substack{n=n_\mathrm{min}+1\\(\text{even } n)}}^{n_\rho} m_{2,a}^\mathrm{c}\mathrm{e}^{-m_{2,a}^\mathrm{c}\frac{a}{\pi}}}_{I_a} + \underbrace{\frac{1}{2}\sum_{\substack{n=n_\rho+2\\(\text{even } n)}}^{n_*-1} m_{2,b}^\mathrm{c}\mathrm{e}^{-m_{2,b}^\mathrm{c}\frac{a}{\pi}}}_{I_b} + \frac{1}{2}\sum_{\substack{n=n_*+1\\(\text{even } n)}}^{\infty} \frac{\pi n}{L-R}\mathrm{e}^{-\frac{an}{L-R}}\,,$$

where the new contributions to Σ_2^s will come solely from I_a and I_b. From I_a, we find the new contributions:

$$I_a \supset \frac{L}{4\pi\rho^2} + \frac{\sqrt{2}}{4\rho} - \frac{2+\pi}{4\pi r_\mathrm{c}} + \frac{R}{8\pi r_\mathrm{c}^2}\,. \tag{4.27a}$$

The sum I_b, as in the even case, cannot be evaluated exactly, so we again have to rely on an asymptotic expansion around $a = 0$. We obtain the following new contributions:

$$I_b \supset -\frac{L}{4\pi\rho^2} - \frac{\sqrt{2}}{4\rho} + \frac{1}{4\pi r_\mathrm{c}} - \frac{1}{4\pi r_\mathrm{c}}\ln\frac{R}{2r_\mathrm{c}}\,. \tag{4.27b}$$

Note that to derive expressions (4.27a) and (4.27b) we assumed that the two limiting values in (4.24) are valid right up to $n \sim n_\rho$. Then, by adding (4.27a) and (4.27b), the terms proportional to L/ρ^2 and $1/\rho$ cancel, in the same way as the

[10] Note that the first sum now starts "two steps" after the transition region because the first step is taken care of by the odd modes. The same is true for the second sum. Note, however, that since individual modes contribute only with $\sim 1/L$ to the sum, in the continuous limit $L \to \infty$ these subtleties could just as well be ignored.

terms $\propto L/r_c^2$ canceled in (4.11), patching together Σ_1^s and Σ_2^s. However, analogous to what we explained in the paragraph around (4.25) regarding region $m \sim r_c^{-1}$, the masses at $m \sim \rho^{-1}$ should also get order-one corrections, since the exact form $(2 \arctan f)/(L-R)$ differs from the approximations in (4.24) at this transition region. But now the number of modes contributing to that correction is $\sim L/\rho$, and hence the expressions (4.27a) and (4.27b) will have terms $\propto \rho^{-1}$ that do not cancel.

Thus, we find that the corrections of both the even and the odd masses modify Σ_2^s according to

$$\Sigma_2^s \to \Sigma_2 = \Sigma_2^s + \mathcal{O}(1)\frac{1}{r_c} + \mathcal{O}(1)\frac{1}{\rho} - \frac{3}{4\pi r_c}\ln\frac{R}{2r_c} + \frac{R}{8\pi r_c^2} + \dots \tag{4.28}$$

The sum, taking care of the "inside" modes, Σ_3^s is unaffected by the correction of the modes in our leading approximation, so

$$\Sigma_3^s = \Sigma_3 + \dots \tag{4.29}$$

Finally, with the modification

$${}^{(2D)}E_s^{reg} \to {}^{(2D)}E^{reg} \equiv \Sigma_1 + \Sigma_2 + \Sigma_3\,, \tag{4.30}$$

the DGP analogue of (4.15), in the first approximation, is

$$\begin{aligned} {}^{(2D)}E_C &= \lim_{\substack{a\to 0\\ L\to\infty}} \left({}^{(2D)}E^{reg} - {}^{(2D)}E_0^{reg}\right), \\ &= -\frac{\pi}{24R} + \mathcal{O}(1)\frac{1}{r_c} + \mathcal{O}(1)\frac{1}{\sqrt{Rr_c}} - \frac{3}{4\pi r_c}\ln\frac{R}{2r_c} + \frac{3}{8\pi}\frac{R}{r_c^2} + \mathcal{O}\left(\frac{R^2}{r_c^3}\right). \end{aligned} \tag{4.31}$$

Let us make a couple of comments about this result. We see that the two terms, which were already present in the sharp transition approximation, $\propto r_c^{-1}$ and $\propto R/r_c^2$, are slightly modified by this more detailed resolution of the transition region, which is expected. However, note that the exact numerical prefactors are sensitive to our rough approximations. The constant term ($\propto r_c^{-1}$) depends on the precise (only numerically accessible) solutions at the transition region. The modification of the linear term comes entirely from $m_{2,a}^c$, where the correction term is $\sim R/r_c$ smaller than the corresponding correction of the even modes, so it is possible that the numerical factor would change further if we would take into account higher correction terms of the even modes.

More importantly, we found two new contributions to the Casimir energy, which are due to the fact that the masses in the region $r_c^{-1} \lesssim m \lesssim R^{-1}$ get corrections from the "DGP nature" of the branes. These corrections vanish only slowly in the limit $R \ll r_c$. In fact, we found that the correction of the masses of the odd modes even increases in the region $r_c^{-1} \lesssim m \lesssim \rho^{-1}$, before again falling off like $\propto n^{-1}$, where the characteristic scale of the turning point is $\rho = \sqrt{Rr_c}$. The growing correction of the odd modes leads to a $\frac{1}{\sqrt{Rr_c}}$-contribution, while the correction $\propto n^{-1}$ gives a logarithmic contribution.

This leads to the (novel) Casimir force

$$ {}^{(2\mathrm{D})}F_{\mathrm{C}} = -\frac{\pi}{24R^2} + \mathcal{O}(1)\frac{1}{R\sqrt{Rr_{\mathrm{c}}}} + \underset{\mathcal{O}(1)\ ?}{\uparrow}\frac{3}{4\pi}\frac{1}{Rr_{\mathrm{c}}} + \mathcal{O}\left(\frac{1}{r_{\mathrm{c}}^2}\right). \tag{4.32} $$

We will see in the next section that the coefficient in front of the term $\propto (Rr_{\mathrm{c}})^{-1}$ gets further modified by an $\mathcal{O}(1)$ factor. Furthermore, we will find that the coefficient in front of the term $\propto 1/(R\sqrt{Rr_{\mathrm{c}}})$ is positive, thus leading to a weakening of the Casimir force. This result reflects the fact that the DGP branes are not just ideal boundary conditions (being completely transparent to soft modes and completely opaque to hard modes) but have a finite transition region, where they "try to keep" the hard modes, but still "leak" some of them. This affects the branes' ability to confine modes inside their interior and hence weakens the Casimir force as compared to the case of perfect conducting plates. Since this leakage effect turns out to be stronger than the effect we discovered in the previous section (leading to a constant increase of the Casimir force), the resulting Casimir force is weaker than in the case of ideal boundary conditions.

4.2.3 Numerical Analysis of the Casimir Energy

The derivation of the Casimir force in the previous section relied on approximations of the quantized masses that have different forms in different regions. Since it is difficult to control the introduced errors in this way, in the present section we will justify, qualitatively, the expression (4.32) and obtain a positive sign for the leading correction by using numerical methods. Our starting point is to numerically solve (2.43) for several different values of R, r_{c} and L. Since this equation has infinitely many solutions, we have to choose where we want to truncate them. We choose the largest mass in such a way that $ma < 100$ because then the exponential factor $\exp(-ma/\pi)$ is sufficiently small, such that the rest of the solutions does not contribute to the Casimir energy anymore. Then, using those numerical solutions, we calculate

$$ {}^{(2\mathrm{D})}E^{\mathrm{ren}} \equiv {}^{(2\mathrm{D})}E^{\mathrm{reg}} - {}^{(2\mathrm{D})}E_0^{\mathrm{reg}} \tag{4.33} $$

as a function of R. The result for $a = 0.1$ and two different sets of parameters r_{c} and L is shown in Figure 4.3.[11] We see that the Casimir energy indeed approaches the form of the standard result, $-\frac{\pi}{24R}$ (blue, solid curve), but it also deviates from it. To see that the difference is not just a constant but actually R-dependent, we also plotted the standard result with a constant shift (gray, dashed curve).

Next, we compare the numerical result to our analytical approximation in Figure 4.4. There, we fitted the leading three terms of (4.31) to the numerical result for $r_{\mathrm{c}} = 150$ and $L = 150$ (red data points), thereby obtaining the coefficients c_1 and c_3 numerically. Both are positive and $\mathcal{O}(1)$. We see that this function already reproduces the numerical result very well. The numerical result for $r_{\mathrm{c}} = 100$ and

[11] In all of the following figures, we express all quantities with dimension of length in some unit l, whereas the energy is expressed in units of l^{-1}. We use dimensionless units by setting $l = 1$.

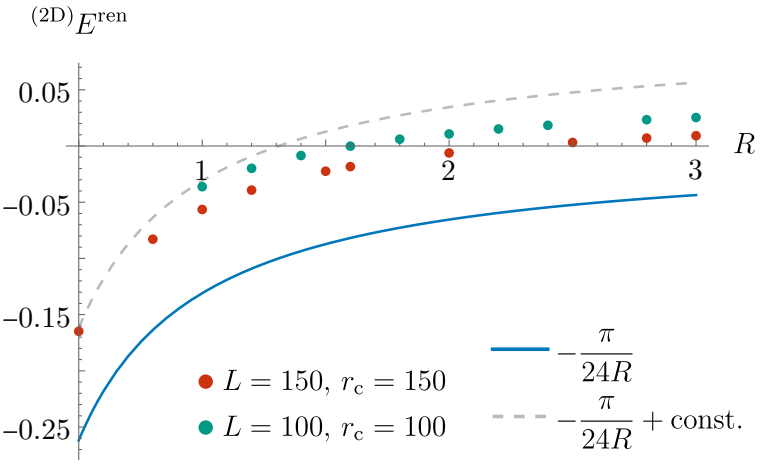

Figure 4.3: Casimir energy, calculated numerically (data points) for $a = 0.1$ and two different sets of parameters r_c and L. Compared to the standard result due to Dirichlet boundary conditions (blue, solid curve) and the shifted version (gray, dashed curve).

$L = 100$ (teal data points) is in slightly worse agreement because, for this value of r_c, the suppression R/r_c is less pronounced, and hence the higher-order terms become more important.

So far, everything is as expected by the previous discussion. However, the numerical analysis shows one feature that was not visible in the analytical analysis. The Casimir energy appears to depend on the cutoff a not just with powers $a, a^2, \ldots$ etc., which vanish in the limit $a \to 0$, but it has an $(\ln a)$-term. To see this, in Figure 4.5 we plotted the Casimir energy (blue points) for the fixed value $R = 1$, as a function of a. Comparing it to the function $-A - B \ln a$ (blue curve), we see that the logarithmic dependence is very robust (for this range of a, the terms with positive powers of a are subleading). We suspect that a term proportional to $r_c^{-1} \ln(a/R)$ arises in (4.31) because of the following reason. In our calculation of Σ_2, we approximated the correction to the even masses in the region $r_c^{-1} \lesssim m \lesssim R^{-1}$ as $\propto n^{-1}$. Therefore, the contribution to Σ_2 from that correction was

$$\sim \frac{1}{r_c} \sum_{n \sim \frac{L}{r_c}}^{n \sim \frac{L}{R}} \frac{1}{n} \mathrm{e}^{-\frac{an}{L-R}} \underset{\substack{\uparrow \\ \text{in the limit} \\ L \to \infty}}{\sim} \frac{1}{r_c} \left(\ln \frac{a}{R} - \ln \frac{a}{r_c} \right) = -\frac{1}{r_c} \ln \frac{R}{r_c} ,$$

so the a-dependence dropped out. Then, for the region $m \gtrsim R^{-1}$, we neglected the correction to the mass and hence did not get any further contribution. However, if we would derive a correction term there as well, it is expected that we would generate a term $\propto r_c^{-1} \ln(a/R)$, coming from the lower limit of $m \sim R^{-1}$. A similar argument holds for the odd masses.

In fact, our numerical analysis shows that the term $\propto r_c^{-1} \ln(a/R)$ enters with a much larger coefficient than the term $\propto r_c^{-1} \ln(2r_c/R)$, which we found in (4.31). In Figure 4.6, we show how the $(\frac{1}{r_c} \ln \frac{a}{R})$-term improves the numerical fit to the data points. Even, if we include another data set (blue points) with an even less

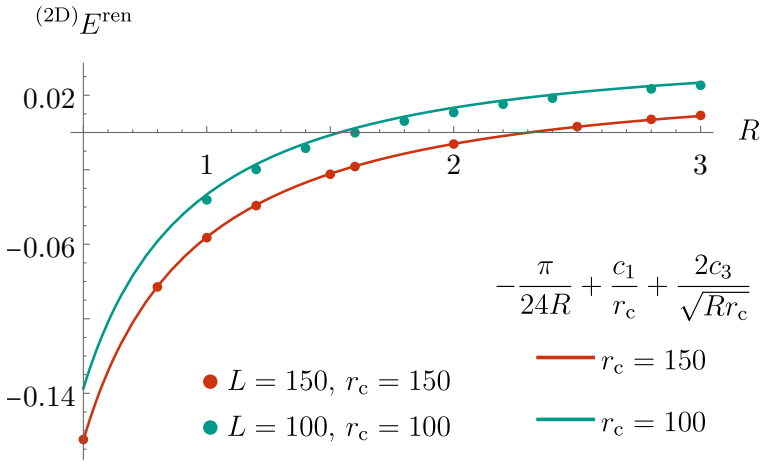

Figure 4.4: Casimir energy, calculated numerically (data points) for $a = 0.1$ and two different sets of parameters r_c and L. We fitted the analytical approximation $-\frac{\pi}{24R} + \frac{c_1}{r_c} + \frac{2c_3}{\sqrt{Rr_c}}$, with free coefficients c_1 and c_3, to the numerical result for $r_c = 150$ and $L = 150$ (red data points). The resulting function, with such determined coefficients $c_1 \simeq 3.32$ and $c_3 \simeq 0.32$, is plotted for $r_c = 150$ (red curve) and $r_c = 100$ (teal curve).

pronounced suppression R/r_c, the fit is very good.[12]

Now, at the first glance, the logarithmic term seems problematic because it depends on a and does not vanish in the limit $a \to 0$. However, the force is the actual observable, and for that the cutoff parameter drops out. Indeed, the term $\propto r_c^{-1} \ln(a/R)$ will contribute to the force in the same way as the third term in (4.32), modifying its numerical factor. To prove that the term $\propto r_c^{-1} \ln(a/R)$, which we found numerically, does not have an R-dependent coefficent (which would invalidate the previous argument), we show in Figure 4.7 the results for different values of R. The fitted curves (solid lines) all have the same slope B. Only the offsets, which of course depend on R, differ.

After we established the correctness of (4.32) numerically and found the magnitudes and signs of the coefficients, we can finally state the Casimir force as

$$ {}^{(2D)}F_C = -\frac{\pi}{24R^2} + \frac{c_3}{R\sqrt{Rr_c}} - \frac{c_4}{Rr_c} + \mathcal{O}\left(\frac{1}{r_c\sqrt{Rr_c}}\right), \tag{4.34} $$

with the coefficients $c_3 \simeq 0.37$ and $c_4 \simeq 0.51$.

Thus, we find indeed that, in the presence of the IR transparency region, the Casimir force becomes weaker, due to the "leakage" of hard modes.

[12]Note that now we had to include a term $\propto L^{-1}$ in the plot of Figure 4.6. In the plot of Figure 4.4 we absorbed it into the term $\propto r_c^{-1}$, since we had $r_c = L$. However, for the data points with $r_c \neq L$ the curve would get a constant shift if we would not take this into account. Of course, other than that, this term is not relevant, since it vanishes in the limit $L \to \infty$.

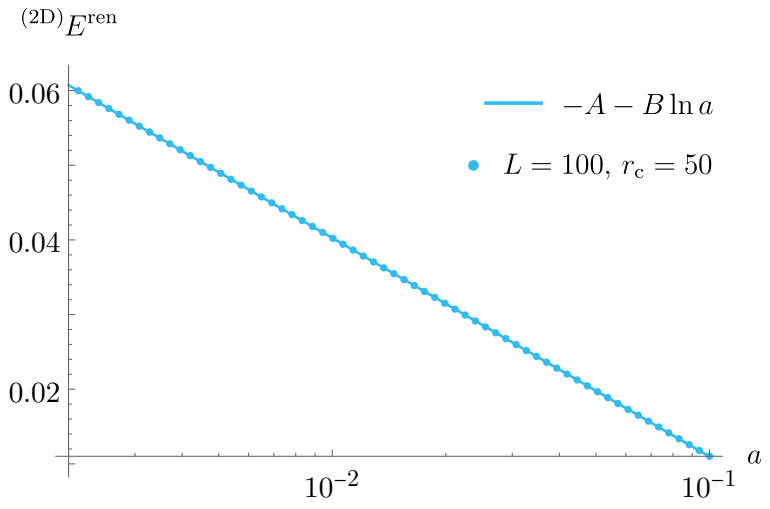

Figure 4.5: Log-linear plot of the numerical Casimir energy (data points) for $R = 1$, $L = 100$ and $r_c = 50$. The function $-A - B \ln a$, with free coefficients A and B, is fitted to the data set. The resulting function, with such determined coefficients ($A, B > 0$), is plotted as the blue curve. We see that the Casimir energy depends logarithmically on a.

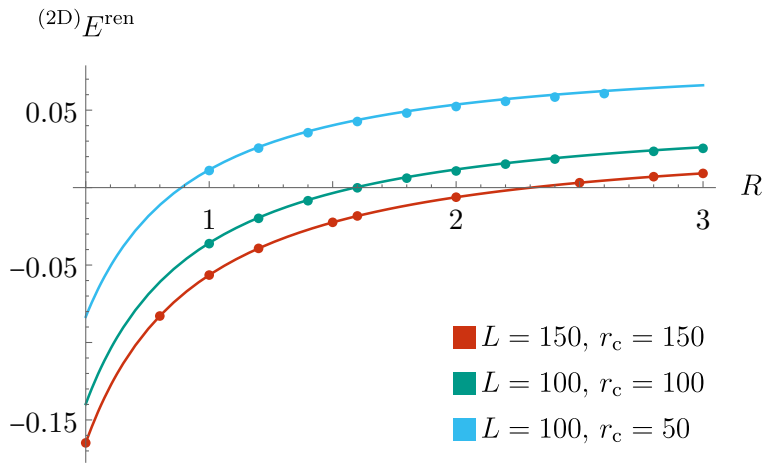

Figure 4.6: Casimir energy, calculated numerically (data points) for $a = 0.1$ and three different sets of parameters r_c and L. We fitted the analytical approximation $-\frac{\pi}{24R} + \frac{c_1}{r_c} + \frac{c_2}{L} + \frac{2c_3}{\sqrt{Rr_c}} - \frac{c_4}{r_c} \ln \frac{a}{R}$, with free coefficients c_i, to the numerical result for $r_c = 150$ and $L = 150$ (red data points). The resulting function, with such determined coefficients $c_1 \simeq 0.50$, $c_2 \simeq 0.48$, $c_3 \simeq 0.37$ and $c_4 \simeq 0.51$, is plotted for $r_c = 150$ (red curve), $r_c = 100$ (teal curve) and $r_c = 50$ (blue curve).

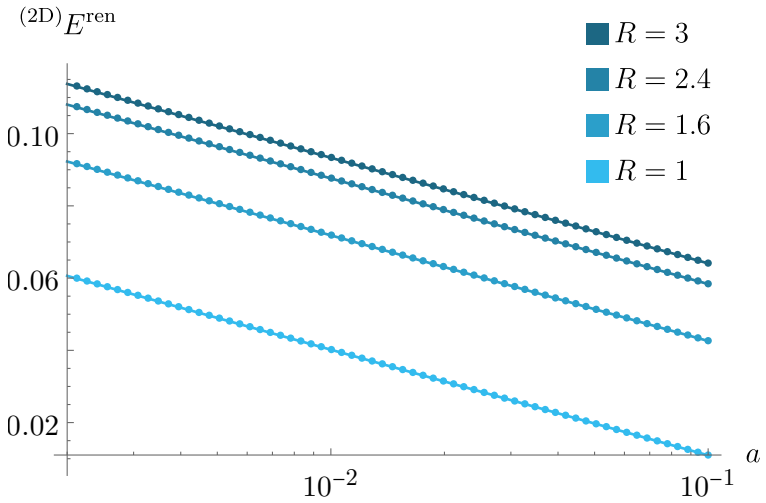

Figure 4.7: Log-linear plot of the functions $-A - B \ln a$ (solid curves), which are fitted to the numerical results for $L = 100$ and $r_{\mathrm{c}} = 50$ (data points) for different values of R. The slopes $B \simeq 0.0127$ are identical for all curves, and only A depends on R.

4.3 Casimir Effect in 4+1 Dimensions

After we have analyzed the properties of the given system in 2D, which led to the novel Casimir force, we can now turn our attention to the system in (the full) five dimensions. In principle, we do not expect a qualitative difference from our previous result, since the branes that produce the effective boundary conditions are still codimension-one objects, and the discrete masses of the KK modes are still given by (2.43). However, the sum that has to be evaluated in order to get the Casimir energy is much more involved in 5D (see (4.2)) than in 2D (see (4.8)). For this reason, we are not able to completely reproduce the analytical analysis and the quantitative results of the previous sections, but have to rely on numerical methods. We will further explain these matters in the following.

Let us start with expression (4.2) and note that we can perform the integration, which leads to

$$E^{\mathrm{reg}} = -\frac{1}{4}\frac{\partial}{\partial a}\sum_{\alpha,m}\frac{m_\alpha^2}{a}K_2\Big(\frac{am_\alpha}{\pi}\Big)\,, \tag{4.35}$$

where K_2 is the modified Bessel function of the second kind.

Now, we would like to calculate an analogue of (4.11) in the (toy model) approximation of a sharp transition, however the sum (4.35), with the masses given by (4.10a) and (4.10b), cannot be solved analytically. Moreover, we were not able to find an asymptotic expansion of this sum.

However, we will show in the next section that in the extreme case $r_\mathrm{c} \to \infty$, where Σ_1^s vanishes (because there is no IR transparency regime anymore), we can use (4.35) to derive the standard Casimir energy, proving that also in 5D the DGP branes, which provide only effective boundary conditions in the finite r_c case, approach Dirichlet boundary conditions in the limit of infinite r_c.

4.3.1 Analytical Result for the Casimir Force in the Limit $r_\mathrm{c} \to \infty$

First, note that the Hamiltonian in the 5D case *does* include the zero-mode ($m_1 = 0$) because, even if it is constant along the extra dimension, the oscillations along the transverse directions still contain energy, $\omega_{0,1}(\vec{k}) \neq 0$ (see (4.1)). Also, $m_1 = 0$ is still a solution of (2.43), even in the limit $r_\mathrm{c} \to \infty$. Thus, separating out this zero-mode and using the masses (4.10b), valid in the limit $r_\mathrm{c} \to \infty$, we get

$$E^{\mathrm{reg}}(r_\mathrm{c}\to\infty) = \frac{3}{2}\frac{\pi^2}{a^4} - \frac{\pi^2}{4}\frac{\partial}{\partial a}\left[\frac{1}{a}\left(\frac{1}{d_1^2}S(d_1) + \frac{1}{d_2^2}S(d_2)\right)\right], \tag{4.36}$$

with

$$S(d_i) \equiv \sum_{n=1}^{\infty} n^2 K_2\Big(\frac{an}{d_i}\Big)\,, \quad d_1 = L - R\,, \quad d_2 = R\,. \tag{4.37}$$

The evaluation of $S(d_i)$ is performed in appendix D. Inserting the result (D.6)

in (4.36), we find

$$E^{\text{reg}}(r_c \to \infty) = \frac{3}{2}\frac{\pi^2}{a^4} - \frac{\pi^2}{4}\left(-\frac{6\pi}{a^5}d_1 + \frac{3}{a^4} + \frac{\zeta'(-4)}{8}\frac{1}{d_1^4} + \mathcal{O}\left(\frac{a^2}{d_1^2}\right) + (d_1 \leftrightarrow d_2)\right),$$
$$= \frac{3\pi^3}{2}\frac{L}{a^5} - \frac{\pi^2\zeta'(-4)}{32}\frac{1}{R^4} - \frac{\pi^2\zeta'(-4)}{32}\frac{1}{(L-R)^4} + \mathcal{O}\left(\frac{a^2}{d_i^2}\right), \quad (4.38)$$

with ζ' the derivative of the Riemann zeta function. In order to renormalize this expression, we have to once again subtract the vacuum energy of a system without branes. The latter is conveniently derivable from (4.35) for masses (4.3). Thus, we get

$$E_0^{\text{reg}} = E^{\text{reg}}(r_c \to 0) = \frac{3}{2}\frac{\pi^2}{a^4} - \frac{\pi^2}{2}\frac{\partial}{\partial a}\left(\frac{1}{a}\frac{1}{d_3^2}S(d_3)\right),$$

with $S(d_3)$ again given by (4.37), for $d_3 = L/2$. Then, again using (D.6), we find

$$E_0^{\text{reg}} = \frac{3\pi^3}{2}\frac{L}{a^5} - \pi^2\zeta'(-4)\frac{1}{L^4} + \mathcal{O}\left(\frac{a^2}{L^2}\right). \quad (4.39)$$

With this, we obtain the Casimir energy (per unit 3-volume) as

$$E_C(r_c \to \infty) = \lim_{\substack{a\to 0 \\ L\to\infty}} \left(E^{\text{reg}}(r_c \to \infty) - E^{\text{reg}}(r_c \to 0)\right),$$
$$= -\frac{\pi^2\zeta'(-4)}{32}\frac{1}{R^4} \quad (4.40)$$

and the Casimir force (per unit 3-volume) as[13]

$$F_C(r_c \to \infty) = -\frac{3\zeta(5)}{32\pi^2}\frac{1}{R^5}. \quad (4.41)$$

Notice that this is the same result as one would obtain for a system with a real, massless, 5D scalar field and two parallel "conducting" plates (with Dirichlet boundary conditions), separated along the fifth dimension [152]. However, we calculated this result in the DGP setup, using the limit $r_c \to \infty$ (after an explicit dimensional reduction). Thus, we proved that the DGP branes can indeed lead to effective Dirichlet boundary conditions, which give rise to the standard Casimir force in the limit of a vanishing IR transparency region.

4.3.2 Numerical Derivation of the Casimir Force

Since we are not able to derive the 5D analogues of (4.17) and (4.32), in the 5D system we have to rely entirely on numerical methods to show that the Casimir force gets weakened due to the leakage of the modes.

In order to calculate (4.35) numerically, we rewrite it as

$$E^{\text{reg}} = \frac{3\pi^2}{2a^4} + \frac{1}{8\pi}\frac{1}{a^2}\sum_{\alpha,m>0} m_\alpha^2\left\{2\pi K_2\left(\frac{am_\alpha}{\pi}\right) + am_\alpha\left[K_1\left(\frac{am_\alpha}{\pi}\right) + K_3\left(\frac{am_\alpha}{\pi}\right)\right]\right\}. \quad (4.42)$$

[13] We used here $\zeta'(-4) = \frac{3\zeta(5)}{4\pi^4}$.

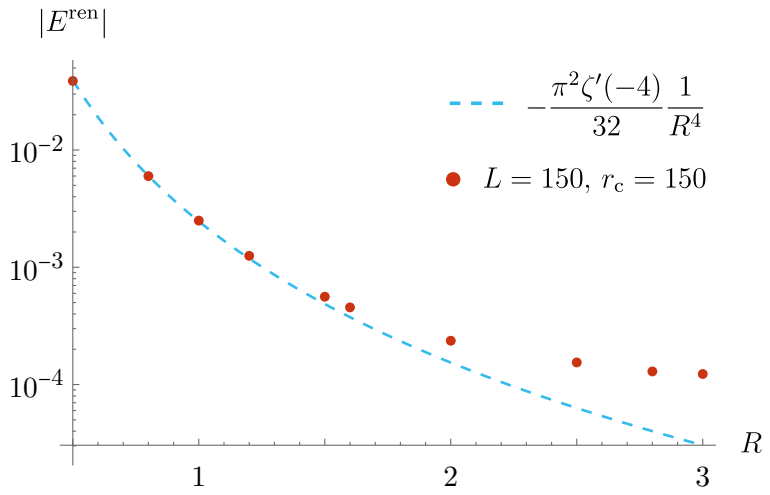

Figure 4.8: Logarithmic plot of the Casimir energy, calculated numerically (data points) for $a = 0.1$, $r_c = 150$ and $L = 150$. The dashed curve represents the standard (5D) Casimir energy (due to Dirichlet boundary conditions). We plotted the absolute values.

The vacuum energy without branes, which we have to subtract from (4.42), is obtained if we insert the masses (4.3) in the above expression (where the zero-mode has already been separated out), leading to

$$E_0^{\mathrm{reg}} = \frac{3\pi^2}{2a^4} + \frac{\pi}{L^2a^2}\sum_{n=1}^{\infty} n^2\left\{2\pi K_2\left(\frac{2an}{L}\right) + am_\alpha\left[K_1\left(\frac{2an}{L}\right) + K_3\left(\frac{2an}{L}\right)\right]\right\}. \quad (4.43)$$

Figure 4.8 shows the result for calculating

$$E^{\mathrm{ren}} \equiv E^{\mathrm{reg}} - E_0^{\mathrm{reg}} \quad (4.44)$$

numerically (for $r_c = 150$, $L = 150$ and $a = 0.1$), where we again shifted the result by an a-dependent constant (i.e. R-independent). We see that the standard Casimir energy (i.e. (4.40)) changes faster than our derived one. Hence, analogous to the 2D case, we find that the DGP branes weaken the resulting Casimir energy.

Guessing the first (non-constant) correction by analogy with the 2D case, (4.31), we suspect a term $\sim (R^3\rho)^{-1}$. We can convince ourselves by looking at Figure 4.9 that this correction gives indeed a good fit to the data. Hence, we finally establish the 5D Casimir force as

$$F_C = -\frac{3\zeta(5)}{32\pi^2}\frac{1}{R^5} + \frac{C}{R^4\sqrt{Rr_c}} + \mathcal{O}\left(\frac{1}{R^4 r_c}\right), \quad (4.45)$$

with the positive coefficient $C \simeq 2.6 \cdot 10^{-3}$. The smallness of this coefficient should not surprise us, since the coefficient of the leading term is already as small as $\frac{3\zeta(5)}{32\pi^2} \simeq 9.8 \cdot 10^{-3}$.[14]

[14] The coefficients in front of the (ordinary) Casimir force usually decrease rapidly with increasing spacetime dimension [152].

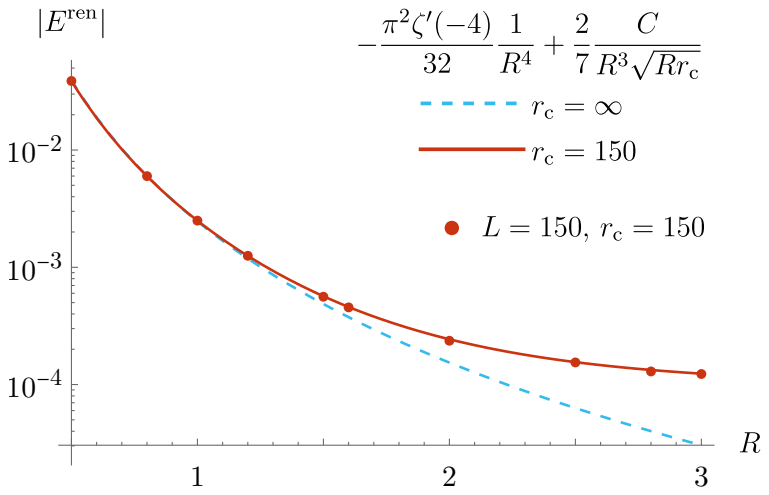

Figure 4.9: Logarithmic plot of the Casimir energy (data points) for the parameters $a = 0.1$, $r_c = 150$ and $L = 150$. Also shown is the plot of the function, stated in the plot legend, that was fitted to the data points, thereby determining the coefficient C. We suppress here the constant shift that we had to apply to the curve in order to fit the points. The dashed curve represents the standard (5D) Casimir energy (due to Dirichlet boundary conditions). We plotted the absolute values.

4.4 Summary and Discussion

We have investigated and established the existence of the Casimir effect in a system without fixed (Dirichlet) boundary conditions, but with surfaces that have the property to suppress the high-energy modes of a quantum field while being transparent to the low-energy modes. The DGP model with two parallel 3-branes in a 5D spacetime, where the DGP branes provide "effective" boundary conditions for the 5D quantum field, provided a particular example of such a system.

Furthermore, we have shown that the just described phenomenon, called IR transparency, has a profound implication for the arising Casimir force: it is weakened.

In order to analyze quantitatively how the IR transparency affects the Casimir force, we have studied in detail the 2D version of the system (two parallel 0-branes, separated along the extra dimension) and found that the IR transparency phenomenon has in fact two opposite contributions to the Casimir force. First, in the case of sharply separated regimes of "opaque" and "IR transparent" branes, the Casimir force increases due to the exclusion of IR modes from the spectrum of vacuum fluctuations between the branes. Second, since the DGP branes distinguish between hard and soft modes in a smooth manner, some of the hard modes "leak" out of the interior region between the branes, thereby weakening the Casimir force. It turns out that the latter effect dominates, and hence the resulting Casimir force decreases.

We have analytically derived the qualitative expressions of the leading correction terms to the Casimir force in the 2D case and justified the expressions by numerical analysis, for both the 2D and 5D system. Regardless of the dimension-

ality, we find that the corrections are suppressed by increasing powers of ρ, where $\rho \equiv \sqrt{Rr_c}$ is the new distance scale (geometric mean between the separation distance of the branes and the DGP cross-over scale) that already arose in this system when we explored its gravitational force law. The similarity between systems of different dimensions is not surprising, since in both cases the effect comes from codimension-one DGP branes, separated along the extra dimension.

We have performed our analysis for a massless, real scalar field with localized kinetic terms on parallel surfaces, thereby showing that the derived effect is very generic. It is beyond the scope of this thesis to repeat the analysis for spin-1 and spin-2 fields. However, as we explained in the beginning of this chapter, we do not expect the results to change, except for numerical $\mathcal{O}(1)$ factors due to the increased number of degrees of freedom. Also, even though a modified gravitational theory such as the DGP model exhibits non-linear behavior at intermediate distances, i.e. where gravity behaves four-dimensional (see the discussion in section 2.1.2), this should not modify our result because the Casimir effect is an IR effect that persists after cutting off the high-energy behavior of the system. Moreover, the Vainshtein radius, below which such non-linearities set in, goes to zero if we are considering a vacuum setup without sources. Of course, the assertions made in this paragraph should be verified in future work.

Since the emergent Casimir force—along with its corrections—is a signature for brane-world scenarios with parallel DGP branes, it might be interesting for future research to further investigate how the presence of this force affects those scenarios. Moreover, since this effect should also be present for a large number of setups, including our 4D world, it is worthwhile to investigate if there are materials that allow for surfaces with a sufficiently low scale r_c such that an observation of this modified Casimir force is possible.

Finally, the presence of the derived effect shows that it is natural to construct "effective" boundary conditions for the graviton in the described way, thereby providing a mechanism to produce the gravitational Casimir effect and the means to probe the quantization of the gravitational field, which otherwise eludes experimental access. However, we want to point out that the parameter r_c for a quasi-localization of gravitons on surfaces in our *four-dimensional* world should be minuscule. But then, the above result is not valid anymore, since we worked in the limit $r_c \gg R$ and implicitly assumed that the width of the branes is much smaller than R (to be able to use the idealization of zero width). Therefore, to trust our result, r_c has to be much larger than the width of the surfaces—a situation which is probably not realized for realistic materials in two-dimensional surfaces in our world.

5

Conclusion and Outlook

If our world is indeed described by an embedding of a lower-dimensional plane, with a DGP curvature term, in a higher-dimensional spacetime, then it might very well be possible that other DGP branes, dislocated from us, exist in the universe. In fact, as mentioned in section 1.1.1, various scenarios exist in the literature that employ a brane-world construction, albeit usually without considering those DGP curvature terms. Yet, it appears natural that a higher-dimensional graviton propagator should receive quantum corrections on branes with localized particle species, thus leading to such DGP branes.

The first part of the present thesis dealt with the exploration of such a scenario. In the preceding chapters we demonstrated that the DGP model, extended through the inclusion of a second brane with a localized curvature term, gives rise to distinctive forces if the brane separation R is parametrically smaller than the DGP cross-over scale r_c. Those forces have both a classical and a quantum mechanical origin.[1]

New Forces

The classical gravitational force in this double-brane setup carries a new length scale, $\rho = \sqrt{Rr_c}$. Whereas for distances much larger than ρ the original results of the single-brane DGP model are recovered, for smaller distances gravity is screened even more, resulting in the fact that the gravitational force has a different form and exhibits phenomenologically interesting new regimes. In particular, we found that the force between point masses on different branes is distance-independent if the worldvolume distance r is much larger than the brane separation R (i.e. $R \ll$

[1] Of course, if the localized curvature term is indeed due to quantum corrections from the SM fields, then both the modified gravitational force and the Casimir force ultimately emerge from quantum mechanics.

$r \ll \rho$). For sources on the same brane, we discovered that the force interpolates between a 4D Newton force for $r \ll \rho$ and a 4D Newton force with half its strength for $r \gg \rho$ (the latter is the ordinary DGP behavior in the $r \ll r_c$ limit).

The same characteristic length scale ρ also appears in the emerging Casimir force, which is quantum mechanical in origin. There, it controls the (weakening) first-order correction to the Casimir force, whose leading term is the same as in the standard result for parallel boundaries with Dirichlet boundary conditions.

We discussed several phenomenological applications of these forces. For example, we outlined the tantalizing implications of the distance-independent gravitational force for galactic dynamics, possibly avoiding the missing mass problem. We also pointed out that the Casimir effect, which emerges naturally in the present setup, can be a probe of the quantization of the gravitational field.

Furthermore, those results can have important implications for the numerous proposals in the brane-world framework. As previously mentioned, it is conceivable that in many scenarios proposed in the literature the branes should be supplemented by the localized DGP terms. Hence, the potentials discussed in the present work could affect those proposals and would possibly modify their predictions. Thus, it might be worthwhile to revisit some of those brane-world scenarios in future work and estimate if the results of this thesis would have a relevant impact.

Moreover, if the higher-dimensional world does indeed incorporate such a setting, the physical effects derived in this thesis will indeed occur, and hence observing them could in turn provide information about that brane-world structure. Although we considered just a special idealization—two parallel branes—there is also the possibility to extend our work and explore scenarios with more than two branes and possibly to consider branes that intersect each other at different angles. It is likely that such generalizations of the present setup still experience the key properties of our result, as long as the generalized configurations are not too much deformed. For example, one could consider two branes that intersect each other at a small angle, or one could include a third brane that has a much greater distance than the separation of the initial two branes. It would be interesting to analyze what new regimes for the forces would open up in these cases. Such an investigation could further increase our diagnostic tool set for exploring the brane-world surrounding us—if it is indeed out there.

Observational Signatures

Besides the fact that the discovered forces are interesting in their own right, with possibly crucial phenomenological implications, they could be powerful experimental signatures not just for the existence of a brane-world but for the DGP model itself (in the presence of more than a single brane) and a further method to test the DGP framework.

Before discussing that, let us briefly summarize some of the existing results of testing the observational viability of the DGP model. First, we have to switch back to the more realistic geometrical model (with the action given in (1.2)), which describes more than just our propagating toy scalar field, in order to discuss the experimental status of the DGP model. Also, since the observational tests are

usually carried out for the original single-brane proposal, we will now discuss that single-brane model.

Experimental tests have been performed on all scales, from laboratory to Hubble distances, but we would like to focus on just two kinds of experimental observations: cosmological surveys and solar system tests (see e.g. Refs. [134, 137] for a more complete discussion, including other tests). Let us start with the solar system tests.

For the DGP model to be able to reproduce the experimentally well-tested 4D Newton's law on solar system scales, it is clear that r_c has to be much larger than the solar system size. This much is already apparent from looking at (2.24) (together with (2.25)). However, as discussed in section 2.1.2, Newton's law (2.24) is only valid for distances that are much larger than the Vainshtein radius r_V, where the linear approximation can be applied and the scalar degree of freedom contributes to the gravitational potential. The *actual* (i.e. observed) 4D Newton's law (with the correct numerical prefactor) is only valid for $r \ll r_V$, where that scalar degree of freedom decouples, due to self-interactions. Hence, the DGP model predicts a deviation from the observed 4D Newton's law already for distances that are much smaller than r_c. For example, if we take $r_c \sim H_0^{-1} \sim 10^9\,\mathrm{pc}$, then the Vainshtein radius for Earth is

$$r_V \sim \left(r_c^2 G M_{\mathrm{Earth}}\right)^{1/3} \sim 1\,\mathrm{pc} \tag{5.1}$$

(see also Ref. [134] for a review).[2] Although this is still parametrically larger than the solar system size, it shows that deviations from 4D Newtonian gravity would set in much earlier, even for a Hubble-size cross-over scale r_c. In other words, measurements in our solar system could test the DGP model and constrain its parameter r_c [131, 132]. A recent overview of completed and planned experimental tests of the DGP model can be found in Ref. [153] (and references therein).

Next, let us have a look at the cosmological observations, which so far appear to have put the tightest constraints on r_c. Cosmological observations can be further divided into "geometric probes" (which include the late-time evolution of the universe) and studies of the formation of large-scale structures. It is useful to combine these observations because whereas the DGP model and the ΛCDM model can predict similar late-time evolutions of the universe, the formation of large-scale structures is also sensitive to the underlying gravitational theory, and in fact observations of the latter can distinguish effectively between the DGP model and the ΛCDM model (see e.g. Refs [135, 154]).[3]

[2]Note that the form of the Vainshtein radius given in (5.1) is valid for compact, spherically symmetric sources on a Minkowski background. If, instead, we consider more realistic cosmological backgrounds like de Sitter (using the normal branch), as we will do in a moment, then the expression gets modified by an additional factor $(1 + 2r_c H_0)^{-2/3}$ [131]. However, if we take $r_c \sim H_0^{-1}$, then r_V just gets an order-one correction. Also note that for $r_c \gtrsim H_0^{-1}$, the Vainshtein radius approaches the distance scale beyond which the cosmological flow dominates over the gravitational effects of the local source. Hence, even if we take into account a brane tension in the following discussion, (5.1) still marks the scale below which gravity behaves approximately as 4D GR, in the single-brane setup.

[3]In addition, weak lensing observations can also help to distinguish between those models [155].

Since cosmological observations indicate that the late-time evolution of the universe exhibits an accelerated expansion (see also the discussion in section 1.1), it can be expected that a tensionless brane, using the normal branch of solutions (see section 1.1.1), i.e. the setup we have been exploring in this thesis, would be much inferior to the ΛCDM model in explaining cosmological data. At least, it would be required to consider a tensionless brane in the self-accelerating branch. Unfortunately, however, cosmological tests even seem to suggest that the self-accelerating branch is disfavored by observations (see e.g Refs. [156, 157], as well as Ref. [158] and references therein), unless a brane cosmological constant is included as well. In the case of the normal branch (and including a brane tension), observations indicate that the DGP model is compatible with observations for $r_c \gtrsim H_0^{-1}$ [147, 157] (or even $r_c \gtrsim 10\, H_0^{-1}$ according to Ref. [159]).

Thus, since the DGP model has neither been experimentally excluded so far nor have its numerous predictions been observed, it might be useful that the setup studied in the present thesis delivers new, distinctive features. As just explained, the DGP model makes the strong prediction that 5D gravity gets screened, and the result is 4D gravity, which interpolates between a region where GR is recovered (below the Vainshtein radius) and a region where scalar-tensor gravity is operating (above the Vainshtein radius but below the cross-over scale). Because the Vainshtein radius of massive objects in the solar system like Earth is so large and the cross-over scale is around the Hubble scale, the effects of the DGP model on solar system physics have not quite been relevant enough, yet. The same is true for the Milky Way and associated galactic-size physics.

However, in the present thesis, we demonstrated that a second DGP brane can further change that behavior by even weakening 4D gravity and producing an intricate novel force with a modified behavior in the region $r \ll \rho$. This adds to the signatures of both the DGP model and brane-world scenarios with more than a single brane, especially if sources are located on the other branes as well. But also for the gravitational force between sources on our brane, we found that at distances $r \simeq \rho$ the force changes; it interpolates between two 4D Newton's laws with a different overall constant. Since $\rho \ll r_c$, we could find ourselves in the fortunate situation that the presence of an additional, nearby brane can improve the observability of the effects of the DGP model.

More precisely, returning to our discussion in section 3.2, there would be the following difference between a single-brane and a double-brane scenario: let us first consider two sources on our brane. If we approximate one of the sources as a point source with the mass of the Milky Way, then, in the single-brane case, the force acting on us (the probe source) would be the standard Newton force (due to the exchange of two tensor degrees of freedom). Since the Vainshtein radius is around 1 Mpc, it is difficult to measure an effect due to DGP inside our galaxy, whose visible part is one to two orders of magnitude smaller. However, if a second (empty) brane would be present at distance R, then the gravitational force would start to change around

$$r \sim \rho = 1\,\mathrm{Mpc}\left(\frac{R}{\mathrm{kpc}}\right)^{1/2} .$$

Hence, for $R \lesssim$ kpc, there might be hope for this change in behavior to be measurable.

Let us next consider the force acting on us from a point source (a "dark galaxy") separated along the extra dimension. As we saw in section 3.2 (see e.g. Figure 3.3), if the source is located in empty space (as in the case of the single-brane scenario), then the force would interpolate between a linear regime and the ordinary 4D Newton force in the transition region $r \sim R$. In the scenario where the dislocated source is attached to a DGP brane, there is also a change in behavior around R, but it is different. Now, the force interpolates between a linear and a constant force. Only later, at $r \sim \rho$, the 4D Newton force is recovered. We already explained in section 3.2 that this new behavior could not only be observable but even be potentially critical for explaining observations in a certain class of galaxies.

In this last-mentioned example, the Vainshtein radius of the "dark galaxy" is even larger than 1 Mpc, and hence it would be hopeless to observe the transition to the scalar-tensor gravity regime (i.e. the regime where the scalar degree of freedom becomes relevant). The reason for this is that (as explained in section 3.2) if we want to consider a "dark galaxy" whose gravitational effect is observationally significant, we have to postulate its mass to be much larger than the Milky Way mass.

Finally, the discovered Casimir effect could also contribute to the phenomenological consequences of the DGP model if the Casimir force between the branes could be measured or deduced through secondary effects. Moreover, we showed that the DGP model would not just generate the standard Casimir force but also induce a distinct correction to it, which scales as

$$\sqrt{\frac{R}{r_c}} = 10^{-3}\left(\frac{R}{\text{kpc}}\right)^{1/2}.$$

Hence, in this case, a brane separation of $R >$ kpc (as long as $R \lesssim r_c \sim 10^6$ kpc) would increasingly raise the correction and hence sharpen the characteristic signature of the DGP model.

Interplay Between Short and Long Distances

Another, possibly important result of our analysis is the implication of a system containing a multitude of DGP branes for the assertion that the modifications of GR at large and short distances are actually interconnected. We explored such a relation by means of the short distance cutoff of semi-classical gravity, obtainable from BH physics. Although we merely touched upon this subject, our investigation shows some indication that the large distance modification of gravity in the simplified scalar field model, which does not take into account all degrees of freedom, is in tension with the short distance modification of GR coupled to quantum fields. As we pointed out in section 3.4.1, a more detailed analysis of the present setup, working in the full spin-2 theory and tracking the effect of the brane bending mode, might be necessary to clarify the relation of the BH bound, in the presence of a large number of particle species, and theories that modify gravity at large distances.

Validity of the Simplified Model

We have repeatedly pointed out that we do not expect any qualitatively different behavior of the results (with the possible caveat expressed in the previous paragraph) if we generalize our analysis to the full-fledged DGP model, which is the theory of a spin-2 particle rather than a spin-0 particle. The main change will be that instead of a scalar mode, the derived effects will be mediated by different degrees of freedom. In the case of the Casimir force, these include the full spectrum of five degrees of freedom: two tensor modes, two vector modes and one scalar mode. In contrast, for the gravitational force between static point masses, two tensor degrees of freedom will contribute at distances below the Vainshtein radius and three degrees of freedom (two tensorial and one scalar) in the region above that scale. Hence, as long as we do not discuss gravitational regimes that include this transition region at r_{V}, we anticipate that the analysis of the complete spin-2 theory would produce results that are merely modified by multiplicative order-one factors with respect to our findings.

We have to mention, however, that the previous conclusion (in the case of the gravitational force) relies on the existence of the Vainsthein mechanism. Although it appears likely, it is important for future research to confirm that such a mechanism, which ensures that the scalar mode decouples below a certain distance scale, is indeed present in the double-brane system. Furthermore, our earlier discussion about the difference between experimental signatures in the single-brane and the double-brane DGP model implicitly assumed that the Vainshtein radius continues to have the form (5.1) and, especially, that it is independent of the new scale ρ. This too has to be verified in future work.

Concerning additional degrees of freedom, we further explained that the potential appearance of a radion mode in the spin-2 theory, due to the presence of a second brane, would not affect our result (according to Ref. [75]) because we are considering a Minkowski brane, embedded in 5D Minkowski space, and hence such a mode is unphysical. As explained above, however, observations indicate that a modification of the current setup is required, prompting us to consider a de Sitter brane (i.e. we have to include a non-vanishing brane tension). In such a situation, a tachyonic radion would indeed appear, leading to a destabilization of the brane separation [75] (see also Refs. [160, 161]). Hence, further detailed analysis would be necessary, including the investigation of possible mechanisms of radion stabilization [162] (see also Ref. [163]). Such issues have to be addressed in future work.

Now, does the addition of a brane tension have another impact on the gravitational dynamics and the Casimir effect derived in this thesis, not related to the threatening radion instability? In the case of the modification of the DGP gravitational laws, since we are still assuming a vanishing bulk cosmological constant, the presence of a brane tension could only affect gravitational dynamics along our brane, e.g. our discussion about the application to galactic rotation curves. However, since the brane cosmological constant has to be extremely small, on observational grounds (its best fit value, obtained from observations, is very close to the value of the ΛCDM model), it would not affect our results for the same reason that in the standard ΛCDM paradigm galactic dynamics are not affected by the

cosmological constant.

The Casimir effect would also likely be not affected, because the space between the branes would still be Minkowski. Also, even though for the infrared modes the constant term from the modified brane action (containing the brane tension) could become increasingly important, it is not a priori obvious to us if it would affect the resulting Casimir force. Moreover, it is not clear if a possible correction would be comparable to the one we found in the phenomenologically relevant regime where R is much smaller than the de Sitter curvature radius, associated with the brane cosmological constant. This question would need to be investigated in future research.

Part II

Dark Matter

6

Superfluid Dark Matter

In this last part of the thesis, we wish to analyze a particular DM model. We will begin this chapter by introducing it and then examine the different parameter regions that lead to diverse DM phenomenology. To be self-contained, we will review some of the well-known properties of that model in the first section, before discussing the new (observational) bounds on the considered scenario in subsequent sections.

Note that we will work exclusively in the non-relativistic limit, since cosmological observations indicate that DM should behave as a non-relativistic fluid, i.e. pressure-less dust (see also section 6.3).

This chapter is based on the collaborative work published in Ref. [3]. Figures 6.2, 6.3, and 6.4 and some of the equations have been reproduced verbatim.

6.1 The Superfluid in the Presence of Gravity

In the following, we will be concerned with a DM model of a massive (with mass m), complex, repulsively self-interacting (with coupling constant $\lambda > 0$) scalar field Φ, minimally coupled to gravity. The corresponding action is given by

$$S = \int \mathrm{d}^4x \sqrt{-g} \left(-\frac{M_\mathrm{P}^2}{2} R + |\partial_\mu \Phi|^2 - m^2 |\Phi|^2 - \frac{\lambda}{2} |\Phi|^4 \right), \tag{6.1}$$

where, as usual, g and R are the (determinant of the) metric and the Ricci scalar, respectively.[1] The equations of motion for this theory read

$$\begin{aligned} &G_{\mu\nu} = M_{\mathrm{P}}^{-2}(\partial_\mu\Phi\partial_\nu\Phi^* + \partial_\mu\Phi^*\partial_\nu\Phi - g_{\mu\nu}\mathcal{L}_M) && \text{(Einstein field equations)}\,, \\ &(g^{\mu\nu}\nabla_\mu\nabla_\nu - m^2 - \lambda|\Phi|^2)\Phi = 0 && \text{(equation of motion for } \Phi)\,, \end{aligned} \tag{6.2}$$

where ∇_μ is the covariant derivative, and

$$\mathcal{L}_M \equiv |\partial_\mu\Phi|^2 - m^2|\Phi|^2 - \frac{\lambda}{2}|\Phi|^4\,. \tag{6.3}$$

If we switched off gravity, the above theory would have the (classical) solution

$$\Phi = v\mathrm{e}^{\mathrm{i}\mu t}\,, \tag{6.4}$$

where v and

$$\mu \equiv \sqrt{m^2 + \lambda v^2} \tag{6.5}$$

are constants. The physical interpretation of these quantities is well studied in the literature (see e.g. the lecture notes in Ref [103]), so we will not discuss this further. The solution (6.4) describes a homogeneous field configuration, which can be interpreted as a Bose-Einstein condensate (since we are at zero temperature, all the DM particles are in the zero-momentum ground state). Due to the U(1) symmetry of the theory (6.1), there is a conserved quantity, the particle number (or number density n), that stabilizes the configuration (6.4) against decay.[2] In the non-gravitational case, the particle number density of the constituents (the DM particles) is not only time-independent but also constant throughout space.

However, in the presence of gravity the picture changes, since now the energy density of the condensate sources the gravitational Newton potential, which, in turn, modifies the energy distribution of the condensate.[3] In order to find a stable configuration, one must then solve the full set of equations (6.2), in the appropriate limit that we consider. Often, this is done in the hydrodynamical description, where the DM substance is treated as a perfect fluid with the equation of state

$$p = \frac{\lambda\rho_{\mathrm{DM}}^2}{8m^4}\,, \tag{6.6}$$

which relates the pressure p to the DM energy density ρ_{DM}, with the relation $\rho_{\mathrm{DM}} = nm$. Then, one can use Euler's equation, together with Poisson's equation, to solve for the now spatially varying ρ_{DM} (see e.g. Ref. [164]). We show the resulting profile below (see (6.9)).

An alternative derivation can be performed using the Lagrangian formalism directly. For this, it is convenient to describe the DM sector not in terms of Φ but to expand around the solution (6.4),

$$\Phi = \Big(v + \chi(x)\Big)\mathrm{e}^{\mathrm{i}[\mu t + \pi(x)]}\,, \tag{6.7}$$

[1] In the present chapter, all quantities are understood to be four-dimensional.

[2] Note that in the non-relativistic limit that we are considering even the decay of the classic solution of a *real* scalar field would be highly suppressed.

[3] Recall that we are considering the non-relativistic (and gravitational weak-field) limit of the theory, in the present chapter.

where χ and π are real scalar field degrees of freedom. It is then straightforward to integrate out χ perturbatively (on the level of equations of motion), using a derivative expansion, thereby deriving a low-energy effective theory for the Goldstone mode π and the gravitational potential $\phi_{\rm N}$.[4] At leading order (i.e. simply neglecting the $(\nabla\chi)^2$-terms), this leads to (see e.g. Refs. [119, 165])

$$S = \int \mathrm{d}^4x \left[M_{\rm P}^2 \phi_{\rm N} \Delta\phi_{\rm N} + \frac{2m^2}{\lambda}\left(\mu_{\rm NR} - m\phi_{\rm N} + \dot{\pi} - \frac{(\nabla\pi)^2}{2m}\right)^2\right], \tag{6.8}$$

with

$$\mu_{\rm NR} \simeq \mu - m$$

(in the non-relativistic limit).

We can thus derive the static configuration, by setting $\pi = 0$ (which is consistent with its equation of motion) and solving the equation for the Newton Potential,

$$\Delta\phi_{\rm N} = \frac{16\pi G m^3}{\lambda}(\mu_{\rm NR} - m\phi_{\rm N})\,.$$

From its solution

$$\phi_{\rm N} = \frac{\mu_{\rm NR}}{m}\left(1 - \frac{\sin(2\pi r/a)}{2\pi r/a}\right)$$

and the Poisson equation

$$\Delta\phi_{\rm N} = 4\pi G \rho_{\rm DM}(r)\,,$$

we can immediately read off the DM density profile

$$\rho_{\rm DM}(r) = \rho_0 \frac{\sin(2\pi r/a)}{2\pi r/a}\,, \tag{6.9}$$

where the size of this profile is given by

$$a \equiv \sqrt{\frac{\pi\lambda}{4Gm^4}}\,, \tag{6.10}$$

and

$$\rho_{\rm DM}(r=0) \equiv \rho_0 = \frac{4m^3}{\lambda}\mu_{\rm NR} = nm \tag{6.11}$$

is the (unperturbed) energy density of the condensate, with n being the conserved particle number density, as introduced above.

The corresponding configuration is depicted in Figure 6.1. It is sometimes called (non-topological) *soliton* in the literature because it is the stationary, minimum-energy solution (for a given particle number) of the theory in (6.1).

Another way to see that the homogeneous configuration (6.4) is not stable in the presence of gravity and to find the characteristic scale a of the stable configuration, given in (6.10), is to keep π switched on in (6.8) and consider perturbations. But

[4] The actual massless mode will be a linear combination of π and χ because of a kinetic mixing term $\dot{\pi}\chi$.

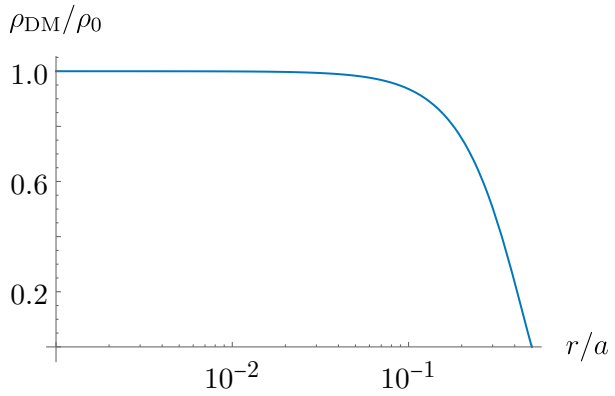

Figure 6.1: Log-linear plot of the density profile (6.9) (normalized by ρ_0) in units of r/a. We see that for $r \lesssim 0.1a$ the profile is given by a constant core.

note that if we also want to account for processes with momentum transfer $k \gtrsim c_{\rm s}m$, where $c_{\rm s}$ is the sound speed of the phonons, (while still being in the non-relativistic regime, $k \ll m$ and $c_{\rm s} \ll 1$) we have to include higher-order terms in the aforementioned derivative expansion [119]. If taking into account the next-to-leading-order term in this expansion, one can derive the dispersion relation of the perturbation π to be (see e.g. Ref. [119])

$$\omega_k^2 = -4\pi G\rho_0 + c_{\rm s}^2 k^2 + \frac{k^4}{4m^2}\,, \quad c_{\rm s}^2 \equiv \frac{\lambda\rho_0}{4m^4}\,. \tag{6.12}$$

It is clear that the first term, which can be considered a tachyonic mass due to gravity, tends to destabilize the perturbations. It leads to the Jeans length, beyond which the structure is not stable anymore, for perturbations of the appropriate wavelengths. The precise critical wavenumber depends on which of the two positive terms dominates the perturbation spectrum. These two terms correspond to different pressure components of the fluid that are responsible for balancing the attractive gravitational force. The quadratic (in k) term, proportional to the sound speed or the coupling constant, is due to the repulsive self-interactions, while the quartic term corresponds to the so-called *quantum pressure*, which is due to the de-localized nature of quantum particles. The critical value for the wavenumber, below which the perturbations cause instabilities, is given by the expression

$$k_*^2 \equiv 2m^2 c_{\rm s}^2\left(-1 + \sqrt{1 + \frac{4\pi G\rho_0}{m^2 c_{\rm s}^4}}\right). \tag{6.13}$$

We see that the dimensionless quantity

$$\xi \equiv \frac{m^2 c_{\rm s}^4}{4\pi G\rho_0}\,, \tag{6.14}$$

$$= \frac{4\pi\rho_0 M_{\rm P}^2\sigma}{m^4} \tag{6.15}$$

controls which is the relevant pressure component that competes with the gravitational attraction. To derive (6.15), we have used the expression for the scattering

cross section

$$\sigma = \frac{\lambda^2}{32\pi m^2}\,. \tag{6.16}$$

For $\xi \ll 1$ (the non-interacting limit),

$$\lim_{\xi\ll 1} k_*^2 = \sqrt{16\pi G\rho_0 m^2}\,, \tag{6.17}$$

while for $\xi \gg 1$, we get

$$\lim_{\xi\gg 1} k_*^2 = \frac{4\pi G\rho_0}{c_{\rm s}^2}\,. \tag{6.18}$$

The first case ($\xi \ll 1$), which we will refer to as the *degeneracy pressure case*, has been explored extensively in the so-called Fuzzy Dark Matter (FDM) scenario [118, 128]. Hence, the second case ($\xi \gg 1$), called *interaction pressure case*, will be the focus of the present work.

Let us estimate ξ for a typical scenario in that we are interested. If we use $\rho_0 \simeq 10^{-25}\,\mathrm{g/cm^3}$, which is the average DM density in inner regions of the Milky Way,[5] we find

$$\xi \simeq 10^{27}\left(\frac{\sigma/m}{\mathrm{cm^2/g}}\right)\left(\frac{m}{\mathrm{eV}}\right)^{-3}\,,$$

using (6.15). Here, we already see that $\xi \gg 1$, unless the scattering cross section (per mass) is extremely low, in which case we are forced to consider an ultra-light DM scenario, with $m \ll \mathrm{eV}$, to stay in the interaction pressure case.

In this regime, high-energy corrections are not important, and thus we can use (6.8). Therefore, the stable density profile is well approximated by expression (6.9), and the Jeans length

$$\ell \equiv 2\pi/k_* = \sqrt{\frac{\pi\lambda}{4Gm^4}} \tag{6.19}$$

precisely coincides with the size of the spherical configuration (see (6.10)). Note that this length scale is independent of the number density of DM particles, which is a feature of the particular scalar field theory (possessing 2-body interactions) but does not generalize to other potentials. We can also express the Jeans length in terms of the scattering cross section

$$\ell = 2\pi\left(\frac{8\pi M_{\rm P}^4}{m^5}\frac{\sigma}{m}\right)^{1/4} \simeq 2\,\mathrm{kpc}\left(\frac{\sigma/m}{\mathrm{cm^2/g}}\right)^{1/4}\left(\frac{m}{\mathrm{meV}}\right)^{-5/4}\,, \tag{6.20}$$

which shows what is the necessary combination of the parameters of the theory in order to achieve a macroscopic (i.e. kpc-size) core.

A comment is in order here regarding the validity of describing the DM in the central regions of galaxies and galaxy clusters in terms of Bose-Einstein condensates, where all particles occupy the ground state. Underlying the above discussion, was the presumption that we deal with zero temperatures, which is of course not realized in real, astrophysical situations. However, if we relate the temperature T

[5] In particular, this is approximately the value for the average density of a thermalized core within a radius between 15 kpc and 60 kpc, determined by using the NFW profile.

to the virial velocity (dispersion) $v \sim 10^{-3}$ in a typical galaxy, by using $T \sim mv^2$, we find

$$T \sim 10^{-6}\,\mathrm{eV}\left(\frac{m}{\mathrm{eV}}\right).$$

The fraction of particles in the condensate with respect to the total number is given by (see e.g. Ref. [166])

$$\frac{n}{n_{\mathrm{tot}}} = 1 - \left(\frac{T}{T_{\mathrm{c}}}\right)^{3/2}, \tag{6.21}$$

where $T_{\mathrm{c}} \sim m^{-5/3}\rho_{\mathrm{DM}}^{2/3}$ is the critical temperature,[6] which again for a typical galactic density can be approximated by

$$T_{\mathrm{c}} \sim 5 \times 10^{-5}\,\mathrm{eV}\left(\frac{m}{\mathrm{eV}}\right)^{-5/3}.$$

Instead of comparing T and T_{c}, we can alternatively compare the energy density to the critical density, which in a typical galaxy is

$$\rho_{\mathrm{c}} \sim m^4 v^3 \sim 10^{-28}\,\mathrm{g/cm^3}\left(\frac{m}{\mathrm{eV}}\right)^4.$$

Hence, we see that for particles whose masses are significantly lighter than eV the zero-temperature approximation is well justified in the inner regions of galaxies. Even though in a physical situation the superfluid cores will always be accompanied by a "normal" gas component, the latter will become significant only outside the cores, when the densities have dropped by several orders of magnitude.

6.2 Formation of the Superfluid Core

Next, we want to discuss in more detail the conditions leading to the formation of the superfluid cores. In order for the Bose-Einstein condensate to form, two conditions must be satisfied. First, the particles must have reached thermal equilibrium.[7] For this, the interaction rate Γ has to satisfy $\Gamma \gtrsim t_{\mathrm{eq}}^{-1}$, where t_{eq} is the time available to achieve the equilibrium. At the very least, the particles need enough time to scatter once on average, which we will denote by $t_1 = \Gamma^{-1}$. Since the interaction rate depends on the particle density, which in turn grows for decreasing distances from the center of the galaxy or cluster, we can associate a thermal radius R_{T} below which thermal equilibrium is reached.

[6] Although the fractional power of 3/2 only holds for a non-interacting Bose gas, we can still use this formula as an estimate for our weakly interacting bosons.

[7] Note that even without thermalization, it would be possible to describe highly degenerate DM particles by the classical, homogeneous field configuration, with the perturbation spectrum given by (6.12). The coherence length in this case is estimated as $l_{\mathrm{c}} \simeq \min(2\pi/k_*, \lambda_{\mathrm{dB}})$ [125], where λ_{dB} denotes the de Broglie wavelength. However, without the additional ingredient of thermal equilibrium, it can be shown (by using typical galactic virial velocities) that l_{c} always reduces to λ_{dB} (unless one is willing to consider masses that are even lighter than in FDM). Hence, without invoking thermalization, one ends up with the FDM scenario, which requires extremely light particles ($\lesssim 10^{-22}\,\mathrm{eV}$) to get a kpc-size core.

Second, the particles need to start populating the ground state, which happens at densities $n \gtrsim n_c \sim (mT)^{3/2}$, as indicated above. Below the radius that we denote as the degeneracy radius $R_{\rm deg}$ the particle density exceeds such a critical density.

Which of these conditions is satisfied first in an astrophysical setting, or equivalently the hierarchy of the radii $R_{\rm T}$ and $R_{\rm deg}$, depends on several parameters (λ, m, $\rho_{\rm DM}$). Additionally, a third length scale enters, namely the Jeans scale, which determines the size of stability of the superfluid cores that can form after both of those conditions are met.

In the following, we want to distinguish two cases, corresponding to the scenarios that either $R_{\rm T} > R_{\rm deg}$ (case **(i)**) or $R_{\rm T} < R_{\rm deg}$ (case **(ii)**). Since a full analysis of the non-linear process responsible for creating the galactic structures is beyond the scope of the present thesis, we will discuss the process in a somewhat qualitative manner, exploring the scenario that in the outside regions of galaxies there is no thermal equilibrium. Thus, we assume that in the outer regions, where the condensate has not formed yet, the density profile of the galaxy is well approximated by the NFW profile (1.7). This assumption appears to be justified by simulations of self-interacting DM scenarios (see e.g. Ref. [121] and references therein).

Then, if we approach smaller radii, one of the two scenarios will be realized, depending on the parameters m and λ. In case **(i)**, the interaction rate is given by the standard expression (see (6.25)). However, if case **(ii)** occurs and hence the DM substance is in a highly degenerate state while thermalization sets in, the interaction rate is enhanced by a degeneracy factor that roughly corresponds to the number of bosons in the same state.

Thus, the interaction rate can be expressed as [167, 168]

$$\Gamma = \frac{\sigma}{m}\rho_{\rm DM} v \mathcal{N}\,, \tag{6.22}$$

where we estimate v as the orbital circular velocity

$$v(r) = \sqrt{\frac{GM(r)}{r}}\,, \tag{6.23}$$

with $M(r)$ the enclosed mass at distance r, and

$$\mathcal{N} = \max\left\{1,\ \frac{\rho_{\rm DM}}{m}\left(\frac{2\pi}{mv}\right)^3\right\} \tag{6.24}$$

is the aforementioned degeneracy factor.

Now, we want to study the two cases in turn. We would also like to note that whenever we will be using the NFW profile in the following sections in order to produce numerical estimates for a Milky Way-like galaxy, we are going to use the total mass $M_{\rm DM} = 10^{12} M_\odot$ and the concentration parameter $c = R_{\rm V}/r_{\rm s} = 6$ (note that the parameter $\rho_{\rm c}$ is then also fixed).

6.2.1 Case (i): Non-Degenerate Thermalization

For $r > R_{\rm T} > R_{\rm deg}$, we have a classical gas of weakly interacting DM particles that approaches local thermal equilibrium at $r \simeq R_{\rm T}$ (while $\mathcal{N} \simeq 1$). Then,

for $R_{\rm T} > r > R_{\rm deg}$, the DM particles are approximately in thermal equilibrium, but since they mostly occupy excited states, the density profile in this region is similar to the one obtained in self-interacting DM models. Finally, at distances $R_{\rm T} > R_{\rm deg} > r$, condensation will occur, and the configuration is expected to be dominated by either one superfluid core of size ℓ or a collection of superfluid islands if $R_{\rm deg} \gg \ell$.

In order to derive the thermalization radius $R_{\rm T}$, we have to solve

$$\Gamma t_{\rm g} = \frac{\sigma}{m}\rho_{\rm DM}(R_{\rm T})v(R_{\rm T})t_{\rm g} = 1\,, \tag{6.25}$$

where we have defined the thermalization radius as the radius below which the DM particles had enough time to scatter once on average, i.e. $t_{\rm eq} = t_1 = \Gamma^{-1}$. For our crude estimates, it suffices to use the rough approximation $t_{\rm g} \simeq 13\,{\rm Gyr}$ (i.e. approximately the Hubble time) for the age of the galaxy. Since we assume the density profile at $r > R_{\rm T}$ to be the NFW profile (1.7), the solution $R_{\rm T}$ is a cumbersome function of σ/m, $\rho_{\rm c}$, and $r_{\rm s}$. To visualize it, we can look at the following limits:

$$R_{\rm T} \simeq r_{\rm s}\Big(\rho_{\rm c} r_{\rm s}\sqrt{2\pi G\rho_{\rm c}}\frac{\sigma}{m}t_{\rm g}\Big)^{\gamma}\,, \quad \text{with} \quad \gamma = \begin{cases} 2\,, & \text{for } R_{\rm T} \ll r_{\rm s}\,, \\ \dfrac{2}{7}\,, & \text{for } R_{\rm T} \gg r_{\rm s}\,. \end{cases} \tag{6.26}$$

We see that $R_{\rm T}$ is a monotonically increasing function of σ/m (which also holds for the full result). So, as expected, the stronger the interactions the earlier the DM particles reach equilibrium (in regions where the densities are lower). However, the self-interactions affect $R_{\rm T}$ more mildly in outer regions ($R_{\rm T} \gg r_{\rm s}$), where the density scales as r^{-3} and hence has to be overcome by stronger self-interactions. On the other hand, for inner regions ($R_{\rm T} \ll r_{\rm s}$) the resulting thermal radius is very sensitive not only to the self-interactions but also to the specific values of $r_{\rm s}$ and $\rho_{\rm c}$ that are characteristic of a given numerical fit to a certain halo.

Since the present case is only valid for $\mathcal{N} \lesssim 1$, we can use the latter inequality to derive a bound for the DM particle mass m. For example, at distances $R_{\rm T} \ll r_{\rm s}$, we find

$$m \gtrsim 20\,{\rm eV}\left(\frac{\sigma/m}{{\rm cm}^2/{\rm g}}\right)^{-5/4}\,. \tag{6.27}$$

Hence, this scenario requires masses that are significantly above eV (for $R_{\rm T} \gg r_{\rm s}$, we get qualitatively the same result, just with a different power law for (6.27)), as long as the scattering cross section satisfies the Bullet Cluster constraint, which we derive below (see (6.36)).

Masses in this region tend to make the Jeans length come out too small to be phenomenologically interesting, as can be seen by using (6.20) together with (6.36), which leads to

$$\ell \lesssim 5 \times 10^{-2}\,{\rm pc}\,.$$

6.2.2 Case (ii): Degenerate Thermalization

In the alternative scenario, we have $R_{\rm deg} > R_{\rm T}$. This scenario incorporates a simpler structure, since the density profile is expected to have the NFW form all

the way down to $r \sim R_{\rm T}$ and hence be similar to the one in the non-self-interacting DM paradigm.[8] Then, at $r < R_{\rm T}$ we expect the phase transition of DM to happen, leading to the emergence of superfluid islands of size ℓ.

Now, in order to find $R_{\rm T}$, we have to solve

$$\Gamma t_{\rm g} = \frac{\sigma}{m}\rho_{\rm DM}(R_{\rm T})v(R_{\rm T})\mathcal{N}t_{\rm g} = 1\,, \quad \text{with} \quad \mathcal{N} = \frac{\rho_{\rm DM}}{m}\left(\frac{2\pi}{mv}\right)^3 \gg 1\,. \tag{6.28}$$

As before, we visualize the solution by considering the two limits:

$$R_{\rm T} \simeq r_{\rm s}\left(\frac{4\pi^2\rho_{\rm c}}{Gm^4r_{\rm s}^2}\frac{\sigma}{m}t_{\rm g}\right)^{\delta}\,, \quad \text{with} \quad \delta = \begin{cases} \dfrac{1}{3}\,, & \text{for } R_{\rm T} \ll r_{\rm s}\,, \\ \dfrac{1}{5}\,, & \text{for } R_{\rm T} \gg r_{\rm s}\,. \end{cases} \tag{6.29}$$

In this case, the result is not particularly sensitive to a change of the NFW parameters, since (6.29) depends only mildly on $r_{\rm s}$ and $\rho_{\rm c}$. Moreover, since now the size of the thermalized region depends on the combination of parameters $(\sigma/m)m^{-4}$ (as opposed to just σ/m as in the non-degenerate case), there exists a wide range of parameters for which a significant fraction of the halo has reached local thermal equilibrium.[9]

The previous analysis indicates that we have to explore the scenario in which $R_{\rm deg} > R_{\rm T}$ if we want to end up with kpc-size superfluid cores.

We would like to finish this section with noting that by using $t_{\rm g}$ as the time scale available for thermalization, we implicitly assumed that dynamical effects (as for example dynamical friction) within the galaxy are not important. If this assumption is not justified, one should rather use the *dynamical time* (see e.g. Ref. [169])

$$t_{\rm dyn} = r/v\,, \tag{6.30}$$

which is the time scale available to DM particles in order to complete an orbit. Although in this case the thermalization radius is reduced, we will now show that the change is only of order one.

The equation for $R_{\rm T}$ now becomes

$$\Gamma t_{\rm dyn} = \frac{\sigma}{m}\rho_{\rm DM}(R_{\rm T})R_{\rm T}\mathcal{N} = 1\,, \tag{6.31}$$

whose solution can again be expressed in the limits

$$R_{\rm T} \simeq r_{\rm s}\left(\sqrt{\frac{8\pi^3\rho_{\rm c}}{G^3}}\frac{1}{m^4r_{\rm s}^2}\frac{\sigma}{m}\right)^{\delta}\,, \quad \text{with} \quad \delta = \begin{cases} \dfrac{2}{5}\,, & \text{for } R_{\rm T} \ll r_{\rm s}\,, \\ \dfrac{2}{7}\,, & \text{for } R_{\rm T} \gg r_{\rm s}\,. \end{cases} \tag{6.32}$$

[8] Note that in contrast to the standard CDM scenario, here there will be a region where, due to the DM particles' large degeneracy, the DM fluid is still described by the homogeneous field configuration (see footnote 7).

[9] This was already shown in Ref. [102].

Comparing (6.29) to (6.32) (using the parameters for a Milky-Way type galaxy), we find

$$\frac{R_{\mathrm{T,dyn}}^{\mathrm{MW}}}{R_{\mathrm{T,g}}^{\mathrm{MW}}} \simeq \begin{cases} \frac{1}{2}\left[\frac{\sigma/m}{\mathrm{cm}^2/\mathrm{g}}\left(\frac{m}{\mathrm{eV}}\right)^{-4}\right]^{1/15}, & \text{for } R_{\mathrm{T}} \ll r_{\mathrm{s}}\,, \\ \left[\frac{\sigma/m}{\mathrm{cm}^2/\mathrm{g}}\left(\frac{m}{\mathrm{eV}}\right)^{-4}\right]^{3/35}, & \text{for } R_{\mathrm{T}} \gg r_{\mathrm{s}}\,. \end{cases} \tag{6.33}$$

We see that since the above ratio depends very weakly on σ/m and m, R_{T} would not be reduced by more than half.

6.3 Revised Bullet Cluster Constraint

We saw in the last section that many of the details of the core formation depend on the values of m and λ (or σ). Thus, let us discuss if we can infer anything about these parameters. Historically, one of the first and most powerful methods to constrain the self-coupling of DM was the observation of a system of two galaxy clusters called *Bullet Cluster* [170]. That system consists of a smaller sub-cluster (the "bullet") that has traversed the larger sub-cluster (the "target") in the distant past. Strikingly, the configuration looks very different depending on whether one observes the gas distributions of the sub-clusters (via X-ray imagery) or if one measures the centers of the total mass distribution (via gravitational microlensing): the latter is offset with respect to the former. In other words, while the baryonic matter of the two sub-clusters has interacted significantly (electromagnetically) during the collisional encounter, the DM halos appear to have passed each other with only gravitational interactions. Hence, that system provides a rare opportunity to derive an upper bound on the strength of DM self-interactions.

Note that other galaxy cluster mergers have been observed as well, leading to similar bounds on the interaction rate. However, for definiteness, we will focus on the Bullet Cluster in this work.

From the aforementioned observation, we can deduce that a DM particle from the bullet cluster has not interacted with a DM particle from the target cluster (on average) even once,

$$\langle N_{\mathrm{sc}} \rangle < 1\,,$$

where $\langle N_{\mathrm{sc}} \rangle$ denotes this average number of scatterings. Taking $2R_{\mathrm{V}}/v_{\text{in-fall}}$ as the crossing time, where R_{V} is the virial radius (and hence effective size) of the target cluster and $v_{\text{in-fall}}$ is the crossing velocity, the above can be expressed as

$$\langle N_{\mathrm{sc}} \rangle = \Gamma \frac{2R_{\mathrm{V}}}{v_{\text{in-fall}}} < 1\,. \tag{6.34}$$

In order to derive a bound on the cross section σ, one has to know the functional form of the interaction rate Γ that, as we have discussed in the previous section, depends on the nature of DM.

The original bound, known as the *Bullet Cluster constraint*, has been derived for non-degenerate DM, subject to 2-body interactions, which leads to

$$\langle N_{\mathrm{sc}} \rangle = 2\frac{\sigma}{m} R_{\mathrm{V}} \rho_{\mathrm{DM}} < 1\,, \tag{6.35}$$

and hence, using $\rho_{\rm DM} \simeq 10^{-25}\,{\rm g/cm^3}$ as the average DM density and $R_{\rm V} \simeq 2\,{\rm Mpc}$,[10] to

$$\frac{\sigma}{m} \lesssim 1\,{\rm cm^2/g}\,. \tag{6.36}$$

If we focus on $m \gg$ eV and translate (6.36) into a bound on the coupling constant, we get

$$\lambda \lesssim \left(\frac{m}{10\,{\rm MeV}}\right)^{3/2}.$$

Hence, for DM particles that are heavier than a few MeV, the theory has to be in the strong coupling regime in order to violate the above Bullet Cluster bound.

We would like to mention that there is another bound that competes with (6.36) for ultra-light DM particles. If we require that this DM candidate behaves as a non-relativistic fluid on cosmological scales, we can derive the following bound for the scattering cross section from its equation of state (which is dominated by the interaction pressure)

$$\left.\frac{p}{\rho_{\rm DM}}\right|_{\rm equality} = \frac{\lambda\rho_{\rm DM}|_{\rm equality}}{8m^4} \ll 1\,, \quad \Rightarrow \quad \frac{\sigma}{m} \ll \left(\frac{m}{2\times 10^{-5}\,{\rm eV}}\right)^5 {\rm cm^2/g}\,, \tag{6.37}$$

where we have used $\rho_{\rm DM}|_{\rm equality} \simeq 0.4\,{\rm eV}^4$ for the DM density at matter-radiation equality.[11] We see that for DM particles that are light enough the bound (6.37) can be even more constraining than (6.36). However, in the following, we shall argue that the bound (6.36) has to be revisited in the present scenario.

As we have already discussed in the previous section, for DM particles that occupy highly degenerate states, the interaction rate is enhanced by the degeneracy factor $\mathcal{N}$ (see (6.28)). It is easy to see that this is precisely the case for the Bullet Cluster system, since for a galaxy cluster with $R_{\rm V} \simeq 2\,{\rm Mpc}$, $R_{\rm V}/r_{\rm s} \simeq 4$, and $\rho_{\rm DM} \simeq 10^{-25}\,{\rm g/cm^3}$, the quantity $\mathcal{N}$ exceeds unity everywhere (using the NFW profile) inside the virial radius if one considers $m \ll$ eV.

Notice that even though $\mathcal{N}_{\rm cluster} \simeq 10^{-3}\mathcal{N}_{\rm galaxy}$ (considering that the velocities in clusters are about an order of magnitude higher than in galaxies), for extremely degenerate galaxies the interaction rates in clusters too can be enhanced.

Thus, using the modified relation (6.28) and the aforementioned typical (average) astrophysical values, we can derive the improved Bullet Cluster bound

$$\frac{\sigma}{m} \lesssim 10^{-2}\left(\frac{m}{\rm eV}\right)^4 {\rm cm^2/g}\,. \tag{6.38}$$

We have to stress that the above bound is only valid if the halos still contain a significant DM fraction in the form of a gaseous, non-condensed medium because the enhancement factor $\mathcal{N}$ was obtained in that situation. If, instead, almost the entirety of particles would occupy the ground state, the transitions to excited states

[10] This value for $\rho_{\rm DM}$ is the average density of the target cluster within 500 kpc, obtained by using an NFW profile [171]. Note that this region is around the size $r_{\rm s}$, i.e. we are averaging over the region that contains most of the halo mass.

[11] Note that if a fraction of the DM is in the excited state, then an additional (linear) contribution to the pressure would be present, which could tighten the bound (6.37).

would not enjoy such an enhancement. Although this issue requires a more detailed investigation in the future, in the present thesis we work on the assumption that the process of thermalization and fragmentation will leave a significant (order one) fraction of DM particles in the excited states.

Using the bound (6.38), together with (6.28), we can derive the upper bounds on the thermal radii of various halos. For the Milky Way, one finds

$$(R_{\rm T})_{\text{Milky Way}} \lesssim 125\,{\rm kpc}\,, \tag{6.39}$$

while the thermal radii of the target and bullet clusters cannot exceed $\approx 0.5\,{\rm Mpc}$. Thus, only the inner regions of DM halos are capable of reaching thermal equilibrium.

Finally, if instead of $t_{\rm g}$ one uses the dynamical time as the available time scale for thermalization, one finds

$$(R_{\rm T}^{\rm dyn})_{\text{Milky Way}} \lesssim 60\,{\rm kpc}\,, \tag{6.40}$$

which is slightly tighter than (6.39), as expected.

6.4 Core Fragmentation and Remaining Parameter Space

Having established the new Bullet Cluster constraint (6.38) and decided to consider the particular scenario where the DM particles reach thermal equilibrium in inner regions of galaxies, while being in a highly degenerate state (case **(ii)**), we are finally in a position to analyze the formation of superfluid cores in the interior of galaxies and galaxy clusters.

Let us begin by focusing on the relation between the Jeans scale ℓ and the thermal radius $R_{\rm T}$. In the interaction-pressure case (large ξ), which we are interested in, the two length scales are controlled by different combinations of m and σ. Although this seems to suggest that we can find parameters for which kpc-size superfluid islands can be generated while $R_{\rm T}$ can vary from values lower than ℓ up to $R_{\rm V}$, this is in fact not possible. We can express ℓ in terms of $R_{\rm T}$ as

$$\left(\frac{\ell}{2\,{\rm kpc}}\right) \simeq \left[\mathcal{F}(R_{\rm T}/{\rm kpc}) \times \left(\frac{m}{\rm meV}\right)^{-1}\right]^{1/4}\,, \tag{6.41}$$

where the function $\mathcal{F}$ is determined by the density profile of a halo and can be deduced from (6.28). We see that for a given $R_{\rm T}$ the Jeans scale depends only mildly on m, and hence we need ultra-low values of the latter in order to have a macroscopic value of the former. More precisely, in order to have $\ell \geq R_{\rm T}$, the DM mass has to enter the regime of the FDM parameter space (i.e. a dispersion relation dominated by the quartic term in (6.12)), which then would violate the condition $\xi \gg 1$. In other words, since ℓ, ξ and $R_{\rm T}$ depend on three different combinations of m and σ/m, the superfluidity condition $\xi \gg 1$ is not satisfied by a generic choice of ℓ and $R_{\rm T}$.

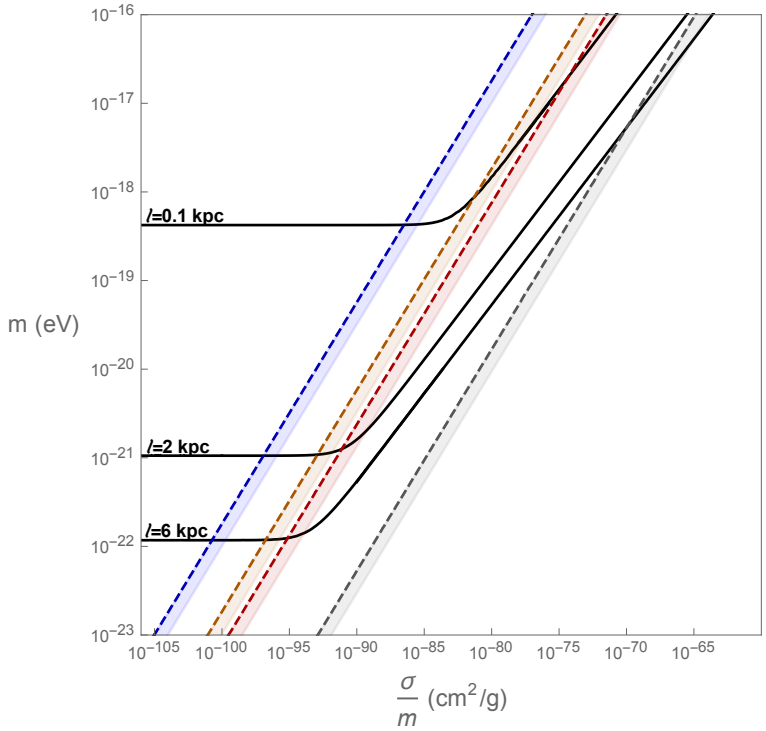

Figure 6.2: The black lines correspond to slices of the parameter space that generate a Jeans scale of 0.1 kpc/2 kpc/6 kpc in the Milky Way DM halo, assuming a DM particle governed by the action (6.1). To obtain them, we evaluated (6.13) numerically, using $\rho_{\rm DM} \simeq 10^{-25}\,{\rm g/cm^3}$. The curves interpolate between the superfluid regime, $\xi \gg 1$ (sloped part), and the "non-interacting" regime, $\xi \ll 1$ (flat part). Blue/Orange/Red, dashed curves highlight the parameter space that generates a thermal radius $R_{\rm T}$ of 0.1 kpc/2 kpc/6 kpc, where $R_{\rm T}$ is the radius within which the particles had the chance to scatter at least once throughout the lifetime of the halo. On the right of the gray line, the Milky Way DM halo is in global thermal equilibrium. The colored regions show how $R_{\rm T}$ changes varying the sufficient mean number of scattering events in the interval 1–10. We see that it is impossible to have an interaction pressure-dominated core with $\ell \gtrsim R_{\rm T}$.

The viable parameter space for which we can get macroscopic superfluid patches within the thermalization radius is shown in Figure 6.2, where we used the full expression for the Jeans scale (6.13) that is valid for arbitrary ξ. We plot different values for the Jeans scale and the thermal radius for a Milky Way-like halo. Note that, even though ℓ is density independent in the interaction pressure case, this is not true for the quantum pressure case. Thus, only the sloped part of the solid curves is equal for all astrophysical structures. For the turning point and the flat part of the solid curves, this is not the case.

We can read off from Figure 6.2 the result that $\ell \gtrsim R_{\mathrm{T}}$ is impossible for halos sustained by the interaction pressure, by observing that in the sloped region (interaction pressure limit) the lines corresponding to a given ℓ do not intersect the lines describing thermal radii with smaller values.

Therefore, we have obtained the result that for DM that consists of a scalar particle with a $(\lambda\Phi^4)$-potential, forming an interaction pressure-supported superfluid core, the only viable scenario is for

$$\ell < R_{\mathrm{T}}\,. \tag{6.42}$$

We would like to remark that this result was obtained for a thermal radius that we defined as the region below which the DM particles had sufficient time to interact once ($t_{\mathrm{eq}} = t_1$). However, the same result is obtained if we use the more conservative assumption that successful thermal equilibrium can only occur if the number of scattering events is increased. We illustrate the result for a number in the interval 1–10 with the colored regions in Figure 6.2.

In order to determine the allowed parameter space of the present DM candidate capable of generating kpc-size solitons in partially thermalized clusters, we combined all the limits discussed in this chapter in Figure 6.3 (which displays the most interesting part of the parameter space) and in Figure 6.4 (which displays the entire parameter space).

The region in pink is excluded due to the upper limit on the self-interaction strength, obtained from the analysis of the collision of the clusters in the degenerate setting (see section 6.3).

We would like to reiterate that the preceding, qualitative analysis is generally sensitive to the particular density profile taken for the halo before thermalization and in particular to the values chosen for the parameters of the NFW profile. Furthermore, if thermalization would affect the outer galactic regions as well, the mean density of the thermal core is expected to drop by one order of magnitude. However, this would neither modify the behavior in the interaction pressure case (because it is density independent) nor the halo's fate to succumb to fragmentation. In fact, the turning point between the different scalings (degeneracy pressure and interaction pressure, respectively) shown in Figure 6.2 would move more to the right because the lower mean density of the thermal core has to be compensated by a stronger self-interaction.

Finally, as pointed out in section 6.3, the bound (6.38) is only applicable if a significant fraction of the halos remains in gaseous form, instead of a scenario where the clusters thermalize completely and undergo the phase transition to (a collection

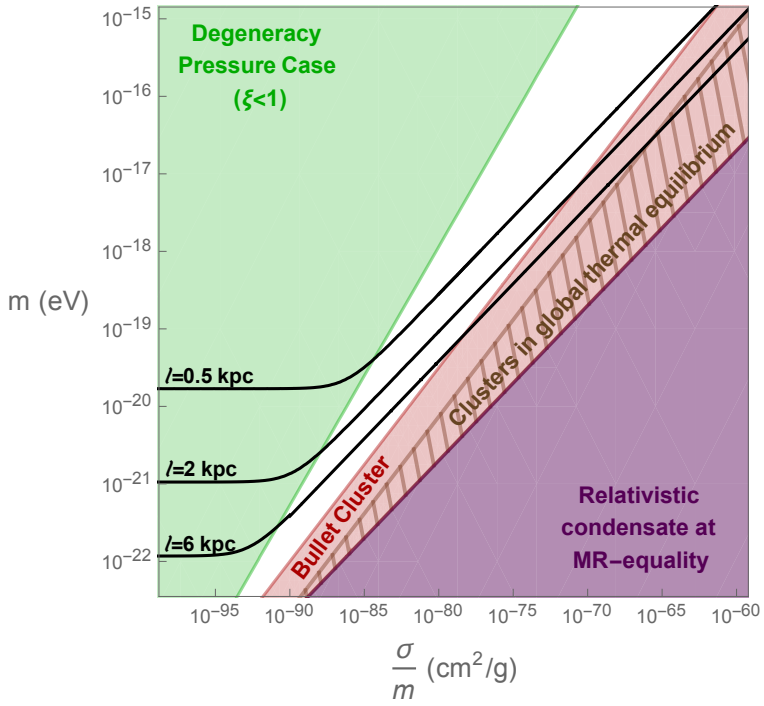

Figure 6.3: Allowed parameter space for the considered scenario. Since we focused on the superfluid regime, we excluded halos sustained by quantum pressure (green region). The pink region is excluded by the Bullet Cluster constraint (6.38), while the purple one represents condensates that were relativistic at matter-radiation equality (see (6.37)). The striped region corresponds to the parameter space where both the bullet and target cluster are in global thermal equilibrium. Black solid lines identify the parameter space that generates a Jeans scale of 0.5 kpc/2 kpc/6 kpc.

of) superfluid cores. Even though the latter scenario appears unlikely, we have highlighted the parameter space in Figure 6.3 (and Figure 6.4) that corresponds to that situation. In this case, the resulting density profile would deviate from the NFW profile and a more detailed analysis would be needed to find constraints on the parameter space. Such an analysis lies beyond the scope of the present work.

To conclude this section, we would like to comment on the implication of our finding on the coupling constant λ. As we can read off from Figure 6.3, superfluid cores with a size $\ell \gtrsim 0.5\,\mathrm{kpc}$ are only possible for cross sections $\sigma/m \lesssim 10^{-63}\,\mathrm{cm}^2/\mathrm{g}$ and masses $m \lesssim 10^{-15}\,\mathrm{eV}$. From this, we can infer that $\lambda \lesssim 10^{-65}$.

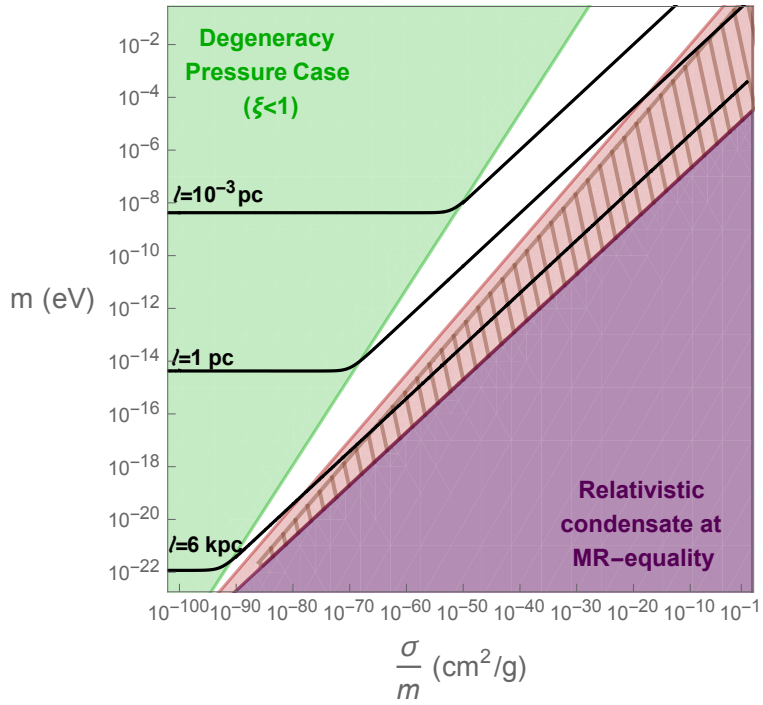

Figure 6.4: This figure is equivalent to Figure 6.3, except that here we plot the whole parameter space, highlighting $\ell = 10^{-3}\,\mathrm{pc}/1\,\mathrm{pc}/6\,\mathrm{kpc}$, for reference.

6.5 Summary

We have argued that for an ultra-light (scalar) DM candidate with repulsive, quartic self-interactions, given by the theory (6.1), the following scenario should arise in an astrophysical setting. As long as the DM particles that begin to clump and form a halo did not have sufficient time to reach thermal equilibrium, their density profile is approximated by the one considered in the CDM paradigm, i.e. it is given by the NFW density profile. However, in interior regions, where the densities are high enough, within the lifetime of the halo, local thermal equilibrium can be reached through the self-interactions. This process can be enhanced due to the fact that the ultra-light bosonic particles occupy highly degenerate states in the phase space.

We have further demonstrated that a scenario including kpc-size cores requires that $R_{\mathrm{deg}} > R_{\mathrm{T}}$, meaning that with decreasing distance to the center of the halo, first a radius is reached where the inter-particle separation is less than the particles' de Broglie wavelength, and only after that the radius emerges where self-scatterings are efficient enough to reach thermal equilibrium. In this way, the thermal equilibration is supported by the large degeneracy.

Moreover, we have shown that the validity of this scenario entails the presence of not just one single core but a collection of superfluid droplets of size ℓ. The latter is the gravitational Jeans length above which the core is unstable and prone to fragmentation. The shape of each superfluid island is approximately given by the superfluid soliton (see (6.9)). We have not further analyzed the resulting dynamics of the droplets, which will influence the precise form of the final density distribution.

However, since the superfluid solitons are expected to behave as weakly interacting effective particles, at scales between ℓ and R_{T} the density profile should resemble its counterpart of the CDM scenario.

Finally, a large portion of the possible parameter space has been removed by the improved Bullet Cluster constraint that we have derived in this work. We have shown that for ultra-light DM particles the interaction rate is enhanced so dramatically that the only way to accommodate the observation in the Bullet Cluster is to have an extremely small scattering cross section. This, however, leads to much smaller Jeans lengths, and hence superfluid core sizes, than might have been expected otherwise.

A

Propagator for Time-Dependent Sources

Here, we will derive the general expression for the propagator in the case of arbitrary (i.e. in general time-dependent) sources. Since we do not need it for our study of the double-brane setup, but only wish to use the derivation to elucidate some of the points addressed in chapter 2, we will perform the calculation for the single-brane case. In order to avoid clutter in our notation, we will refrain from using the superscript "1B".

Let us start with the derivation for the scalar field theory in order to expose the essential parts of the calculation. For simplicity, we will derive the propagator between points where one of the points is located at the brane (at the origin). A generalization to arbitrary locations along the extra dimension is straightforward. The propagator $G(x^\mu, y)$ then fulfills the equation

$$\Big(\Box - \partial_y^2 + r_\mathrm{c}\delta(y)\Box\Big)G(x^\mu, y) = -\delta^{(4)}(x^\mu)\delta(y)\,. \tag{A.1}$$

Fourier transforming with respect to the worldvolume coordinates, using

$$\overline{G}(k^\mu, y) = \int \mathrm{d}^4x\, \mathrm{e}^{\mathrm{i}k_\mu x^\mu} G(x^\mu, y)\,,$$

and with respect to the extra dimension, using

$$\widetilde{G}(k^\mu, k^5) = \int \mathrm{d}y\, \mathrm{e}^{-\mathrm{i}k^5 y} \overline{G}(k^\mu, y)\,,$$

we arrive at

$$\widetilde{G}(k^\mu, k^5) = \frac{1}{(k^5)^2 - k^2}\Big(r_\mathrm{c} k^2 \overline{G}(k^\mu, 0) - 1\Big)\,,$$

with $k^2 \equiv k_\mu k^\mu$. Transforming back to the y-coordinates leads to

$$\overline{G}(k^\mu, y) = A(k,y)\Big(r_\mathrm{c} k^2 \overline{G}(k^\mu, 0) - 1\Big)\,, \tag{A.2}$$

with $A(k,y)$ as defined in (2.15). From (A.2), we can find

$$\overline{G}(k^\mu, 0) = \frac{1}{r_\mathrm{c} k^2 - A^{-1}(k,0)}\,, \tag{A.3}$$

and hence

$$\overline{G}(k^\mu, y) = \frac{A(k,y)}{A(k,0)} \frac{1}{r_\mathrm{c} k^2 - A^{-1}(k,0)}\,. \tag{A.4}$$

In order to calculate $A(k,y)$, we have to prescribe how the integration contour should go around the poles (which will be encountered for $k^2 > 0$). We choose the prescription

$$A(k,y) = \lim_{\varepsilon \to 0} \int \frac{\mathrm{d}k^5}{2\pi} \frac{\mathrm{e}^{\mathrm{i}k^5 y}}{(k^5)^2 - k^2 - \mathrm{i}\varepsilon}\,, \tag{A.5}$$

which is consistent with the iε-prescription for the Feynman propagator. With this, we find

$$A(k,y) = \frac{\mathrm{i}}{2} \frac{\mathrm{e}^{\mathrm{i}k|y|}}{k}\,, \quad k \equiv \sqrt{k^2}\,. \tag{A.6}$$

Thus, the propagator is given by

$$\overline{G}(x^\mu, y) = \int \frac{\mathrm{d}^4 k}{(2\pi)^4} \frac{\mathrm{e}^{-\mathrm{i}k_\mu x^\mu} \mathrm{e}^{\mathrm{i}k|y|}}{r_\mathrm{c} k^2 + 2\mathrm{i}k}\,. \tag{A.7}$$

It is now straightforward to repeat the appropriate calculation for the graviton in the full DGP theory. We can rewrite (2.14), using (2.16), as

$$\overline{h}_{\mu\nu}(k,y) - \eta_{\mu\nu}\overline{h}(k,y) = \frac{A(k,y)}{A(k,0)}\Big(\overline{h}_{\mu\nu}(k,0) - \eta_{\mu\nu}\overline{h}(k,0)\Big)\,.$$

From this, it follows that

$$\overline{h}_{\mu\nu}(k,y) = \mathrm{e}^{\mathrm{i}k|y|}\overline{h}_{\mu\nu}(k,0)\,, \tag{A.8}$$

and hence

$$h_{\mu\nu}(x^\mu, y) = \frac{2}{M_*^3} \int \mathrm{d}^4 k\, \frac{1}{r_\mathrm{c}} \frac{\mathrm{e}^{-\mathrm{i}k_\alpha x^\alpha} \mathrm{e}^{\mathrm{i}k|y|}}{k^2 - m^2(k)} \left[\overline{T}_{\mu\nu}(k) - \frac{1}{3}\left(\eta_{\mu\nu} - \frac{k_\mu k_\nu}{m^2(k)}\right)\overline{T}(k)\right], \tag{A.9}$$

where we employed (A.6) and (2.19). We also used a normalization factor in front, which is appropriate for the 5D graviton.

We can now read off the propagator (see also section 2.1.2) for propagation between a point on the brane and a point along the extra dimension. In (world-volume) momentum space, it reads

$$\overline{D}_{\mu\nu,\alpha\beta}(k^\mu, y) = \frac{1}{r_\mathrm{c}} \frac{\mathrm{e}^{\mathrm{i}k|y|}}{k^2 - m^2(k)} \left[\frac{1}{2}(P_{\mu\alpha}P_{\nu\beta} + P_{\mu\beta}P_{\nu\alpha}) - \frac{1}{3}P_{\alpha\beta}P_{\mu\nu}\right], \tag{A.10}$$

with $m^2(k)$ and $P_{\mu\nu}$ as given in (2.17) and (2.22), respectively.

B

Mode Functions

B.1 Infinite Extra Dimension

In order to find the solutions $\psi_{m,\alpha}(y)$ of (2.34), we have to solve the harmonic oscillator equation in the three regions I, II and III (see Figure B.1) and then match the solutions at the boundaries of those regions (this is the standard procedure for Schroedinger-type equations with delta-function potentials). In particular, the matching conditions (at the branes) between the regions I and II and the regions II and III are: continuity of $\psi_m(y)$ at $y = -\frac{R}{2}$ and $y = \frac{R}{2}$; discontinuity of $\frac{\mathrm{d}\psi_m(y)}{\mathrm{d}y}$ at $y = -\frac{R}{2}$ and $y = \frac{R}{2}$.[1] This calculation leads to

$$\psi_m(y) = \begin{cases} A_m \cos my + B_m \sin my\,, & y < -\dfrac{R}{2}\,, \\ C_m \cos my + D_m \sin my\,, & -\dfrac{R}{2} \le y \le \dfrac{R}{2}\,, \\ E_m \cos my + F_m \sin my\,, & y > \dfrac{R}{2}\,, \end{cases}$$

where 4 of the 6 integration constants are fixed as

$$\begin{aligned} A_m &= C_m\left[1 + r_\mathrm{c} m \sin\left(\frac{mR}{2}\right)\cos\left(\frac{mR}{2}\right)\right] - r_\mathrm{c} m D_m \sin^2\left(\frac{mR}{2}\right), \\ B_m &= D_m\left[1 - r_\mathrm{c} m \sin\left(\frac{mR}{2}\right)\cos\left(\frac{mR}{2}\right)\right] + r_\mathrm{c} m C_m \cos^2\left(\frac{mR}{2}\right), \\ E_m &= C_m\left[1 + r_\mathrm{c} m \sin\left(\frac{mR}{2}\right)\cos\left(\frac{mR}{2}\right)\right] + r_\mathrm{c} m D_m \sin^2\left(\frac{mR}{2}\right), \\ F_m &= D_m\left[1 - r_\mathrm{c} m \sin\left(\frac{mR}{2}\right)\cos\left(\frac{mR}{2}\right)\right] - r_\mathrm{c} m C_m \cos^2\left(\frac{mR}{2}\right), \end{aligned}$$

[1] $\lim\limits_{\varepsilon\to 0} \frac{\mathrm{d}\psi_m(y)}{\mathrm{d}y}\Big|_{\pm\frac{R}{2}-\varepsilon}^{\pm\frac{R}{2}+\varepsilon} + m^2 r_\mathrm{c}\psi_m(\pm\frac{R}{2}) = 0.$

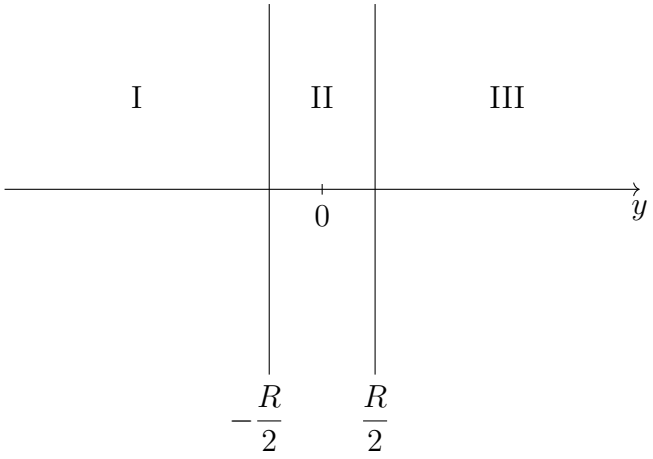

Figure B.1: The setup: Two DGP branes along the (infinite) extra dimension y (with suppressed transverse dimensions). I, II and III are the regions we need to match in order to find the field solution.

with two arbitrary integration constants C_m and D_m. In principle, every choice of C_m and D_m parametrizes a different solution in the two-dimensional solution-space. However, since the operator acting on $\psi_{m,\alpha}(y)$ in (2.34) is symmetric around $y = 0$, we can find solutions that are either even ($\alpha = 1$) or odd ($\alpha = 2$). Hence, our mode functions are

$$\psi_{m,1}(y) = \begin{cases} A_m \cos my + B_m \sin my\,, & y < -\dfrac{R}{2}\,, \\ C_m \cos my\,, & -\dfrac{R}{2} \le y \le \dfrac{R}{2}\,, \\ A_m \cos my - B_m \sin my\,, & y > \dfrac{R}{2}\,, \end{cases} \qquad \text{(even)}\,, \quad \text{(B.1)}$$

with

$$A_m = C_m\Big[1 + r_c m \sin\left(\frac{mR}{2}\right)\cos\left(\frac{mR}{2}\right)\Big] \quad \text{and} \quad B_m = r_c m C_m \cos^2\left(\frac{mR}{2}\right), \tag{B.2}$$

and

$$\psi_{m,2}(y) = \begin{cases} A_m \cos my + B_m \sin my\,, & y < -\dfrac{R}{2}\,, \\ D_m \sin my\,, & -\dfrac{R}{2} \le y \le \dfrac{R}{2}\,, \\ -A_m \cos my + B_m \sin my\,, & y > \dfrac{R}{2}\,, \end{cases} \qquad \text{(odd)}\,, \quad \text{(B.3)}$$

with

$$A_m = -r_c m D_m \sin^2\left(\frac{mR}{2}\right) \quad \text{and} \quad B_m = D_m\Big[1 - r_c m \sin\left(\frac{mR}{2}\right)\cos\left(\frac{mR}{2}\right)\Big]. \tag{B.4}$$

It is straightforward to establish that these mode functions satisfy condition (2.35). Performing that lengthy calculation, fixes the coefficients

$$C_m^2 = \frac{1}{\pi} \frac{1}{\cos^2\left(\frac{mR}{2}\right) + \left[\sin\left(\frac{mR}{2}\right) + r_c m \cos\left(\frac{mR}{2}\right)\right]^2}\,, \tag{B.5}$$

$$D_m^2 = \frac{1}{\pi} \frac{1}{\sin^2\left(\frac{mR}{2}\right) + \left[\cos\left(\frac{mR}{2}\right) - r_c m \sin\left(\frac{mR}{2}\right)\right]^2}\,. \tag{B.6}$$

B.2 Compact Extra Dimension

To find the solutions $\psi_{m,\alpha}(y)$ of (2.34) subject to periodic boundary conditions, we proceed analogously to the derivation in appendix B.1. Now the three regions I, II and III are defined as shown in Figure 2.1. The matching conditions (at the branes) between the regions I and II and the regions II and III are as before: continuity of $\psi_m(y)$ at $y = -\frac{R}{2}$ and $y = \frac{R}{2}$; discontinuity of $\frac{\mathrm{d}\psi_m(y)}{\mathrm{d}y}$ at $y = -\frac{R}{2}$ and $y = \frac{R}{2}$. This calculation leads to

$$\psi_m(y) = \begin{cases} \widetilde{A}_m \mathrm{e}^{\mathrm{i}my} + \widetilde{B}_m \mathrm{e}^{-\mathrm{i}my}\,, & -\dfrac{L}{2} < y < -\dfrac{R}{2}\,, \\ \widetilde{C}_m \mathrm{e}^{\mathrm{i}my} + \widetilde{D}_m \mathrm{e}^{-\mathrm{i}my}\,, & -\dfrac{R}{2} < y < \dfrac{R}{2}\,, \\ \widetilde{E}_m \mathrm{e}^{\mathrm{i}my} + \widetilde{F}_m \mathrm{e}^{-\mathrm{i}my}\,, & \dfrac{R}{2} < y < \dfrac{L}{2}\,, \end{cases}$$

where 4 of the 6 integration constants (we choose here a representation with generally complex coefficients) are fixed as

$$\begin{aligned} \widetilde{A}_m &= \widetilde{C}_m\Big(1 - \frac{\mathrm{i}mr_c}{2}\Big) - \widetilde{D}_m \frac{\mathrm{i}mr_c}{2} \mathrm{e}^{\mathrm{i}mR}\,, \\ \widetilde{B}_m &= \widetilde{C}_m \frac{\mathrm{i}mr_c}{2} \mathrm{e}^{-\mathrm{i}mR} + \widetilde{D}_m\Big(1 + \frac{\mathrm{i}mr_c}{2}\Big)\,, \\ \widetilde{E}_m &= \widetilde{C}_m\Big(1 + \frac{\mathrm{i}mr_c}{2}\Big) + \widetilde{D}_m \frac{\mathrm{i}mr_c}{2} \mathrm{e}^{-\mathrm{i}mR}\,, \\ \widetilde{F}_m &= -\widetilde{C}_m \frac{\mathrm{i}mr_c}{2} \mathrm{e}^{\mathrm{i}mR} + \widetilde{D}_m\Big(1 - \frac{\mathrm{i}mr_c}{2}\Big)\,, \end{aligned}$$

with two arbitrary integration constants $\widetilde{C}_m$ and $\widetilde{D}_m$.

The conditions of periodicity, $\psi_m(\frac{L}{2}) = \psi_m(-\frac{L}{2})$ and $\partial_y \psi_m|_{\frac{L}{2}} = \partial_y \psi_m|_{-\frac{L}{2}}$, lead to the quantization of the masses according to

$$\mathrm{e}^{\mathrm{i}mL} = \frac{b_\alpha^*(m)}{b_\alpha(m)}\,, \qquad \text{for} \begin{cases} \widetilde{C}_m = \widetilde{D}_m\,, & \alpha = 1\,, \\ \widetilde{C}_m = -\widetilde{D}_m\,, & \alpha = 2\,, \end{cases} \tag{B.7}$$

with

$$b_{1,2}(m) = \frac{1}{2}\Big(1 + \frac{\mathrm{i}mr_c}{2}\Big(1 \pm \mathrm{e}^{-\mathrm{i}mR}\Big)\Big)\,. \tag{B.8}$$

Notice that the solutions (automatically) split into even ($\alpha = 1$) and odd ($\alpha = 2$). The mass quantization equation (B.7) can be rewritten as

$$\tan\frac{mL}{2} = -\frac{\mathrm{Im}\left[b_\alpha(m)\right]}{\mathrm{Re}\left[b_\alpha(m)\right]}\,, \tag{B.9}$$

which leads to the expression given in (2.43).

Putting everything together, the (real-valued) solutions for the mode functions are

$$\psi_{m,1}(y) = \begin{cases} C_1(m_1)b_1(m_1)\mathrm{e}^{-\mathrm{i}m_1 y} + \text{c.c.}\,, & -\dfrac{L}{2} < y < -\dfrac{R}{2}\,, \\ C_1(m_1)\cos m_1 y\,, & -\dfrac{R}{2} < y < \dfrac{R}{2}\,, \\ C_1(m_1)b_1(m_1)\mathrm{e}^{\mathrm{i}m_1 y} + \text{c.c.}\,, & \dfrac{R}{2} < y < \dfrac{L}{2}\,, \end{cases} \quad \text{(even)}\,, \tag{B.10}$$

and

$$\psi_{m,2}(y) = \begin{cases} \mathrm{i}C_2(m_2)b_2(m_2)\mathrm{e}^{-\mathrm{i}m_2 y} + \text{c.c.}\,, & -\dfrac{L}{2} < y < -\dfrac{R}{2}\,, \\ C_2(m_2)\sin m_2 y\,, & -\dfrac{R}{2} < y < \dfrac{R}{2}\,, \\ -\mathrm{i}C_2(m_2)b_2(m_2)\mathrm{e}^{\mathrm{i}m_2 y} + \text{c.c.}\,, & \dfrac{R}{2} < y < \dfrac{L}{2}\,, \end{cases} \quad \text{(odd)}\,, \tag{B.11}$$

with $b_\alpha(m_\alpha)$ and m_α given by (B.8) and the solutions of (B.9), respectively.[2]

The integration constants $C_\alpha(m_\alpha)$ can be fixed by requiring a normalization according to (2.41). We find

$$C_\alpha(m_\alpha) = \frac{1}{\sqrt{2}}\left(|b_\alpha(m_\alpha)|^2(L-R) + \frac{R}{4} + \frac{\mathrm{Im}\left[b_\alpha(m_\alpha)\right]}{m_\alpha}\right)^{-1/2}, \qquad \text{for } m_\alpha \neq 0\,, \tag{B.12}$$

and[3]

$$C_1(0) = \frac{1}{\sqrt{2r_\mathrm{c} + L}}\,, \qquad \text{for } m_1 = 0\,. \tag{B.13}$$

It is now straightforward to check that the above results reduce to the results of the infinite-dimension case (see appendix B.1) if one takes the limit $L \to \infty$, leading to

$$C_1 \overset{L\to\infty}{\longrightarrow} \sqrt{\frac{2\pi}{L}}C\,,$$
$$C_2 \overset{L\to\infty}{\longrightarrow} \sqrt{\frac{2\pi}{L}}D\,,$$

and goes over to the cosine- and sine-basis.[4] In this limit, the masses regain their continuous spectrum.

[2] As opposed to the previous case (infinite dimension), now we distinguish between m_1 and m_2 because the masses do not take continuous values anymore but are the solutions of two distinct quantization equations.

[3] As explained in section 4.2, there is no zero-mode for $\alpha = 2$.

[4] Notice that the factor $\sqrt{\frac{2\pi}{L}}$ appears because the mode functions are plane-wave normalized in the infinite-dimension case.

C

Numerical Demonstration of the Validity of Integral Approximations

C.1 Point Sources on Different Branes

In order to show that the leading-order approximations, which we found for the three specified regimes in section 3.1.1, are correct, we compare the numerical value of J (obtained by numerical integration of (3.5)), as a function of r, to the two asymptotes $F_{\mathrm{DGP}}(r/2)$ (see (2.25)), valid for $r \gg \rho$, and $\frac{\pi}{\sqrt{2}}\frac{r}{\rho}$, valid for $r \ll \rho$, respectively. Since J can be viewed as a function of the dimensionless variables r/R and r_{c}/R, all functions plotted in Figure C.1 depend just on r and r_{c}, expressed in units of R. We see that J is approximated excellently by the given leading-order expressions for the two regimes $r \ll \rho$ and $r \gg \rho$. Furthermore, if the ratio r_{c}/R is large enough, J can be approximated by a constant, for $\rho \ll r \ll r_{\mathrm{c}}$.

Next, let us verify that also the corrections to the leading-order terms of J, given in section 3.1.1, are accurate. Since in section 3.2 we are interested mostly in the force along the brane, where the terms linear in r will drop out, in the remainder of this section, we will perform our numerical analysis exclusively for the force (3.24). In order to plot a dimensionless quantity f, we define the physical (dimensionfull) force as

$$F_{\mathrm{r}} \equiv -\frac{1}{16\pi M_{\mathrm{P}}^2}\frac{1}{R^2} f(r, r_{\mathrm{c}})\,, \tag{C.1}$$

so that[1]

$$f \equiv -\frac{2}{\pi}R^2 \frac{\partial}{\partial r}\left(\frac{J}{r}\right). \tag{C.2}$$

[1] In order to extract a numerical result, we pull the derivative inside the integral of (3.5) and then integrate numerically.

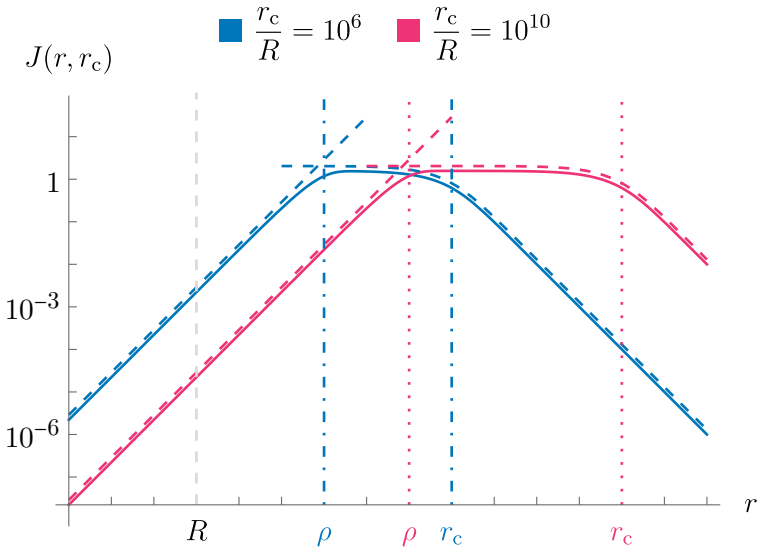

Figure C.1: Log-log plot of the numerical value of J (see (3.5)), as a function of r (in units of R), for two different values of r_c/R (solid curves). The dashed curves are the functions $F_{\text{DGP}}(r/2)$ (see (2.25)), for $r \gtrsim \rho$, and $\frac{\pi}{\sqrt{2}}\frac{r}{\rho}$, for $r \lesssim \rho$, in two different colors, depending on the value of r_c/R. We see that J is approximated very well by the two asymptotes in the two regimes, separated by ρ (we have plotted the asymptotes with an offset because otherwise the curves would lie on top of each other). We observe that J does not change its leading-order behavior by crossing $r \simeq R$. At $r \simeq \rho$, J crosses over from a linear behavior to the "DGP behavior", where J is approximately constant for $r \ll r_c$ and then crosses over to a $(1/r)$-scaling for $r \gg r_c$. The constant part is more pronounced for larger ratios r_c/R.

We, again, consider f as a function of r and r_c (in units of R). Figure C.2 shows the force along the brane between two point sources on different branes. We see that the leading-order terms of (3.24) approximate the actual behavior of the force very accurately in the regimes (I)-(III).

To justify the corrections to the leading-order terms in the expression (3.24), let us consider regimes (I) and (II) separately. For $R \ll r \ll \rho$, we compare the numerical value of f where we subtracted the leading-order term $\frac{R}{r_c}$ to the correction terms given in (3.24), in Figure C.3 (the numerical prefactors are specified in the caption of that figure). We see that the two given corrections in (3.24) are in good agreement with the numerical result, where $\frac{1}{\pi r^2}\frac{R}{r_c}$ dominates for smaller r, while $\frac{2\sqrt{2}}{3}\frac{r}{\rho^3}$ dominates for larger r, in the regime (II).

Next, we compare the corrections for $\rho \ll r$, given in (3.24), to the numerical value of f where we subtracted the leading-order term $\frac{R^2}{r^2}$. We show in Figure C.4 that the two corrections, given in (3.24), are again quite good approximations for the numerical result, where the correction $\frac{\sqrt{2}}{r\rho}e^{-\sqrt{2}\frac{r}{\rho}}$ dominates for $r \to \rho$, while the correction $\frac{2}{\pi}\frac{1}{r r_c}$ dominates for $r \to r_c$.

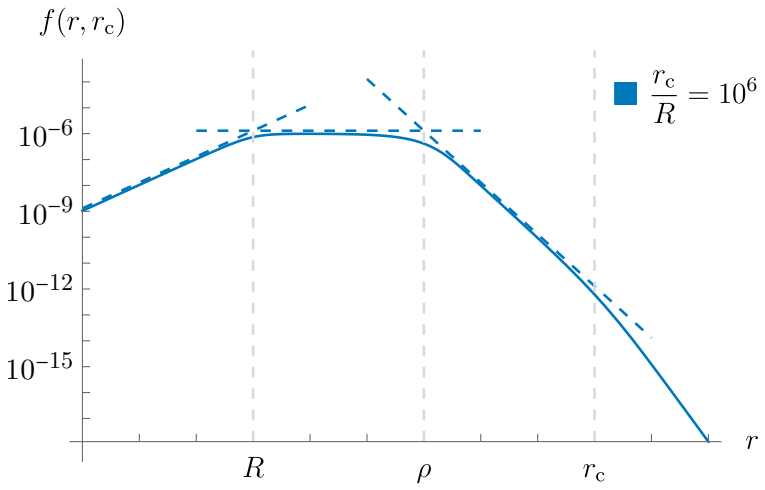

Figure C.2: Log-log plot of the numerical value of f, defined in (C.2), as a function of r (in units of R), shown as the solid curve. The dashed curves show the functions $\frac{r}{r_c}$ for $r \lesssim R$, $\frac{R}{r_c}$ for $R \lesssim r \lesssim \rho$ and $\frac{R^2}{r^2}$ for $r \gtrsim \rho$. We see that f is approximated very well by the three asymptotes in the stated regimes. We observe that already for $r_c/R = 10^6$, the regime (II), where the force can be approximated as constant, extends over almost three orders of magnitude. Increasing r_c/R, extends this region. For $r \ll R$, the force vanishes linearly, while for $r \gg \rho$ it interpolates between a $(1/r^2)$- and a $(1/r^3)$-behavior.

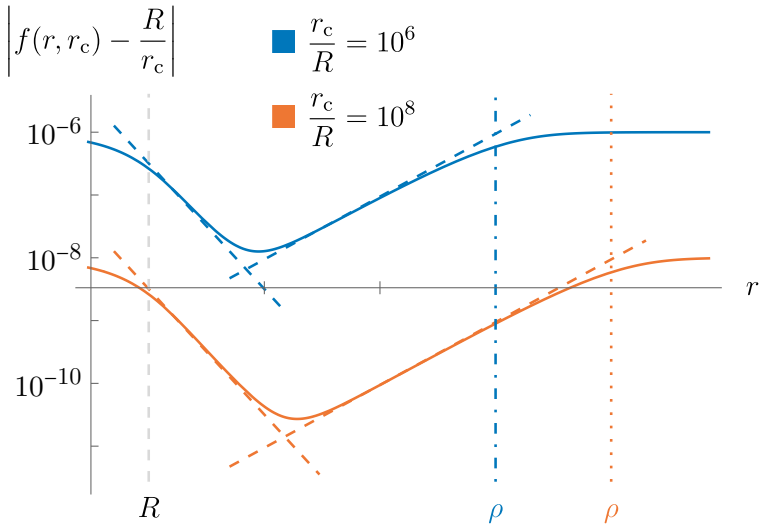

Figure C.3: Log-log plot of the numerical value of $f - \frac{R}{r_c}$ (since the leading correction terms in regime (II) always have the opposite sign from the leading term, we plot here the absolute value), as a function of r and r_c (in units of R), for two different values of r_c/R (solid curves). The dashed curves are the functions $\frac{R^3}{\pi r^2 r_c}$, for $r \to R$, and $\frac{2\sqrt{2}}{3}\frac{r\sqrt{R}}{r_c^{3/2}}$, for $r \to \rho$, in two different colors, depending on the value of r_c/R. We see that the corrections given in (3.24) are good approximations for the numerical result of F_r, with $\frac{1}{\pi r^2}\frac{R}{r_c}$ dominating for smaller r and $\frac{2\sqrt{2}}{3}\frac{r}{\rho^3}$ dominating for larger r, in the regime (II). The vertical lines show the scales that separate the regimes. We see that for larger r_c/R the approximation gets better.

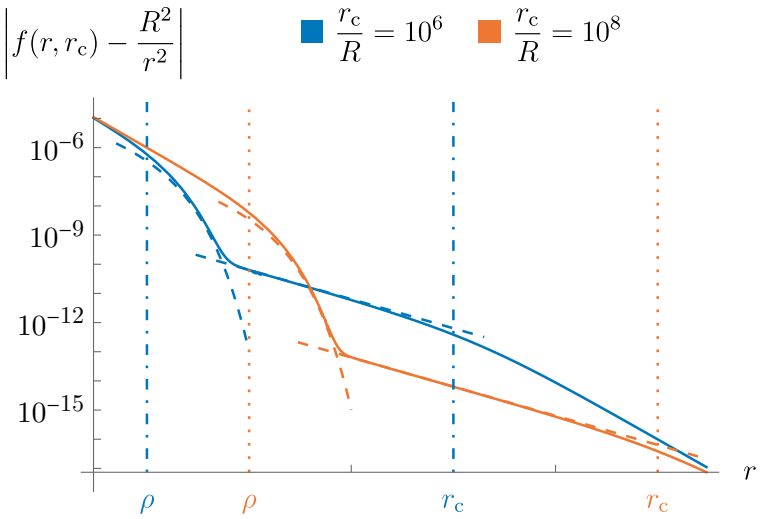

Figure C.4: Log-log plot of the numerical value of $f - \frac{R^2}{r^2}$ (since the leading correction terms in regime (I) always have the opposite sign from the leading term, we plot here the absolute value), as a function of r (in units of R), for two different values of r_c/R (solid curves). The dashed curves are the functions $\sqrt{2}\frac{R^{3/2}}{r\sqrt{r_c}}e^{-\sqrt{2}\frac{r}{\rho}}$, for $r \to \rho$, and $\frac{2}{\pi}\frac{R^2}{rr_c}$ for $r \to r_c$, again for two different values of r_c/R. We see that the corrections given in (3.24) are good approximations for the numerical result of F_r, with $\frac{\sqrt{2}}{r\rho}e^{-\sqrt{2}\frac{r}{\rho}}$ dominating for smaller r and $\frac{2}{\pi}\frac{1}{rr_c}$ dominating for larger r, in the regime (I). The vertical lines show the scales that separate the regimes. We see that for larger r_c/R the approximation gets better.

C.2 Point Sources on the Same Brane

The potential energy due to two point sources on "our" brane, in the presence of an empty second DGP brane, is given by (3.30) with (2.31). This leads to the "baryonic" potential energy

$$V_{\mathrm{b}}(r) = -\frac{g^2}{4\pi^2}\frac{1}{r r_{\mathrm{c}}} J_{\mathrm{b}}\,, \tag{C.3}$$

with

$$J_{\mathrm{b}} = 2\int_0^\infty \mathrm{d}x\, \sin x \frac{2\frac{r}{r_{\mathrm{c}}} + x - x\,\mathrm{e}^{-2\frac{R}{r}x}}{\left(2\frac{r}{r_{\mathrm{c}}} + x\right)^2 - x^2\,\mathrm{e}^{-2\frac{R}{r}x}}\,. \tag{C.4}$$

The plot in Figure C.5 shows the numerical result for (C.4), for two different values of r_{c}/R. We see that for $r \ll \rho$, $J_{\mathrm{b}} = \pi$, so we recover the standard Newton potential. In particular, there is no change of behavior in going from $r \lesssim R$ to $r \gtrsim R$. Only when r approaches ρ, does the potential energy cross over to the DGP-behavior, found in Ref. [64]. Interestingly, if r_{c}/R is large enough, there will still be a region (for $\rho \ll r \ll r_{\mathrm{c}}$) where the potential is approximately Newtonian, but with half its value.[2] One of the results of the present work is that we found the length scale that differentiates between these two behaviors to be ρ.

[2]The reason for the factor 1/2 is easy to understand: in the region $\rho \ll r \ll r_{\mathrm{c}}$ the brane distance is effectively zero ($\rho \to 0$ for $R \to 0$), so the propagator is the one for two branes on top of each other, i.e. $r_{\mathrm{c}} \to 2r_{\mathrm{c}}$. Since the propagator scales as r_{c}^{-1} for $r \ll r_{\mathrm{c}}$, the Newton potential gets halved. See also the discussion in the paragraph below (3.3).

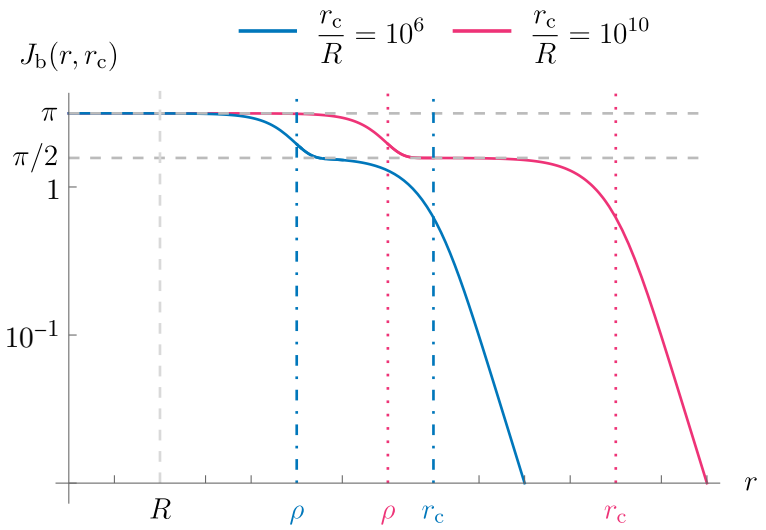

Figure C.5: Log-log plot of the numerical value of J_b (see (C.4)), as a function of r (in units of R), for two different values of r_c/R (solid curves). The dashed horizontal lines go through the points π and $\pi/2$. We see that J_b starts with a constant value of π for $r \ll \rho$, does not change across R, and then crosses over to a DGP-behavior at $r \sim \rho$, where it then goes from a constant value of $\pi/2$ to a $(1/r)$-behavior. Again, the constant region $(\pi/2)$ is more pronounced for larger values of r_c/R.

D

Evaluation of the Bessel Function Sum

In order to evaluate the sum (4.37), we will closely follow Ref. [172], where several asymptotic expansions of Bessel function sums that are similar to ours are derived. We start by defining the new variable

$$\tau := \frac{a}{d_i} \tag{D.1}$$

and taking the Mellin transform of

$$S\Big(\frac{a}{d_i}\Big) = S(\tau) = \sum_{n=1}^{\infty} n^2 K_2(\tau n)\,,$$

which leads to

$$\begin{aligned}\widetilde{S}(s) &= \int_0^\infty \mathrm{d}\tau\, \tau^{2s-1} S(\tau)\,, \\ &= \sum_{n=1}^{\infty} n^2 \underbrace{\int_0^\infty \mathrm{d}\tau\, \tau^{2s-1} K_2(\tau n)}_{I}\,. \end{aligned} \tag{D.2}$$

This expression converges for $\mathrm{Re}(s) > s_0$, with s_0 specified below. The integral, I, in (D.2) can be easily performed, giving

$$I = \frac{1}{4} 2^{2s} \Gamma(s-1)\Gamma(s+1) n^{-2s}\,,$$

with the Gamma function Γ. Now we can take the sum

$$\sum_{n=1}^{\infty} n^{2-2s} = \zeta(2s-2)\,,$$

where ζ is the Riemann zeta function, and find

$$\widetilde{S}(s) = \frac{1}{4} 2^{2s} \Gamma(s-1)\Gamma(s+1)\zeta(2s-2)\,.$$

Finally, we take the inverse Mellin transform

$$\begin{aligned} S(\tau) &= \frac{1}{\pi \mathrm{i}} \int\limits_{s_0-\mathrm{i}\infty}^{s_0+\mathrm{i}\infty} \mathrm{d}s\, \tau^{-2s} \widetilde{S}(s)\,, \\ &= \frac{1}{4\pi \mathrm{i}} \int\limits_{s_0-\mathrm{i}\infty}^{s_0+\mathrm{i}\infty} \mathrm{d}s\, \tau^{-2s} 2^{2s} \Gamma(s-1)\Gamma(s+1)\zeta(2s-2)\,. \end{aligned} \tag{D.3}$$

The integrand in (D.3) has an infinite set of poles, originating from both the Riemann zeta function (pole at $s = \frac{3}{2}$) and the Gamma functions. The poles at $s = \frac{3}{2}, 1, 0$ are simple, while the ones at $s = -1, -2, \ldots$ are double poles. We now see that $s_0 = \frac{3}{2}$, so the integration contour in (D.3) has to be on the right-hand side of this in order for $S(\tau)$ to converge. Using the residue theorem, we can rewrite the above expression as

$$S(\tau) = \frac{1}{2} \sum_{s_i} \mathrm{Res}\Big(f(s), s_i\Big)\,, \tag{D.4}$$

where we sum over all the residues of

$$f(s) = 4^s \tau^{-2s} \Gamma(s-1)\Gamma(s+1)\zeta(2s-2)\,, \tag{D.5}$$

with the poles s_i given above. Expression (D.4) is correct if the integration along the contour around all the poles to the left of s_0 vanishes. It can be shown that this is indeed the case, by carefully analyzing the asymptotic behavior of $\zeta(2s-2)$ and $\Gamma(s \pm 1)$ (see e.g. Ref. [172]).

Now, we do not have to consider all the residues in (D.4) because we are only interested in the terms of $S(\tau)$ that are not higher than second order in τ, since all higher orders will lead to positive powers of a in (4.36). But these will not contribute to the Casimir energy in the limit $a \to 0$. Hence, we only have to consider the poles higher than and up to $s = -1$. We find

$$S(\tau) = \frac{1}{2}\left[\frac{3\pi}{\tau^3} - \frac{2}{\tau^2} + \frac{\zeta'(-4)}{4}\tau^2 + \mathcal{O}\Big(\tau^4\Big)\right], \tag{D.6}$$

where ζ' is the derivative of ζ (and τ as defined in (D.1)).

List of Figures

Bibliography

[1] M. Warkentin, "Modification of the laws of gravity in the DGP model by the presence of a second DGP brane", *JHEP* **03** (2020) 015 [1908.01227].

[2] M. Warkentin, "The Casimir effect in the presence of infrared transparency", *JHEP* **05** (2021) 071 [2011.02985].

[3] L. Berezhiani, G. Cintia and M. Warkentin, "Core fragmentation in simplest superfluid dark matter scenario", *Phys. Lett. B* **819** (2021) 136422 [2101.08117].

[4] S.G. Turyshev, "Experimental Tests of General Relativity", *Ann. Rev. Nucl. Part. Sci.* **58** (2008) 207 [0806.1731].

[5] C.M. Will, "The Confrontation between General Relativity and Experiment", *Living Rev. Rel.* **17** (2014) 4 [1403.7377].

[6] E. Berti et al., "Testing General Relativity with Present and Future Astrophysical Observations", *Class. Quant. Grav.* **32** (2015) 243001 [1501.07274].

[7] J.F. Donoghue, "General relativity as an effective field theory: The leading quantum corrections", *Phys. Rev. D* **50** (1994) 3874 [gr-qc/9405057].

[8] J.F. Donoghue, "Introduction to the effective field theory description of gravity", in *Advanced School on Effective Theories*, 6, 1995 [gr-qc/9512024].

[9] C.P. Burgess, "Quantum gravity in everyday life: General relativity as an effective field theory", *Living Rev. Rel.* **7** (2004) 5 [gr-qc/0311082].

[10] Supernova Search Team collaboration, "Observational evidence from supernovae for an accelerating universe and a cosmological constant", *Astron. J.* **116** (1998) 1009 [astro-ph/9805201].

[11] Supernova Cosmology Project collaboration, "Measurements of Ω and Λ from 42 high redshift supernovae", *Astrophys. J.* **517** (1999) 565 [astro-ph/9812133].

[12] WMAP collaboration, "First year Wilkinson Microwave Anisotropy Probe (WMAP) observations: Determination of cosmological parameters", *Astrophys. J. Suppl.* **148** (2003) 175 [astro-ph/0302209].

[13] SDSS collaboration, "Detection of the Baryon Acoustic Peak in the Large-Scale Correlation Function of SDSS Luminous Red Galaxies", *Astrophys. J.* **633** (2005) 560 [astro-ph/0501171].

[14] J.P. Ostriker and P.J. Steinhardt, "The Observational case for a low density universe with a nonzero cosmological constant", *Nature* **377** (1995) 600.

[15] V. Mukhanov, *Physical Foundations of Cosmology*, Cambridge University Press, Oxford (2005).

[16] S.M. Carroll, *Spacetime and Geometry*, Cambridge University Press (7, 2019).

[17] D. Huterer and M.S. Turner, "Prospects for probing the dark energy via supernova distance measurements", *Phys. Rev. D* **60** (1999) 081301 [astro-ph/9808133].

[18] S. Perlmutter, M.S. Turner and M.J. White, "Constraining dark energy with SNe Ia and large scale structure", *Phys. Rev. Lett.* **83** (1999) 670 [astro-ph/9901052].

[19] P.J.E. Peebles and B. Ratra, "The Cosmological Constant and Dark Energy", *Rev. Mod. Phys.* **75** (2003) 559 [astro-ph/0207347].

[20] Planck collaboration, "Planck 2018 results. VI. Cosmological parameters", *Astron. Astrophys.* **641** (2020) A6 [1807.06209].

[21] S. Weinberg, "The Cosmological Constant Problem", *Rev. Mod. Phys.* **61** (1989) 1.

[22] G. Dvali, G. Gabadadze and M. Shifman, "Diluting cosmological constant in infinite volume extra dimensions", *Phys. Rev. D* **67** (2003) 044020 [hep-th/0202174].

[23] G. Dvali, G. Gabadadze and M. Shifman, "Diluting cosmological constant via large distance modification of gravity", in *18th IAP Colloquium on the Nature of Dark Energy: Observational and Theoretical Results on the Accelerating Universe*, pp. 566–581, 8, 2002, DOI [hep-th/0208096].

[24] N. Arkani-Hamed, S. Dimopoulos, G. Dvali and G. Gabadadze, "Nonlocal modification of gravity and the cosmological constant problem", hep-th/0209227.

[25] G. Dvali, S. Hofmann and J. Khoury, "Degravitation of the cosmological constant and graviton width", *Phys. Rev. D* **76** (2007) 084006 [hep-th/0703027].

[26] M. Kolanovic, M. Porrati and J.-W. Rombouts, "Regularization of brane induced gravity", *Phys. Rev. D* **68** (2003) 064018 [hep-th/0304148].

[27] G. Gabadadze and M. Shifman, "Softly massive gravity", *Phys. Rev. D* **69** (2004) 124032 [hep-th/0312289].

[28] G.R. Dvali and G. Gabadadze, "Gravity on a brane in infinite volume extra space", *Phys. Rev. D* **63** (2001) 065007 [hep-th/0008054].

[29] C. de Rham, G. Dvali, S. Hofmann, J. Khoury, O. Pujolas, M. Redi et al., "Cascading gravity: Extending the Dvali-Gabadadze-Porrati model to higher dimension", *Phys. Rev. Lett.* **100** (2008) 251603 [0711.2072].

[30] C. de Rham, J. Khoury and A.J. Tolley, "Flat 3-Brane with Tension in Cascading Gravity", *Phys. Rev. Lett.* **103** (2009) 161601 [0907.0473].

[31] G. Dvali, "S-Matrix and Anomaly of de Sitter", *Symmetry* **13** (2020) 3 [2012.02133].

[32] G. Dvali, "On S-Matrix Exclusion of de Sitter and Naturalness", 2105.08411.

[33] G. Dvali and C. Gomez, "Quantum Compositeness of Gravity: Black Holes, AdS and Inflation", *JCAP* **01** (2014) 023 [1312.4795].

[34] G. Dvali and C. Gomez, "Quantum Exclusion of Positive Cosmological Constant?", *Annalen Phys.* **528** (2016) 68 [1412.8077].

[35] G. Dvali, C. Gomez and S. Zell, "Quantum Break-Time of de Sitter", *JCAP* **06** (2017) 028 [1701.08776].

[36] N.J. Secrest, S. von Hausegger, M. Rameez, R. Mohayaee, S. Sarkar and J. Colin, "A Test of the Cosmological Principle with Quasars", *Astrophys. J. Lett.* **908** (2021) L51 [2009.14826].

[37] K. Migkas, F. Pacaud, G. Schellenberger, J. Erler, N.T. Nguyen-Dang, T.H. Reiprich et al., "Cosmological implications of the anisotropy of ten galaxy cluster scaling relations", *Astron. Astrophys.* **649** (2021) A151 [2103.13904].

[38] J. Colin, R. Mohayaee, M. Rameez and S. Sarkar, "Evidence for anisotropy of cosmic acceleration", *Astron. Astrophys.* **631** (2019) L13 [1808.04597].

[39] L. Perivolaropoulos and F. Skara, "Challenges for ΛCDM: An update", 2105.05208.

[40] P. Bull et al., "Beyond ΛCDM: Problems, solutions, and the road ahead", *Phys. Dark Univ.* **12** (2016) 56 [1512.05356].

[41] F. Zwicky, "Die Rotverschiebung von extragalaktischen Nebeln", *Helv. Phys. Acta* **6** (1933) 110.

[42] V.C. Rubin and W.K. Ford, Jr., "Rotation of the Andromeda Nebula from a Spectroscopic Survey of Emission Regions", *Astrophys. J.* **159** (1970) 379.

[43] V.C. Rubin, N. Thonnard and W.K. Ford, Jr., "Rotational properties of 21 SC galaxies with a large range of luminosities and radii, from NGC 4605 /R = 4kpc/ to UGC 2885 /R = 122 kpc/", *Astrophys. J.* **238** (1980) 471.

[44] L. Roszkowski, E.M. Sessolo and S. Trojanowski, "WIMP dark matter candidates and searches—current status and future prospects", *Rept. Prog. Phys.* **81** (2018) 066201 [1707.06277].

[45] G. Bertone and D. Hooper, "History of dark matter", *Rev. Mod. Phys.* **90** (2018) 045002 [1605.04909].

[46] J.S. Bullock and M. Boylan-Kolchin, "Small-Scale Challenges to the ΛCDM Paradigm", *Ann. Rev. Astron. Astrophys.* **55** (2017) 343 [1707.04256].

[47] M. Milgrom, "A Modification of the Newtonian dynamics as a possible alternative to the hidden mass hypothesis", *Astrophys. J.* **270** (1983) 365.

[48] M. Milgrom, "A Modification of the Newtonian dynamics: Implications for galaxies", *Astrophys. J.* **270** (1983) 371.

[49] M. Milgrom, "A modification of the Newtonian dynamics: implications for galaxy systems", *Astrophys. J.* **270** (1983) 384.

[50] J. Bekenstein and M. Milgrom, "Does the missing mass problem signal the breakdown of Newtonian gravity?", *Astrophys. J.* **286** (1984) 7.

[51] B. Famaey and S. McGaugh, "Modified Newtonian Dynamics (MOND): Observational Phenomenology and Relativistic Extensions", *Living Rev. Rel.* **15** (2012) 10 [1112.3960].

[52] J.D. Bekenstein, "Relativistic gravitation theory for the MOND paradigm", *Phys. Rev. D* **70** (2004) 083509 [astro-ph/0403694].

[53] G. Dvali, "Infrared modification of gravity", in *Nobel Symposium 127: Cosmology and String Theory*, 2, 2004 [hep-th/0402130].

[54] G. Dvali, "Predictive Power of Strong Coupling in Theories with Large Distance Modified Gravity", *New J. Phys.* **8** (2006) 326 [hep-th/0610013].

[55] C. Deffayet, G. Dvali, G. Gabadadze and A.I. Vainshtein, "Nonperturbative continuity in graviton mass versus perturbative discontinuity", *Phys. Rev. D* **65** (2002) 044026 [hep-th/0106001].

[56] H. van Dam and M.J.G. Veltman, "Massive and massless Yang-Mills and gravitational fields", *Nucl. Phys. B* **22** (1970) 397.

[57] V.I. Zakharov, "Linearized gravitation theory and the graviton mass", *JETP Lett.* **12** (1970) 312.

[58] A.I. Vainshtein, "To the problem of nonvanishing gravitation mass", *Phys. Lett. B* **39** (1972) 393.

[59] K. Hinterbichler, "Theoretical Aspects of Massive Gravity", *Rev. Mod. Phys.* **84** (2012) 671 [1105.3735].

[60] N. Arkani-Hamed, H. Georgi and M.D. Schwartz, "Effective field theory for massive gravitons and gravity in theory space", *Annals Phys.* **305** (2003) 96 [hep-th/0210184].

[61] M.A. Luty, M. Porrati and R. Rattazzi, "Strong interactions and stability in the DGP model", *JHEP* **09** (2003) 029 [hep-th/0303116].

[62] C. de Rham and G. Gabadadze, "Generalization of the Fierz-Pauli Action", *Phys. Rev. D* **82** (2010) 044020 [1007.0443].

[63] A. Nicolis and R. Rattazzi, "Classical and quantum consistency of the DGP model", *JHEP* **06** (2004) 059 [hep-th/0404159].

[64] G.R. Dvali, G. Gabadadze and M. Porrati, "4-D gravity on a brane in 5-D Minkowski space", *Phys. Lett. B* **485** (2000) 208 [hep-th/0005016].

[65] G.R. Dvali and M.A. Shifman, "Dynamical compactification as a mechanism of spontaneous supersymmetry breaking", *Nucl. Phys. B* **504** (1997) 127 [hep-th/9611213].

[66] G.R. Dvali, G. Gabadadze and M. Porrati, "Metastable gravitons and infinite volume extra dimensions", *Phys. Lett. B* **484** (2000) 112 [hep-th/0002190].

[67] E. Witten, "The Cosmological constant from the viewpoint of string theory", in *4th International Symposium on Sources and Detection of Dark Matter in the Universe (DM 2000)*, pp. 27–36, 3, 2000 [hep-ph/0002297].

[68] T. Clifton, P.G. Ferreira, A. Padilla and C. Skordis, "Modified Gravity and Cosmology", *Phys. Rept.* **513** (2012) 1 [1106.2476].

[69] A. Nicolis, R. Rattazzi and E. Trincherini, "The Galileon as a local modification of gravity", *Phys. Rev. D* **79** (2009) 064036 [0811.2197].

[70] G. Dvali, G. Gabadadze, M. Kolanovic and F. Nitti, "The Power of brane induced gravity", *Phys. Rev. D* **64** (2001) 084004 [hep-ph/0102216].

[71] G.R. Dvali, G. Gabadadze, M. Kolanovic and F. Nitti, "Scales of gravity", *Phys. Rev. D* **65** (2002) 024031 [hep-th/0106058].

[72] G. Dvali, G. Gabadadze and M.A. Shifman, "(Quasi)localized gauge field on a brane: Dissipating cosmic radiation to extra dimensions?", *Phys. Lett. B* **497** (2001) 271 [hep-th/0010071].

[73] G.R. Dvali and S.H.H. Tye, "Brane inflation", *Phys. Lett. B* **450** (1999) 72 [hep-ph/9812483].

[74] G.R. Dvali and G. Gabadadze, "Nonconservation of global charges in the brane universe and baryogenesis", *Phys. Lett.* **B460** (1999) 47 [hep-ph/9904221].

[75] A. Padilla, "Ghost free brane world bigravity", *Class. Quant. Grav.* **21** (2004) 2899 [hep-th/0402079].

[76] K. Izumi, K. Koyama and T. Tanaka, "Unexorcized ghost in DGP brane world", *JHEP* **04** (2007) 053 [hep-th/0610282].

[77] Y. Yamashita and T. Tanaka, "Mapping the ghost free bigravity into braneworld setup", *JCAP* **06** (2014) 004 [1401.4336].

[78] C. Deffayet, "Cosmology on a brane in Minkowski bulk", *Phys. Lett. B* **502** (2001) 199 [hep-th/0010186].

[79] C. Deffayet, G.R. Dvali and G. Gabadadze, "Accelerated universe from gravity leaking to extra dimensions", *Phys. Rev. D* **65** (2002) 044023 [astro-ph/0105068].

[80] C. Charmousis, R. Gregory, N. Kaloper and A. Padilla, "DGP Specteroscopy", *JHEP* **10** (2006) 066 [hep-th/0604086].

[81] G. Dvali, "Black Holes and Large N Species Solution to the Hierarchy Problem", *Fortsch. Phys.* **58** (2010) 528 [0706.2050].

[82] G. Dvali and M. Redi, "Black Hole Bound on the Number of Species and Quantum Gravity at LHC", *Phys. Rev. D* **77** (2008) 045027 [0710.4344].

[83] G. Dvali and C. Gomez, "Quantum Information and Gravity Cutoff in Theories with Species", *Phys. Lett. B* **674** (2009) 303 [0812.1940].

[84] N. Arkani-Hamed, S. Dimopoulos and G.R. Dvali, "The Hierarchy problem and new dimensions at a millimeter", *Phys. Lett. B* **429** (1998) 263 [hep-ph/9803315].

[85] G. Dvali and O. Pujolas, "Micro Black Holes and the Democratic Transition", *Phys. Rev. D* **79** (2009) 064032 [0812.3442].

[86] G. Dvali, "Nature of Microscopic Black Holes and Gravity in Theories with Particle Species", *Int. J. Mod. Phys. A* **25** (2010) 602 [0806.3801].

[87] M. Aryal, L.H. Ford and A. Vilenkin, "Cosmic Strings and Black Holes", *Phys. Rev. D* **34** (1986) 2263.

[88] A. Achucarro, R. Gregory and K. Kuijken, "Abelian Higgs hair for black holes", *Phys. Rev. D* **52** (1995) 5729 [gr-qc/9505039].

[89] L. Randall and R. Sundrum, "A Large mass hierarchy from a small extra dimension", *Phys. Rev. Lett.* **83** (1999) 3370 [hep-ph/9905221].

[90] L. Randall and R. Sundrum, "An Alternative to compactification", *Phys. Rev. Lett.* **83** (1999) 4690 [hep-th/9906064].

[91] H.B.G. Casimir, "On the Attraction Between Two Perfectly Conducting Plates", *Indag. Math.* **10** (1948) 261.

[92] S.J. Minter, K. Wegter-McNelly and R.Y. Chiao, "Do Mirrors for Gravitational Waves Exist?", *Physica E* **42** (2010) 234 [0903.0661].

[93] G.R. Dvali and M.A. Shifman, "Domain walls in strongly coupled theories", *Phys. Lett. B* **396** (1997) 64 [hep-th/9612128].

[94] M. Bordag, D. Hennig and D. Robaschik, "Vacuum energy in quantum field theory with external potentials concentrated on planes", *J. Phys. A* **25** (1992) 4483.

[95] N. Graham, R.L. Jaffe, V. Khemani, M. Quandt, M. Scandurra and H. Weigel, "Calculating vacuum energies in renormalizable quantum field theories: A New approach to the Casimir problem", *Nucl. Phys. B* **645** (2002) 49 [hep-th/0207120].

[96] N. Graham, R.L. Jaffe, V. Khemani, M. Quandt, M. Scandurra and H. Weigel, "Casimir energies in light of quantum field theory", *Phys. Lett. B* **572** (2003) 196 [hep-th/0207205].

[97] N. Graham, R.L. Jaffe, V. Khemani, M. Quandt, O. Schroeder and H. Weigel, "The Dirichlet Casimir problem", *Nucl. Phys. B* **677** (2004) 379 [hep-th/0309130].

[98] K.A. Milton, "Casimir energies and pressures for delta function potentials", *J. Phys. A* **37** (2004) 6391 [hep-th/0401090].

[99] K.A. Milton, "The Casimir effect: Recent controversies and progress", *J. Phys. A* **37** (2004) R209 [hep-th/0406024].

[100] L. Berezhiani and J. Khoury, "Dark Matter Superfluidity and Galactic Dynamics", *Phys. Lett. B* **753** (2016) 639 [1506.07877].

[101] L. Berezhiani and J. Khoury, "Theory of dark matter superfluidity", *Phys. Rev. D* **92** (2015) 103510 [1507.01019].

[102] L. Berezhiani, B. Famaey and J. Khoury, "Phenomenological consequences of superfluid dark matter with baryon-phonon coupling", *JCAP* **09** (2018) 021 [1711.05748].

[103] J. Khoury, "Dark Matter Superfluidity", in *Les Houches summer school on Dark Matter*, 9, 2021 [2109.10928].

[104] V. Faraoni, E. Gunzig and P. Nardone, "Conformal transformations in classical gravitational theories and in cosmology", *Fund. Cosmic Phys.* **20** (1999) 121 [gr-qc/9811047].

[105] E.G.M. Ferreira, "Ultra-light dark matter", *Astron. Astrophys. Rev.* **29** (2021) 7 [2005.03254].

[106] J.F. Navarro, C.S. Frenk and S.D.M. White, "The Structure of cold dark matter halos", *Astrophys. J.* **462** (1996) 563 [astro-ph/9508025].

[107] D.S. Reed, S.M. Koushiappas and L. Gao, "Non-universality of halo profiles and implications for dark matter experiments", *Mon. Not. Roy. Astron. Soc.* **415** (2011) 3177 [1008.1579].

[108] A.A. Dutton and A.V. Macciò, "Cold dark matter haloes in the Planck era: evolution of structural parameters for Einasto and NFW profiles", *Mon. Not. Roy. Astron. Soc.* **441** (2014) 3359 [1402.7073].

[109] S. McGaugh, F. Lelli and J. Schombert, "Radial Acceleration Relation in Rotationally Supported Galaxies", *Phys. Rev. Lett.* **117** (2016) 201101 [1609.05917].

[110] F. Lelli, S.S. McGaugh, J.M. Schombert and M.S. Pawlowski, "One Law to Rule Them All: The Radial Acceleration Relation of Galaxies", *Astrophys. J.* **836** (2017) 152 [1610.08981].

[111] S.S. McGaugh, "The Mass discrepancy - acceleration relation: Disk mass and the dark matter distribution", *Astrophys. J.* **609** (2004) 652 [astro-ph/0403610].

[112] S.S. McGaugh, J.M. Schombert, G.D. Bothun and W.J.G. de Blok, "The Baryonic Tully-Fisher relation", *Astrophys. J. Lett.* **533** (2000) L99 [astro-ph/0003001].

[113] S. McGaugh, "The Baryonic Tully-Fisher Relation of Gas Rich Galaxies as a Test of LCDM and MOND", *Astron. J.* **143** (2012) 40 [1107.2934].

[114] F. Lelli, S.S. McGaugh and J.M. Schombert, "The Small Scatter of the Baryonic Tully–fisher Relation", *Astrophys. J. Lett.* **816** (2016) L14 [1512.04543].

[115] R.B. Tully and J.R. Fisher, "A New method of determining distances to galaxies", *Astron. Astrophys.* **54** (1977) 661.

[116] V.P. Debattista and J.A. Sellwood, "Dynamical friction and the distribution of dark matter in barred galaxies", *Astrophys. J. Lett.* **493** (1998) L5 [astro-ph/9710039].

[117] E.C. Ostriker, "Dynamical friction in a gaseous medium", *Astrophys. J.* **513** (1999) 252 [astro-ph/9810324].

[118] L. Hui, J.P. Ostriker, S. Tremaine and E. Witten, "Ultralight scalars as cosmological dark matter", *Phys. Rev. D* **95** (2017) 043541 [1610.08297].

[119] L. Berezhiani, B. Elder and J. Khoury, "Dynamical Friction in Superfluids", *JCAP* **10** (2019) 074 [1905.09297].

[120] D.N. Spergel and P.J. Steinhardt, "Observational evidence for selfinteracting cold dark matter", *Phys. Rev. Lett.* **84** (2000) 3760 [astro-ph/9909386].

[121] M. Kaplinghat, S. Tulin and H.-B. Yu, "Dark Matter Halos as Particle Colliders: Unified Solution to Small-Scale Structure Puzzles from Dwarfs to Clusters", *Phys. Rev. Lett.* **116** (2016) 041302 [1508.03339].

[122] J. Goodman, "Repulsive dark matter", *New Astron.* **5** (2000) 103 [astro-ph/0003018].

[123] Z. Slepian and J. Goodman, "Ruling Out Bosonic Repulsive Dark Matter in Thermal Equilibrium", *Mon. Not. Roy. Astron. Soc.* **427** (2012) 839 [1109.3844].

[124] A. Sharma, J. Khoury and T. Lubensky, "The Equation of State of Dark Matter Superfluids", *JCAP* **05** (2019) 054 [1809.08286].

[125] A.H. Guth, M.P. Hertzberg and C. Prescod-Weinstein, "Do Dark Matter Axions Form a Condensate with Long-Range Correlation?", *Phys. Rev. D* **92** (2015) 103513 [1412.5930].

[126] E.D. Schiappacasse and M.P. Hertzberg, "Analysis of Dark Matter Axion Clumps with Spherical Symmetry", *JCAP* **01** (2018) 037 [1710.04729].

[127] D.J.E. Marsh, "Axion Cosmology", *Phys. Rept.* **643** (2016) 1 [1510.07633].

[128] W. Hu, R. Barkana and A. Gruzinov, "Cold and fuzzy dark matter", *Phys. Rev. Lett.* **85** (2000) 1158 [astro-ph/0003365].

[129] S. May and V. Springel, "Structure formation in large-volume cosmological simulations of fuzzy dark matter: Impact of the non-linear dynamics", 2101.01828.

[130] A. Gruzinov, "On the graviton mass", *New Astron.* **10** (2005) 311 [astro-ph/0112246].

[131] A. Lue and G. Starkman, "Gravitational leakage into extra dimensions: Probing dark energy using local gravity", *Phys. Rev. D* **67** (2003) 064002 [astro-ph/0212083].

[132] G. Dvali, A. Gruzinov and M. Zaldarriaga, "The Accelerated universe and the moon", *Phys. Rev. D* **68** (2003) 024012 [hep-ph/0212069].

[133] G. Gabadadze and A. Iglesias, "Schwarzschild solution in brane induced gravity", *Phys. Rev. D* **72** (2005) 084024 [hep-th/0407049].

[134] A. Lue, "The phenomenology of dvali-gabadadze-porrati cosmologies", *Phys. Rept.* **423** (2006) 1 [astro-ph/0510068].

[135] Y.-S. Song, I. Sawicki and W. Hu, "Large-Scale Tests of the DGP Model", *Phys. Rev. D* **75** (2007) 064003 [astro-ph/0606286].

[136] G. Dvali and C. Gomez, "Strong Coupling Holography", 0907.3237.

[137] C. de Rham, "Massive Gravity", *Living Rev. Rel.* **17** (2014) 7 [1401.4173].

[138] E. Poisson, *A Relativist's Toolkit: The Mathematics of Black-Hole Mechanics*, Cambridge University Press (12, 2009), 10.1017/CBO9780511606601.

[139] A. Zee, *Quantum field theory in a nutshell* (2003).

[140] J. Garriga and T. Tanaka, "Gravity in the brane world", *Phys. Rev. Lett.* **84** (2000) 2778 [hep-th/9911055].

[141] S.B. Giddings, E. Katz and L. Randall, "Linearized gravity in brane backgrounds", *JHEP* **03** (2000) 023 [hep-th/0002091].

[142] P.D. Mannheim, "Are galactic rotation curves really flat?", *The Astrophysical Journal* **479** (1997) 659 [astro-ph/9605085].

[143] A. Borriello and P. Salucci, "The Dark matter distribution in disk galaxies", *Mon. Not. Roy. Astron. Soc.* **323** (2001) 285 [astro-ph/0001082].

[144] Y. Sofue and V. Rubin, "Rotation curves of spiral galaxies", *Ann. Rev. Astron. Astrophys.* **39** (2001) 137 [astro-ph/0010594].

[145] S.S. McGaugh, V.C. Rubin and W.J.G. de Blok, "High - resolution rotation curves of low surface brightness galaxies: Data", *Astron. J.* **122** (2001) 2381 [astro-ph/0107326].

[146] K.A. Oman, J.F. Navarro, A. Fattahi, C.S. Frenk, T. Sawala, S.D.M. White et al., "The unexpected diversity of dwarf galaxy rotation curves", *MNRAS 452 (2015) 3650-3665* (2015) [1504.01437].

[147] A. Barreira, A.G. Sánchez and F. Schmidt, "Validating estimates of the growth rate of structure with modified gravity simulations", *Phys. Rev. D* **94** (2016) 084022 [1605.03965].

[148] G. Veneziano, "Large-N bounds on, and compositeness limit of, gauge and gravitational interactions", *JHEP 0206 (2002) 051* (2001) [hep-th/0110129].

[149] M. Bordag, G.L. Klimchitskaya, U. Mohideen and V.M. Mostepanenko, *Advances in the Casimir effect*, vol. 145, Oxford University Press (2009).

[150] F.-L. Lin, "Casimir effect of graviton and the entropy bound", *Phys. Rev. D* **63** (2001) 064026 [hep-th/0010127].

[151] J.Q. Quach, "Gravitational casimir effect", *Physical Review Letters* **114** (2015) .

[152] J. Ambjørn and S. Wolfram, "Properties of the vacuum. i. mechanical and thermodynamic", *Annals of Physics* **147** (1983) 1.

[153] P. Brax, S. Casas, H. Desmond and B. Elder, "Testing Screened Modified Gravity", *Universe* **8** (2021) 11 [2201.10817].

[154] A. Joyce, L. Lombriser and F. Schmidt, "Dark Energy Versus Modified Gravity", *Ann. Rev. Nucl. Part. Sci.* **66** (2016) 95 [1601.06133].

[155] F. Schmidt, "Weak Lensing Probes of Modified Gravity", *Phys. Rev. D* **78** (2008) 043002 [0805.4812].

[156] W. Fang, S. Wang, W. Hu, Z. Haiman, L. Hui and M. May, "Challenges to the DGP Model from Horizon-Scale Growth and Geometry", *Phys. Rev. D* **78** (2008) 103509 [0808.2208].

[157] L. Lombriser, W. Hu, W. Fang and U. Seljak, "Cosmological Constraints on DGP Braneworld Gravity with Brane Tension", *Phys. Rev. D* **80** (2009) 063536 [0905.1112].

[158] Z. Zhai, M. Blanton, A. Slosar and J. Tinker, "An Evaluation of Cosmological Models from the Expansion and Growth of Structure Measurements", *Astrophys. J.* **850** (2017) 183 [1705.10031].

[159] L. Xu, "Confronting DGP braneworld gravity with cosmico observations after Planck data", *JCAP* **02** (2014) 048 [1312.4679].

[160] Z. Chacko and P.J. Fox, "Wave function of the radion in the dS and AdS brane worlds", *Phys. Rev. D* **64** (2001) 024015 [hep-th/0102023].

[161] P. Binetruy, C. Deffayet and D. Langlois, "The Radion in brane cosmology", *Nucl. Phys. B* **615** (2001) 219 [hep-th/0101234].

[162] W.D. Goldberger and M.B. Wise, "Modulus stabilization with bulk fields", *Phys. Rev. Lett.* **83** (1999) 4922 [hep-ph/9907447].

[163] P.J. Steinhardt, "General considerations of the cosmological constant and the stabilization of moduli in the brane world picture", *Phys. Lett. B* **462** (1999) 41 [hep-th/9907080].

[164] S. Chandrasekhar and S. Chandrasekhar, *An introduction to the study of stellar structure*, vol. 2, Courier Corporation (1957).

[165] D.T. Son and M. Wingate, "General coordinate invariance and conformal invariance in nonrelativistic physics: Unitary Fermi gas", *Annals Phys.* **321** (2006) 197 [cond-mat/0509786].

[166] J.F. Annett et al., *Superconductivity, superfluids and condensates*, vol. 5, Oxford University Press (2004).

[167] P. Sikivie and Q. Yang, "Bose-Einstein Condensation of Dark Matter Axions", *Phys. Rev. Lett.* **103** (2009) 111301 [0901.1106].

[168] O. Erken, P. Sikivie, H. Tam and Q. Yang, "Cosmic axion thermalization", *Phys. Rev. D* **85** (2012) 063520 [1111.1157].

[169] J. Binney and S. Tremaine, *Galactic dynamics*, Princeton university press (2011).

[170] M. Markevitch, A.H. Gonzalez, D. Clowe, A. Vikhlinin, L. David, W. Forman et al., "Direct constraints on the dark matter self-interaction cross-section from the merging galaxy cluster 1E0657-56", *Astrophys. J.* **606** (2004) 819 [astro-ph/0309303].

[171] D. Clowe, A. Gonzalez and M. Markevitch, "Weak lensing mass reconstruction of the interacting cluster 1E0657-558: Direct evidence for the existence of dark matter", *Astrophys. J.* **604** (2004) 596 [astro-ph/0312273].

[172] R. Paris, "The evaluation of single Bessel function sums", *Mathematica Æterna* **8** (2018) 71.

Acknowledgments

My deepest and heartfelt gratitude belongs to Gia Dvali, who gave me the tremendous opportunity to produce this work, by letting me join his research group as a PhD student, and who stimulated most of the research directions undertaken in the present thesis. Moreover, I thank him for having benefited so much from his seemingly bottomless insight into fundamental physics, which he shared so generously and lucidly, on countless occasions, in lectures, seminars, group meetings and private discussions.

My further appreciation goes to my alma mater, the Ludwig-Maximilians-Universität, which nurtured me since my beginnings as an ignorant but overly confident freshman in physics, impatient to learn how the world functions, up until my latest stage as a vastly more knowledgeable but humble doctoral candidate, becoming increasingly aware that the universe's greatest mysteries still remain uncovered. This intriguing progression was facilitated by the amazing professors at the LMU Munich and further eased by the supportive non-scientific staff and the pleasant culture.

During the course of my doctoral studies, I profited immensely from numerous scientific exchanges and inspiring discussions, not only about physics but also on various other fascinating topics. I want to thank all those individuals who supported me and expanded my horizon. Primarily, this includes my collaborators Lasha Berezhiani and Giordano Cintia, who were always available for fruitful discussions and eager to answer my questions. Furthermore, I notably thank Lukas Eisemann for his great support at several stages of the research for the present thesis and for his continuing presence as a physics sparring partner, and as a friend. Moreover, I am indebted to Marco Michel for his scientific support and the daily, welcome distractions. I am also grateful to my "roomies" Karan Tiwana and Oto Sakhelashvili, who never got tired of discussing physics and everything else. Great thanks go out to Giorgos Karananas for his kindness and constantly available support in whatever area I could think of. It is impossible to overstate my thankfulness to all of my remaining colleagues and fellow students, who, over the years, helped to shape me as a physicist and as a person.

A special thanks belongs to Herta Wiesbeck-Yonis, who has been an enormous supporter and guardian angel in the frightening wilderness of academic bureaucracy.

I am grateful to Gia Dvali, Lasha Berezhiani, Giordano Cintia and Silas Zelmer for reading parts of the manuscript and helping to improve it with their invaluable feedback. Furthermore, I wish to thank Gia Dvali, Goran Senjanović, Harald Lesch, and Andreas Burkert for making up my PhD committee.

Finally, I have the pleasure to thank Simone for her patience, understanding,

scientific and mental support, critical questions, encouragement, helpful and exciting physics discussions, and, first and foremost, her love. Of all the expected and unexpected events that contributed to the delay of the completion of this thesis, the arrival of my daughter Philina was the most wonderful one. I want to thank her for reminding me of a simple but remarkable fact: although contemporary high energy physicists have ascended to fantastic theoretical spheres, inhabited by constructs such as curved spacetimes, black holes, quantum gravity, and colliding particles with unimaginable energies, even "ordinary", everyday physics, like a cup falling off a toddler chair, can still appear marvelous and inspire a deep sense of wonderment about this world.